Spin Torques in Systems with Spin Filtering and Spin Orbit Interaction

Dissertation by

Christian Ortiz Pauyac

In Partial Fulfillment of the Requirements

For the Degree of

Doctor of Philosophy

King Abdullah University of Science and Technology, Thuwal,

Kingdom of Saudi Arabia

The Dissertation of Christian Ortiz Pauyac is approved by the examination committee

Committee Chairperson: Aurelien Manchon

Committee Member: Mairbek Chshiev

Committee Member: Udo Schwingenschloegl

Committee Member: Boon Ooi

Committee Member: Tao Wu

ABSTRACT

Spin Torques in Systems with Spin Filtering and Spin Orbit Interaction

Christian Ortiz Pauyac

In the present thesis we introduce the reader to the field of spintronics and explore new phenomena, such as spin transfer torques, spin filtering, and three types of spin-orbit torques, Rashba, spin Hall, and spin swapping, which have emerged very recently and are promising candidates for a new generation of memory devices in computer technology. A general overview of these phenomena is presented in Chap. 1. In Chap. 2 we study spin transfer torques in tunnel junctions in the presence of spin filtering. In Chap. 3 we discuss the Rashba torque in ferromagnetic films, and in Chap. 4 we study spin Hall effect and spin swapping in ferromagnetic films, exploring the nature of spin-orbit torques based on these mechanisms. Conclusions and perspectives are summarized in Chap. 5.

ACKNOWLEDGEMENTS

First and foremost I want to thank my supervisor Aurelien Manchon and co-supervisor Mairbek Chshiev for introducing me to the the world of spintronics. I met Prof. Mairbek Chshiev in Lyon - France while studying a master in engineering. He was eager to accept me as his student for my Master thesis. This was the beginning of my spintronics journey that ended up with a PhD at King Abdullah University of Science and Technology (KAUST) under the supervision of Prof. Aurelien Manchon. Working with them has been a wonderful experience as I was able to develop my theoretical skills in condensed matter physics. I would also like to thank Dr. Xuhui Wang for always showing me the fundamental physics behind a mathematical problem. Special thanks to Collins Akosa and Sergiy Grytsiuk, who came to KAUST as PhD students under the supervisions of Prof. Aurelien Manchon and Prof. Udo Schwingenschlogl, respectively. They have been close friends and always free (although busy) to discuss about spintronics and many other things, as well as spending enjoyable times abroad while going to conferences of magnetism. Last, I want to thank my family for always giving me words of motivation.

TABLE OF CONTENTS

Copyright **1**

Examination Committee Approval **2**

Abstract **3**

Acknowledgements **4**

List of Figures **7**

1 Introduction **8**

1.1 Motivation 8

1.2 Spin transfer torques 11

1.3 Spin filtering 13

1.4 Spin orbit torques 14

1.4.1 Intrinsic spin-orbit torque 15

1.4.2 Extrinsic spin-orbit torque 16

2 Spin Transfer Torques in Spin Filter Tunnel Junctions **18**

2.1 Introduction 18

2.2 Free-electron model based in WKB approximation 19

2.2.1 Eigenenergies and eigenfunctions in a ferromagnet 19

2.2.2 Wavefunctions in ideal spin filter tunnel junctions 20

2.2.3 Charge and spin current densities in spin filter tunnel junctions 24

2.2.4 In-plane and out-of-plane spin torques 27

2.3 Tight binding model based in Keldysh Formalism 29

2.3.1 Tight binding Hamiltonian in second quantization 30

2.3.2 Isolated Green's functions 36

2.3.3 Coupled Green's functions 39

2.3.4 Quantum kinetic equation 41

2.3.5 Spin current densities and spin transfer torques 47

2.4 Results and discussion 50
2.4.1 Partial Spin Filter Tunnel Junction 50
2.4.2 Symmetric Spin Filter Tunnel Junction 53
2.4.3 Spin Filter Tunnel Junctions with insulating spacers 56
2.5 Conclusion 60

3 Rashba Torque in Ferromagnetic Films 62
3.1 Introduction 62
3.2 Quantum kinetic equation 63
3.2.1 Kinetic equation in Keldysh space 63
3.2.2 Wigner expansion 66
3.2.3 Density matrix 72
3.2.4 Diffusion equations 74
3.2.5 Spin-orbit torques 76
3.3 Results and discussion 77
3.4 Conclusions 86

4 Spin Swapping and Spin Hall Effect in Ferromagnetic Films 87
4.1 Introduction 87
4.2 Quantum kinetic equation 88
4.2.1 Unperturbed Green's function 88
4.2.2 Spin orbit coupled impurities 90
4.2.3 Self-energy 92
4.2.4 Momentum relaxation 93
4.2.5 Kinetic equation 96
4.2.6 Quantum Boltzmann equations 103
4.2.7 Diffusion Equations 110
4.3 Results and discussion 112
4.4 Conclusions 116

5 Concluding Remarks 117
5.1 Summary 117
5.2 Perspectives 119

References 123

LIST OF FIGURES

1.1 Tunneling magnetoresistance 10
1.2 Spin transfer torques 11
1.3 Spin filtering 13
1.4 Intrinsic spin orbit torques 15
1.5 Extrinsic spin orbit torques 17

2.1 Scheme of a spin filter tunnel junction (SFTJ) 21
2.2 Potential profile of a SFTJ 22
2.3 Tight binding scheme of a SFTJ 33
2.4 Tight binding Hamiltonian of a SFTJ 39
2.5 Bias dependence of a partial SFTJ 51
2.6 Torque efficiency of a partial SFTJ 52
2.7 Angular dependence of a symmetric SFTJ 55
2.8 Torque efficiency of a partial SFTJ in the presence of spacers 57
2.9 Bias dependence of SFTJs in the presence of spacers 59

3.1 Scheme of a heavy metal/ferromagnet bilayer 77
3.2 Spin density for various values of the Rashba constant 78
3.3 Rashba torque for various exchange splitting values 79
3.4 Spatial distribution of the Rashba torque 80
3.5 Angular dependence of the Rashba torque for $\boldsymbol{m}$ along the $xz-$plane 83
3.6 Angular dependence of the Rashba torque in all directions 85

4.1 Scheme of a squared lattice and a diamond-like ferromagnet 112
4.2 Spin accumulation arising from spin swapping or spin Hall effect . . . 113
4.3 Spin accumulation in ferromagnets with spin-orbit coupled impurities 114
4.4 Spin accumulation in a diamond-like geometry 116

Chapter 1

Introduction

1.1 Motivation

Conventional micro-electronics is based on measuring the tiny electrical charge of electrons passing through electronic circuits; an alternative approach, which emerged after the discovery of the electron's spin through the Stern-Gerlach [1] and the fine structure [2] experiments, revealed that not only the electron's charge but also the fundamental quantum-mechanical property known as the *spin* can be used to reproduce micro-electronic logic/memory devices. Referred to as *spintronics*, this alternative approach offered potential advantages over conventional micro-electronic devices. Whereas the latter requires semiconductor materials in order to control the flow of the charge through transistors, the former can be measured in common metals and ferromagnets since the spin behaves like tiny magnetic fields that can store and transfer information. Therefore, less power consumption is needed to change the electron's spin than to generate a current to maintain electron charges in a device. Moreover, because the electron's spin is not energy-dependent, spin is non-volatile, meaning that information stored in the spin will remain fixed even after loss of power.

It was not until 1988, with the discovery of *giant magnetoresistance* (GMR) by 2007 Nobel Prize in Physics Albert Fert and Peter Grunberg [3], that the first application of spintronics to computers shed its lights. GMR revealed that the electrical

resistance (magnetoresistance) changes as high as 50% at low temperatures in multilayered Fe-Cr structures. It was shown to be much stronger than the usual anisotropic magnetoresistance [4] and was explained in terms of spin-flip scattering of the conduction electrons caused by the antiparallel alignment of the magnetizations in the Fe-layers. This discovery found immediate applications such as magnetic sensors and magnetic random access memories (MRAM), which in contrast to previous memory types, e.g., SRAM, DRAM, FLASH, HDD, offered non-volatility, high-speed reading and writing, random access to data, and low cost.

In the same decade, the phenomenon of *spin-dependent tunneling* (SDT), found on junctions between very thin superconducting aluminum films and ferromagnetic nickel films [5], led to the discovery of *tunneling magnetoresistance* (TMR) in *magnetic tunnel junctions* (MTJs), i.e., a stack of ferromagnetic layers (FM) separated by an insulating barrier (I), see top schemes in Fig. 1.1. The pioneering work in 1975 revealed a modest change in tunneling resistance (14%) when the magnetization of the electrodes were switched from parallel to antiparallel configuration [6]. It was understood in terms of the difference in electronic density of states at the Fermi level between spin-up and spin-down electrons in the magnetized ferromagnets. Because electrons preserve their spin orientation during tunneling processes, they can only tunnel into the sub-band of the same spin orientation. When a bias voltage is placed across the barrier, electrons will tunnel, e.g., from left to right, depending on the availability of free states for its spin direction. Thus, if two FM layers are parallel, see Fig. 1.1(a), a majority of electrons in one FM will find many states of similar orientation in the other FM, causing a large current to tunnel through and a lowering of the overall resistance. However, if they are antiparallel, see Fig. 1.1(b), both spin directions will encounter a bottleneck resulting in a higher total resistance. Initially, TMR did not attract too much attention due to its low magnetoresistance value compared to GMR devices; however, in 2001 a dramatic variation was predicted

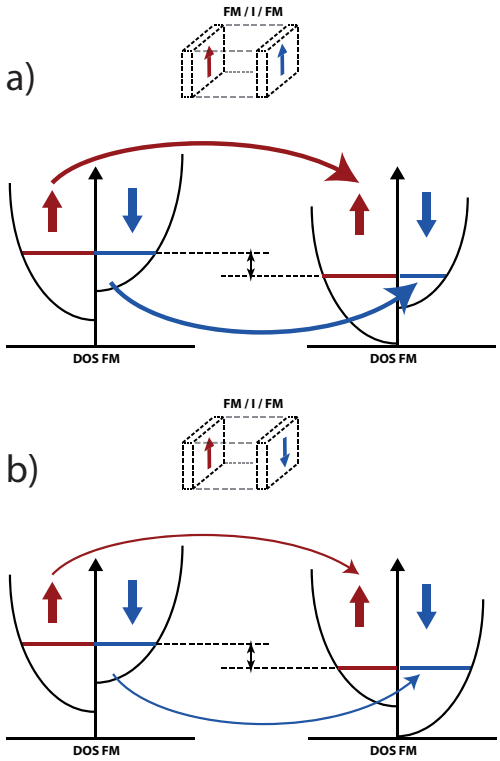

Figure 1.1: Density of states of a magnetic tunnel junction of the form ferromagnet/insulator/ferromagnet ($FM/I/FM$) in a) parallel configuration and b) antiparallel configurations.

considering Fe as the ferromagnets and MgO as the insulator [7]. It was explained that in these type of junctions the symmetric crystallographic structure allowed coherent wave function symmetry filtering, which implied that only bloch states with a defined symmetry of wave functions can tunnel through. The same year, the first experimental results in MgO-based tunnel junctions were given [8]; and in the following years, giant TMR values over 200% were obtained in Fe/MgO/Fe systems [9] and over 600% in CoFeB/MgO/CoFeB junctions [10]. These results led to a new kind of MRAM technology based on TMR; nonetheless, it encountered some difficulties centered around two factors, stability and scalability. Since external fields were needed to switch the magnetization vectors, as the system scaled down parasitic field disturbances appeared leading to data loss. These difficulties were solved considering a new generation of MRAM devices, which based its functionalities in the spin

transfer torque (STT) phenomenon. And more recently (to the date of publication of this thesis), a new kind of MRAM technology is emerging considering the spin-orbit torque (SOT) phenomenon. Coined SOT-MRAM, it offers potential advantages over conventional STT-MRAM devices, e.g., lower switching currents and lower density.

In this chapter we briefly introduce the phenomena behind novel approaches in STT- and SOT- MRAM technologies, i.e., spin transfer torques, spin filtering, and three types of spin-orbit torques: Rashba, spin Hall, and spin swapping. And in the following chapters we discuss in detail these novel approaches, which may impact the future of MRAM technology.

1.2 Spin transfer torques

The intensive search for innovative devices enabling the efficient electrical control of magnetization direction has led to the discovery of Spin Transfer Torque (STT) [11]. In contrast to TMR and GMR, which refer to a controllable electron flow by playing with the relative directions of the magnetic states, STT considers a flowing charge current that is polarized by the first (reference) magnetic layer and exerts a torque on the second (free) magnetic layer as a result or spin transfer from conduction electrons in junctions with non-collinear magnetizations [12], see Fig. 1.2.

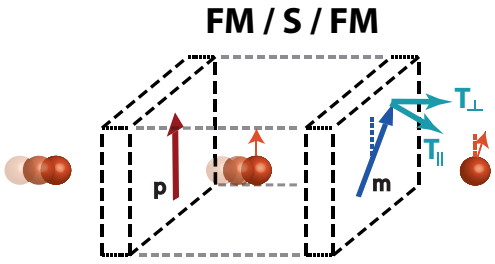

Figure 1.2: Spin transfer torques, $T_{\parallel}$ and $T_{\perp}$, in tunnel junctions of the form, ferromagnet/spacer/ferromagnet (FM/S/FM). The spacer can be either metallic or insulating.

STT has emerged as an efficient mechanism to induce magnetization reversal and excitations, resulting in immediate applications such as magnetic random access

memories (MRAM) and spin torque oscillators, respectively [13]. Conventionally, the torque is partitioned into an out-of-plane component, $T_\perp$, along $\boldsymbol{m} \times \boldsymbol{p}$, and an in-plane component, $T_\parallel$, along $\boldsymbol{m} \times (\boldsymbol{m} \times \boldsymbol{p})$ direction, where $\boldsymbol{m}$ ($\boldsymbol{p}$) represents the free (reference) layer magnetization unit vector, see Fig. 1.2. The relative magnitude of these spin torque components is dependent on material and device structure and is critical in determining the threshold currents for magnetization switching or magnetization oscillations. From the expressions, it is inferred that the in-plane (out-of-plane) torque is odd (even) in $\boldsymbol{m}$, and therefore acts as an antidamping (real field) component [14].

Initially studied in metallic spin valves [15], STT was soon extended to magnetic tunnel junctions (MTJs), where the spacer was replaced by non-magnetic insulating barriers such as Al_2O_3 [16] or MgO [17]. The latter, in contact with Fe(100) electrodes, captured the attention due to its crystallographic configuration that allowed coherent wave function symmetry filtering [18], giving rise to large tunneling magnetoresistance [19]. Meanwhile, STT in MgO-based tunnel junctions became the most promising ingredient for high-density, nonvolatile MRAM devices due to the combination of large TMR and low critical switching current. Substantial studies in ballistic regime [20, 21] revealed, for low bias (V), the following form of the spin torque components,

$$T_\parallel = a_1 V + a_2 V^2, \tag{1.1}$$

$$T_\perp = b_0 + b_1 V + b_2 V^2, \tag{1.2}$$

where the extra linear term of $T_\perp$, b_1, only appears due to symmetry breaking [22] originated from band filling mismatch of the electrodes [23], asymmetric barriers [24, 25], or interfacial disorders [26].

1.3 Spin filtering

Alternative tunneling systems have been proposed after the discovery of GMR and TMR. As an extension of conventional MTJs we have ferroelectrics and magnetic insulators (MI). Ferroelectric junctions display electro-resistance due to the electrical control of charge accumulation at the interfaces [27], whereas magnetic insulators exhibit *spin filtering* effect, which in contrast to symmetry filtering, selectively filters majority carriers due to the spin-dependent evanescence of the wave function in the barrier [28]. Consequently, even when considering a normal metal (NM) reference layer, higher spin polarization is obtained as a result of charge current being exponentially dependent on the exchange splitting of the barrier (Δ_B) [29], see Fig. 1.3.

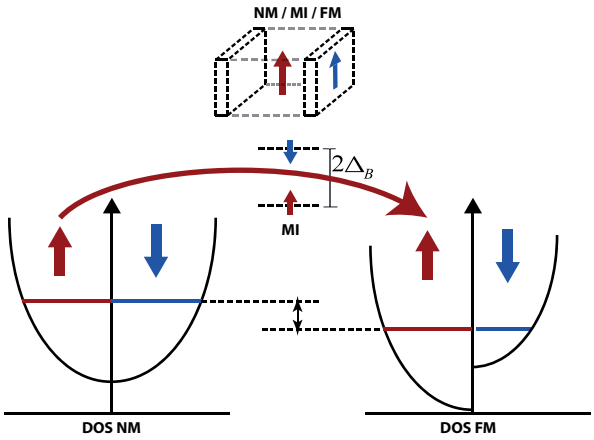

Figure 1.3: Density of states in parallel configuration of a spin filter tunnel junction of the form, normal metal/magnetic insulator/ferromagnet.

Magnetic insulators have attracted also increasing interest in magnonics and spin-caloritronics devices due to its ultra-low damping coefficient [30]. Several architectures of spin filter based tunnel junctions (SFTJs) have been proposed, such as single junctions [31], double junctions [32], partial junctions [33], and symmetric junctions of the form FM/MI/FM [34]. These structures rely on either ferromagnetic or ferrimagnetic insulating barriers. The former includes Eu chalcogenides materials such

as EuS [35], EuSe [36], and EuO [37], which present low Curie temperature (T_c), i.e, $\sim$ 69K [37]. The latter covers spinel-based materials such as $CoFe_2O_4$ [38], $NiFe_2O_4$ [39], $NiMn_2O_4$ [40], $BiMnO_3$ [41], and $CoCr_2O_4$ [42], which exhibit T_c values above room temperature. Most of the works on these architectures have focused on understanding spin polarization and TMR, where the latter tends to be much larger than conventional MTJs. However, the spin transfer torque has been mostly overlooked and little has been done from a theoretical perspective [43].

1.4 Spin orbit torques

The concept of current-driven spin-orbit torques in ultrathin ferromagnetic heterostructures [44] and diluted magnetic semiconductors [45] started to attract attention very recently (to the date of publication of this thesis) for providing an efficient magnetization switching mechanism using just one ferromagnet. In contrast to the spin transfer torque mechanism that requires inhomogeneous magnetic textures (non-collinear magnetizations), the spin-orbit torque accomplishes magnetization switching by transferring angular momentum between the spin and orbital degrees of freedom through a spin-orbit coupling. In the following, we introduce two types of systems where spin-orbit torques can be evidenced. First, in §1.4.1, we consider ferromagnetic heterostructures, typically made of magnetic trilayers comprising an ultrathin ferromagnetic film sandwiched between a noble metal and an insulator. We show that intrinsic spin-orbit torques are evidenced as a result of Rashba and spin Hall effect. Then, in §1.4.2, bilayer structures, comprising a normal metal layer in the presence of spin-orbit coupled impurities and a ferromagnet adjacent to it, are considered. We show that extrinsic spin-orbit torques are evidenced as a result of spin swapping and spin Hall effect.

1.4.1 Intrinsic spin-orbit torque

Experiments and theories have uncovered spin-orbit torques of the form [46, 47, 48]

$$\mathbf{T} = T_{\parallel}\mathbf{m} \times (\hat{\mathbf{y}} \times \mathbf{m}) + T_{\perp}\hat{\mathbf{y}} \times \mathbf{m}, \tag{1.3}$$

in ferromagnetic heterostructures of the form given in Fig. 1.4. In Eq. (1.3), $\mathbf{m}$ is the magnetization direction and $\hat{\mathbf{y}}$ is the directional unit vector. Similar to the spin transfer torque components discussed in §1.2, the two components in Eq. (1.3) are usually referred to as *in-plane* ($T_{\parallel}$) and *out-of-plane* ($T_{\perp}$) torques. The current understanding of the origin of this type of spin-orbit torque in ferromagnetic heterostructures in the presence of intrinsic spin-orbit coupling combines spin-Hall effect [49] and spin-orbit field effects. In the former, a spin current is generated by the spin-Hall effect in the noble metal layer and injected into the ferromagnet to produce a torque [50, 51]. As shown in Fig. 1.4(a), the spin current generated by the spin Hall effect is independent of magnetization direction; therefore, the torque is considered even as a function of $\boldsymbol{m}$ and exhibits a damping-like character.

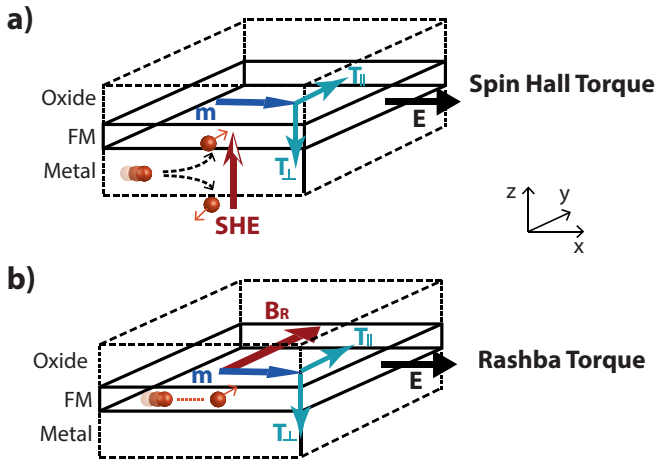

Figure 1.4: Intrinsic spin-orbit torques, a) Spin Hall torque and b) Rashba torque

In the latter, symmetry breaking across the interface between the noble metal and the ferromagnet induces a spin splitting in the band structure, leading to a non-

vanishing current-induced spin-orbit field, $\mathbf{B_R} \propto \hat{\mathbf{z}} \times \mathbf{E}$, where $\boldsymbol{E}$ is the applied electric field directed parallel to the thin film ferromagnet. This field eventually gives rise to a non-equilibrium spin-orbit torque known as Rashba torque. As shown in Fig. 1.4(b), the Rashba torque depends on magnetization direction; therefore, the torque is considered odd as a function of $\boldsymbol{m}$ and exhibits a field-like character. However, it has been shown very recently (to the date of publication of this thesis), considering semiclassical Boltzmann equations, that both effects contribute to both types of torques [51]; consequently, further studies are needed to clarify the experimental results.

1.4.2 Extrinsic spin-orbit torque

Extrinsic spin Hall effect, which converts a charge current into a transverse spin current, is generated in normal metals as a result of the scattering with the spin-orbit coupled impurities. This spin current will eventually induce a torque in an adjacent ferromagnet, see Fig. 1.5(a). Two distinct mechanisms of extrinsic spin Hall effect, or anomalous Hall effect in ferromagnets [52], have been identified, i) *skew scattering*, and ii) *side-jump scattering*. The former scatters asymmetrically as a result of a scattering cross section that depends not only on the scattering angle, but also on the relative sign of the orbital and the spin angular momentum [53], whereas the latter originates from the anomalous form of the velocity operator [54].

An additional extrinsic effect was recently predicted in a similar structure. Referred to as *spin swapping*, Lifshits and D'yakonov showed that, in contrast to the spin Hall effect, spin swapping converts a primary spin current into a secondary spin current with interchanged spin direction and the direction of flow [55]. Initially derived as an extrinsic mechanism [56], it was soon extended to appear from intrinsic contributions such as Rashba [57]. To detect spin swapping, bilayer structures have been proposed, where a polarized current is generated in a ferromagnetic layer and

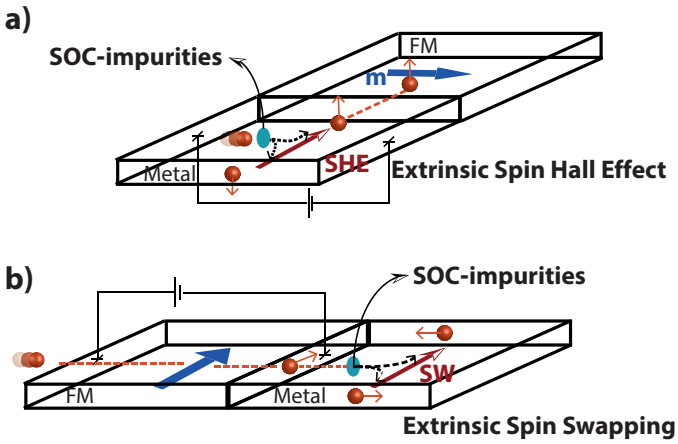

Figure 1.5: Extrinsic spin-orbit torques, a) spin Hall effect and b) spin swapping.

injected in the normal metal where the spin swapping is studied [58], see Fig. 1.5(b).

Based on these phenomena we proceed in the following chapters to study novel avenues in MRAM technology. In Chapter 2 we discuss the interplay of spin transfer torques and spin filtering and in Chapter 3 and Chapter 4, we study new approaches in current-induced spin-orbit torques.

Chapter 2

Spin Transfer Torques in Spin Filter Tunnel Junctions

2.1 Introduction

In the present chapter we study spin transfer torques in magnetic tunnel junctions in the presence of magnetic insulators. Referred to as spin filter tunnel junctions, these junctions consist of one ferromagnet (FM) adjacent to a magnetic insulator (MI) or two FM separated by a MI. Based in free electron (§2.2) and tight binding (§2.3) models we find (§2.4) that the presence of the magnetic insulator dramatically enhances the magnitude of the spin torque components compared to conventional magnetic tunnel junctions, offering novel avenues in STT-MRAM technology. The out-of-plane torque is driven by the spin-dependent reflection at MI/FM interface, which results in a small reduction of its amplitude when an insulating spacer (S) is inserted to decouple MI and FM layers. Meanwhile, the in-plane torque is dominated by the tunnelling electrons that experience the lowest barrier height. We propose a device of the form FM/(S)/MI/(S)/FM that takes advantage of these characteristics and allows for tuning the spin torque magnitudes over a wide range just by rotation of the magnetization of the insulating layer. Conclusions are summarized in §2.5.

2.2 Free-electron model based in WKB approximation

In this section, considering a free-electron model based in *Wensetz-Kramers-Brillouin* approximation, we develop analytical expressions for the in-plane and out-of-plane spin torque components in partial spin filter tunnel junctions, i.e., NM/MI/FM. An important feature of tunnel junctions with dimensions in the scale of 1-5 nm is that transport is considered to be in the ballistic regime; therefore, the electron does not lose track of its $k-$vector and a plane wave solution is a good approximation. In a free-electron model interactions are neglected, e.g., electron-electron, electron-phonon, electron-impurities. Consequently, the plane wave solutions are treated by matching the wave-functions and its derivatives at the interfaces. In particular, in Wensetz-Kramers-Brillouin approach, to be referred to as WKB approximation, Schrodinger equation is solved considering a wavefunction solution in the barrier that requires a slowly varying potential. Details of this approach are neglected in the present thesis as this model is well established and appears in many textbooks of quantum mechanics [59]. We therefore address, in the following, the most important mathematical details in calculating the in-plane and out-of-plane spin torque components.

2.2.1 Eigenenergies and eigenfunctions in a ferromagnet

In a free-electron approximation of the spin-polarized conduction electrons inside the ferromagnet, the one-electron Hamiltonian may be written as,

$$H_0 = \frac{\hbar^2 \mathbf{k^2}}{2m} - J\hat{\boldsymbol{\sigma}} \cdot \mathbf{m}. \tag{2.1}$$

The first term in Eq. (2.1) represents the kinetic part, where $\mathbf{p} = \hbar\mathbf{k}$ is the momentum and m is the mass of the electron. The second term is the s-d exchange

interaction. J is the exchange coupling parameter, $\hat{\boldsymbol{\sigma}} = (\sigma_x, \sigma_y, \sigma_z)$ is the Pauli matrix vector, and $\mathbf{m}$ is the magnetization unit vector, which in spherical coordinates is defined by the angles θ and ϕ. Two possible eigenenergies are obtained, $E_s = \frac{\hbar^2\mathbf{k}^2}{2m} - sJ$, where $s = \pm 1$ or $\Uparrow$ ($\Downarrow$). In principle we consider $E_+ = \frac{\hbar^2\mathbf{k}^2}{2m} - J$ the energy for majority carriers and $E_- = \frac{\hbar^2\mathbf{k}^2}{2m} + J$ the energy for minority carriers. The eigenfunctions of the Hamiltonian are,

$$\Psi^{\Uparrow} = \begin{bmatrix} \cos\frac{\theta}{2}e^{-i\phi} \\ \sin\frac{\theta}{2} \end{bmatrix} \psi^{\uparrow}, \qquad \Psi^{\Downarrow} = \begin{bmatrix} -\sin\frac{\theta}{2}e^{-i\phi} \\ \cos\frac{\theta}{2} \end{bmatrix} \psi^{\downarrow}. \tag{2.2}$$

$\Psi^{\Uparrow(\Downarrow)}$ is the eigenfunction for spin-up (-down) state and $\psi^{\uparrow(\downarrow)}$ is the plane-wave associated to it, e.g., $\psi^{\uparrow(\downarrow)} = e^{i\mathbf{k}^{\uparrow(\downarrow)}\mathbf{r}}$. In tunnel junctions, $\psi^{\uparrow(\downarrow)}$ becomes a linear combination of incident and reflected waves. Considering $\boldsymbol{m}$ to be restricted to the $xz-$plane and defining basis states along the z-quantization axis, i.e., $|\Uparrow\rangle_{\mathbf{z}} = [1 \;\; 0]^t$ and $|\Downarrow\rangle_{\mathbf{z}} = [0 \;\; 1]^t$, the total eigenfunction, $\Psi = \Psi^{\Uparrow} + \Psi^{\Downarrow}$, becomes,

$$\Psi = \left[\cos\frac{\theta}{2}\psi^{\uparrow} - \sin\frac{\theta}{2}\psi^{\downarrow}\right] |\Uparrow\rangle_{\mathbf{z}} + \left[\sin\frac{\theta}{2}\psi^{\uparrow} + \cos\frac{\theta}{2}\psi^{\downarrow}\right] |\Downarrow\rangle_{\mathbf{z}}, \tag{2.3}$$

2.2.2 Wavefunctions in ideal spin filter tunnel junctions

In the present analysis we consider semi-infinite ferromagnetic electrodes separated by a finite magnetic insulator of thickness d. In the electrodes the magnetization vectors, $\mathbf{m}_L$ and $\mathbf{m}_R$, are constraint to the $xz-$plane, transverse to the propagation direction, given along y, whereas in the barrier $\mathbf{m}_B = \hat{\mathbf{z}}$. At position $y = |d/2|$ we are at the barrier - electrode interface, See Fig. 2.1.

The Hamiltonians for each layer are given as follow,

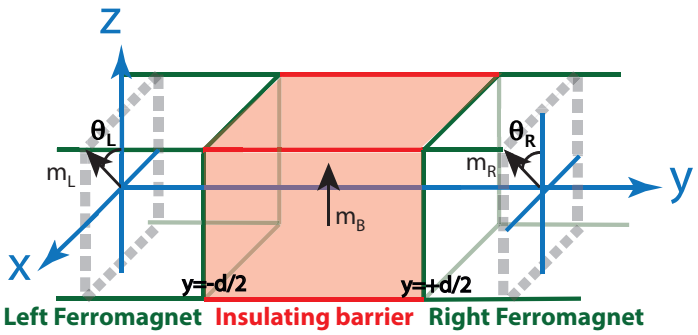

Figure 2.1: Spin filter tunnel junction made of two semi-infinite ferromagnetic layers and a finite magnetic insulating barrier. The magnetization vectors in the ferromagnetic layers, $\mathbf{m}_L$ and $\mathbf{m}_R$, are constraint to the $xz-$plane and therefore are defined by θ_L and θ_R, respectively. The magnetization vector in the barrier is set to $\mathbf{m}_B = \hat{\mathbf{z}}$.

$$\hat{H}_L = \frac{\mathbf{p}^2}{2m} - J_L \hat{\boldsymbol{\sigma}} \cdot \mathbf{m_L} + \frac{eV}{2}, \qquad y \leq -d/2, \tag{2.4}$$

$$\hat{H}_B = \frac{\mathbf{p}^2}{2m} + U_0 - J_B \hat{\boldsymbol{\sigma}} \cdot \mathbf{m_B} - \frac{eV}{d} y, \qquad -d/2 \leq y \leq d/2, \tag{2.5}$$

$$\hat{H}_R = \frac{\mathbf{p}^2}{2m} - J_R \hat{\boldsymbol{\sigma}} \cdot \mathbf{m_R} - \frac{eV}{2}, \qquad d/2 \leq y. \tag{2.6}$$

L (R) stands for the left (right) ferromagnetic layer and B for the insulating barrier. As shown in Fig. 2.2, U_0 is the barrier potential, d is the barrier thickness, and eV is the voltage drop across the sample. Other parameters were defined in §2.2.1

To describe the propagation of the electron along y, transmitted and reflected one-dimensional plane waves are considered, i.e., $e^{ik_y(y-y_0)}$ ($e^{-ik_y(y-y_0)}$) describes a plane wave going from left to right (right to left). Notice that for $y = y_0$ the plane-wave vanishes; therefore, $y_0 = +d/2(-d/2)$ in the right (left) electrode. Considering Eq. (2.3), the wavefunctions in the electrodes are,

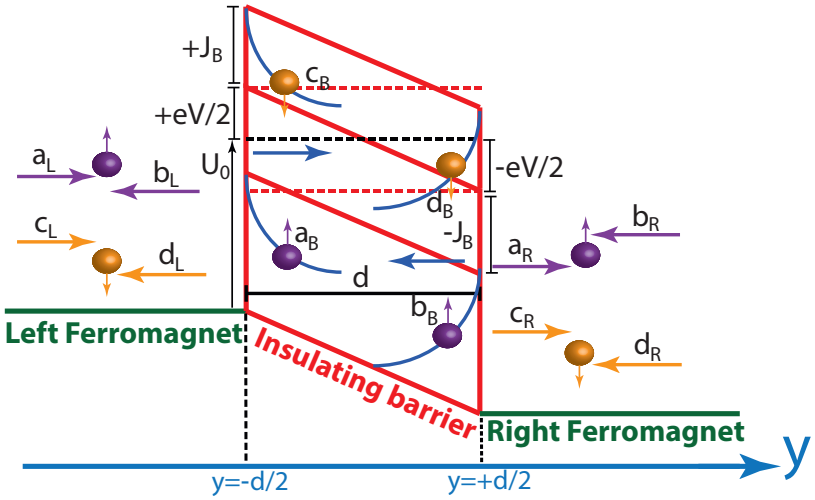

Figure 2.2: Schematic illustration of the transmitted and reflected waves in the electrodes and the evanescent waves in the barrier.

$$\Psi_L = [\psi_L^{\uparrow} \cos\frac{\theta_L}{2} - \ {}^{\downarrow}_{L} \sin\frac{\theta_L}{2}] \, |\Uparrow\rangle_{\mathbf{z}} + [\psi_L^{\uparrow} \sin\frac{\theta_L}{2} + \ {}^{\downarrow}_{L} \cos\frac{\theta_L}{2}] \, |\Downarrow\rangle_{\mathbf{z}}, \tag{2.7}$$

$$\Psi_R = [\psi_R^{\uparrow} \cos\frac{\theta_R}{2} - \ {}^{\downarrow}_{R} \sin\frac{\theta_R}{2}] \, |\Uparrow\rangle_{\mathbf{z}} + [\psi_R^{\uparrow} \sin\frac{\theta_R}{2} + \ {}^{\downarrow}_{R} \cos\frac{\theta_R}{2}] \, |\Downarrow\rangle_{\mathbf{z}}, \tag{2.8}$$

with

$${}^{\uparrow}_{L} = (a_L e^{ik_L^{\uparrow}(y+d/2)} + b_L e^{-ik_L^{\uparrow}(y+d/2)}), \tag{2.9}$$

$${}^{\downarrow}_{L} = (c_L e^{ik_L^{\downarrow}(y+d/2)} + d_L e^{-ik_L^{\downarrow}(y+d/2)}), \tag{2.10}$$

$${}^{\uparrow}_{R} = (a_R e^{ik_R^{\uparrow}(y-d/2)} + b_R e^{-ik_R^{\uparrow}(y-d/2)}), \tag{2.11}$$

$${}^{\downarrow}_{R} = (c_R e^{ik_R^{\downarrow}(y-d/2)} + d_R e^{-ik_R^{\downarrow}(y-d/2)}), \tag{2.12}$$

and

$$k_L^{\uparrow(\downarrow)} = \sqrt{\frac{2m}{\hbar^2}(E \pm J_L - \frac{eV}{2} - E_{||})} = \sqrt{\frac{2m}{\hbar^2}(E \pm J_L - \frac{eV}{2}) - k_{||}^2}, \tag{2.13}$$

$$k_R^{\uparrow(\downarrow)} = \sqrt{\frac{2m}{\hbar^2}(E \pm J_R + \frac{eV}{2} - E_{||})} = \sqrt{\frac{2m}{\hbar^2}(E \pm J_R + \frac{eV}{2}) - k_{||}^2}. \tag{2.14}$$

In Eqs. (2.9) - (2.12), $a_{L(R)}(b_{L(R)})$ and $c_{L(R)}(d_{L(R)})$ account for the coefficients of spin up and spin down plane waves going from left (right) to right (left), respectively. As shown in Fig. 2.2, a total of 4 plane waves are defined in each electrode. In Eqs. (2.13) and (2.14), $E_{||} = \frac{\hbar^2(k_x^2+k_z^2)}{2m} = \frac{\hbar^2 k_{||}^2}{2m}$ is the in-plane energy and $k_y = k_{L(R)}$ is wave-vector in the electrode.

In the barrier the wavefunction is given by,

$$\Psi_B = \psi_B^{\uparrow} \left|\Uparrow\right\rangle_{\mathbf{z}} + \psi_B^{\downarrow} \left|\Downarrow\right\rangle_{\mathbf{z}} \tag{2.15}$$

with

$$\overset{\uparrow}{}_B = (\frac{a_B}{\sqrt{\kappa^{\uparrow}(y)}} e^{-\xi^{\uparrow}(y)} + \frac{b_B}{\sqrt{\kappa^{\uparrow}(y)}} e^{\xi^{\uparrow}(y)}), \tag{2.16}$$

$$\overset{\downarrow}{}_B = (\frac{c_B}{\sqrt{\kappa^{\downarrow}(y)}} e^{-\xi^{\downarrow}(y)} + \frac{d_B}{\sqrt{\kappa^{\downarrow}(y)}} e^{\xi^{\downarrow}(y)}), \tag{2.17}$$

and

$$\kappa^{\uparrow(\downarrow)}(y) = \sqrt{\frac{2m}{\hbar^2}(U_0 - \frac{eV}{d} y \mp J_B - E + E_{||})}, \tag{2.18}$$

$$\xi^{\uparrow(\downarrow)}(y) = \int_{y_0}^{y} \kappa^{\uparrow(\downarrow)}(u) du = (\frac{d\hbar^2}{3meV}) \left[\kappa^{3\uparrow(\downarrow)}(y_0) - \kappa^{3\uparrow(\downarrow)}(y)\right], \tag{2.19}$$

where we have considered WKB approximation and $\boldsymbol{m}_B = \boldsymbol{z}$. In Eqs. (2.16) and (2.17), $a_B(b_B)$ and $c_B(d_B)$ are the spin-up and spin-down coefficients of the evanescent waves going from left (right) to right (left), respectively, see Fig. 2.2. $\kappa^{\uparrow(\downarrow)}(y)$ defines the wave-vector in the barrier and $e^{-\xi^{\uparrow(\downarrow)}(y)(+\xi^{\uparrow(\downarrow)}(y))}$ describes the evanescent decaying exponential wave from left (right) to right (left). Notice that our wavefunctions are normalized with respect to the wave-vector, e.g., For a spin-up (down) electron incident from left to right we have $a_L = 1/\sqrt{2k_L^{\uparrow}}$ ($c_L = 1/\sqrt{2k_L^{\downarrow}}$). To finalize, we solve Eq. (2.19) for $y = d/2$ and get

$$\xi^{\uparrow(\downarrow)}(d/2) = \int_{-d/2}^{d/2} \kappa^{\uparrow(\downarrow)}(u)du = (\frac{d\hbar^2}{3meV})\Big[\Big(\frac{2m}{\hbar^2}(U_0 + eV/2 \mp J_B - E + E_{||})\Big)^{3/2} - \Big(\frac{2m}{\hbar^2}(U_0 - eV/2 \mp J_B - E + E_{||})\Big)^{3/2}\Big]. \tag{2.20}$$

Considering that WKB approximation is valid for low voltage, then we can perform a Taylor expansion in terms of eV. Consequently, Eq. (2.20) reduces to,

$$\xi^{\uparrow(\downarrow)}(d/2) = d\sqrt{\frac{2m}{\hbar^2}(U_0 \mp J_B - E + E_{||})} - d\frac{\sqrt{\frac{m}{\hbar^2}(U_0 \mp J_B - E + E_{||})}}{48\sqrt{2}(U_0 \mp J_B - E + E_{||})^2}eV^2, \tag{2.21}$$

which shows that $\xi(d/2)$ is independent of the sign of eV. Moreover, for $eV = 0$, it reduces to the case of a spatially independent barrier potential [60].

2.2.3 Charge and spin current densities in spin filter tunnel junctions

The charge (ρ) and spin ($\boldsymbol{S}$) densities are defined as,

$$\rho = e\sum_{\sigma}\psi^{*}_{\sigma}\psi_{\sigma} = e(\psi^{*}_{\uparrow}\psi_{\uparrow} + \psi^{*}_{\downarrow}\psi_{\downarrow}), \tag{2.22}$$

$$\mathbf{S} = \sum_{\sigma,\sigma'}\psi^{*}_{\sigma}\mathbf{s}_{\sigma,\sigma'}\psi_{\sigma'}, \tag{2.23}$$

where e is the charge of the electron, $\sigma =\uparrow (\downarrow)$ represents the spin orientation, $\hat{\boldsymbol{\sigma}}$ is the Pauli matrix vector, and $\mathbf{s} = \frac{\hbar}{2}\hat{\boldsymbol{\sigma}} = \frac{\hbar}{2}(\sigma_x, \sigma_y, \sigma_z)$ is the spin operator. Similarly, the charge ($\mathbf{j}_e$) and spin ($\mathbf{J}^s$) current densities are defined as,

$$\boldsymbol{j}_e = e\sum_{\sigma}\psi^{*}_{\sigma}\mathbf{v}\psi_{\sigma} = -e(\frac{i\hbar}{m})(\psi^{*}_{\uparrow}\nabla\psi_{\uparrow} + \psi^{*}_{\downarrow}\nabla\psi_{\downarrow}), \tag{2.24}$$

$$\boldsymbol{J}^s = \sum_{\sigma\sigma'}\psi^{*}_{\sigma}\mathbf{s}_{\sigma\sigma'}\otimes\mathbf{v}\psi_{\sigma'}, \tag{2.25}$$

where $\mathbf{v} = -\frac{i\hbar}{m}\boldsymbol{\nabla}$ is the velocity operator, $\hbar$ is Planck's constant, and m is the mass of the electron. In three dimensional systems, a total of 9 components are given for the spin current density. However, in tunnel junctions, where transport is given along $y-$axis, only the $y-$components survive, i.e., J^x_y, J^y_y, J^z_y (upper index refers to the spin space and sub-index to the spatial space). We proceed now to calculate the spin current densities, J^x_y and J^y_y at the right interface (y=d/2) in spin filter tunnel junctions. Considering the local representation we have,

$$J^x_y = -\frac{i\hbar^2}{2m}(\psi^{*\uparrow}_R\frac{\partial\psi^{\downarrow}_R}{\partial y} + \psi^{*\downarrow}_R\frac{\partial\psi^{\uparrow}_R}{\partial y}), \tag{2.26}$$

$$J^y_y = \frac{\hbar^2}{2m}(-\psi^{*\uparrow}_R\frac{\partial\psi^{\downarrow}_R}{\partial y} + \psi^{*\downarrow}_R\frac{\partial\psi^{\uparrow}_R}{\partial y}), \tag{2.27}$$

where $\psi^{\uparrow}_R$ and $\psi^{\downarrow}_R$ are defined in Eqs. (2.11) and (2.12), respectively.

Let's consider first spin-up and spin-down electrons incident from left to right,

i.e., $b_R = 0$ and $d_R = 0$. Replacing Eqs. (2.11) and (2.12) in Eqs. (2.26) and (2.27) we have,

$$J_y^x(y = d/2)_{L\to R}^{\uparrow(\downarrow)} = \frac{\hbar^2}{2m}(a_R^* c_R k_R^{\downarrow} + a_R c_R^* k_R^{\uparrow}), \tag{2.28}$$

$$J_y^y(y = d/2)_{L\to R}^{\uparrow(\downarrow)} = \frac{i\hbar^2}{2m}(-a_R^* c_R k_R^{\downarrow} + a_R c_R^* k_R^{\uparrow}), \tag{2.29}$$

where the coefficients are derived by matching the wavefunctions and its derivatives at the interfaces. Considering then electrons from right to left we get different expressions for up and down spins. For spin up ($\uparrow$) electrons flowing from right to left ($R \to L$) we have $d_R = 0$ and $b_R = 1/\sqrt{2k_R^{\uparrow}}$, then

$$J_y^x(y = d/2)_{R\to L}^{\uparrow} = \frac{\hbar^2}{4m\sqrt{k_R^{\uparrow}}}[c_R k_R^{\downarrow}(\sqrt{2} + 2a_R^*\sqrt{k_R^{\uparrow}}) + c_R^* k_R^{\uparrow}(-\sqrt{2} + 2a_R\sqrt{k_R^{\uparrow}})], \tag{2.30}$$

$$J_y^y(y = d/2)_{R\to L}^{\uparrow} = -\frac{i\hbar^2}{4m\sqrt{k_R^{\uparrow}}}[c_R k_R^{\downarrow}(\sqrt{2} + 2a_R^*\sqrt{k_R^{\uparrow}}) + c_R^* k_R^{\uparrow}(\sqrt{2} - 2a_R\sqrt{k_R^{\uparrow}})]. \tag{2.31}$$

For spin-down ($\downarrow$) electrons flowing from right to left ($R \to L$) we have $b_R = 0$ and $d_R = 1/\sqrt{2k_R^{\downarrow}}$, then

$$J_y^x(y=d/2)^{\downarrow}_{R\to L} = \frac{\hbar^2}{4m\sqrt{k_R^{\downarrow}}}[a_R^* k_R^{\downarrow}(-\sqrt{2}+2c_R\sqrt{k_R^{\downarrow}}) + a_R k_R^{\uparrow}(\sqrt{2}+2c_R^*\sqrt{k_R^{\downarrow}})], \tag{2.32}$$

$$J_y^y(y=d/2)^{\downarrow}_{R\to L} = \frac{i\hbar^2}{4m\sqrt{k_R^{\downarrow}}}[a_R^* k_R^{\downarrow}(-2c_R\sqrt{k_R^{\downarrow}}+\sqrt{2}) + a_R k_R^{\uparrow}(\sqrt{2}+2c_R^*\sqrt{k_R^{\downarrow}})]. \tag{2.33}$$

Finally, in equilibrium, the total spin current density measured on the right electrode at $y = d/2$ shall be given by summing up the 4 contributions, i.e.,

$$J_y^i(\text{total}) = J_y^i(y=d/2)^{\uparrow}_{L\to R} + J_y^i(y=d/2)^{\downarrow}_{L\to R} + J_y^i(y=d/2)^{\uparrow}_{R\to L} + J_y^i(y=d/2)^{\downarrow}_{R\to L}, \tag{2.34}$$

2.2.4 In-plane and out-of-plane spin torques

In this section we proceed to study the spin transfer torque mechanism. In the literature, for transport given along y, the spin torque components are defined as

$$T_{||} = J_y^x, \tag{2.35}$$

$$T_{\perp} = J_y^y. \tag{2.36}$$

$T_{||}$ is the in-plane torque and $T_{\perp}$ is the out-of-plane torque. As shown, the spin torque components are equivalent to the spin current densities that are transverse to the magnetization direction. These definitions are found in many textbooks and reviews, we therefore won't give much details about its derivations. Notice that the above definitions are correct as long as we work in the local representation.

Considering the definitions given, we proceed to study partial spin filter tunnel junctions, i.e., NM/MI/FM, where $J_L = 0$ in Eq. (2.13) and therefore $k_L = k_L^{\uparrow(\downarrow)}$. In the thick barrier limit, to the lowest order in the transmission, the out-of-plane component of the spin torque for electrons flowing from left to right ($L \to R$) and right to left ($R \to L$) read,

$$\mathrm{T}_{\perp}^{L\to R} = \frac{8\hbar^2}{m\eta_{\theta_R}}(k_R^{\downarrow 2} - k_R^{\uparrow 2})k_L q_R^{\downarrow} q_R^{\uparrow} \sum_{\sigma}\left[\sigma \frac{e^{-2\xi^{\sigma}} q_L^{\sigma}}{k_L^2 + q_L^{\sigma 2}}\right] \sin\theta_R, \tag{2.37}$$

$$\mathrm{T}_{\perp}^{R\to L} = \frac{2\hbar^2}{m\eta_{\theta_R}}(k_R^{\downarrow} - k_R^{\uparrow})(q_R^{\downarrow} - q_R^{\uparrow})(k_R^{\downarrow}k_R^{\uparrow} - q_R^{\downarrow}q_R^{\uparrow}) \sin\theta_R. \tag{2.38}$$

$\eta_{\theta_R} = [(k_R^{\downarrow} + k_R^{\uparrow})(q_R^{\downarrow} + q_R^{\uparrow}) - (k_R^{\downarrow} - k_R^{\uparrow})(q_R^{\downarrow} - q_R^{\uparrow})\cos\theta_R]^2 + 4(q_R^{\downarrow}q_R^{\uparrow} - k_R^{\downarrow}k_R^{\uparrow})^2$, $\kappa^{\uparrow(\downarrow)}(+d/2) = q_R$, $\kappa^{\uparrow(\downarrow)}(-d/2) = q_L$, and $\xi^{\uparrow(\downarrow)} \equiv \xi^{\uparrow(\downarrow)}(d/2)$. In Eqs. (2.37) and (2.38) η_{θ_R} depends on the free layer magnetization direction and is driven by the exchange splitting of the barrier. This term brings an out-of-plane torque angular dependence that deviates from the conventional $\sin\theta_R$ dependence encountered in MTJs. Of great importance is the non-vanishing zeroth-order term of $\mathrm{T}_{\perp}^{R\to L}$, given in Eq. (2.38), which demonstrates that the out-of-plane torque is dominated by the spin-dependent reflection at MI/FM interface, depending strongly on $q_R^{\uparrow} - q_R^{\downarrow}$ and $k_R^{\uparrow} - k_R^{\downarrow}$ and being independent of the barrier width. Meanwhile, the in-plane components, for electrons flowing from left to right and right to left, are both second order in barrier transmission, $\sim e^{-2\xi^{\uparrow(\downarrow)}}$ and strongly depend on the barrier width. $\mathrm{T}_{\parallel}$ for MTJs and p-SFTJs to the lowest order in the thick barrier limit are given by,

$$T_{\parallel(MTJ)}^{L\to R} = \frac{2\hbar^2}{m}\frac{(k_L^{\downarrow}-k_L^{\uparrow})(k_R^{\downarrow}+k_R^{\uparrow})(k_L^{\downarrow}k_L^{\uparrow}-q_L^2)(k_R^{\downarrow}k_R^{\uparrow}+q_R^2)q_Lq_Re^{-2\xi}}{(k_L^{\downarrow 2}+q_L^2)(k_L^{\uparrow 2}+q_L^2)(k_R^{\downarrow 2}+q_R^2)(k_R^{\uparrow 2}+q_R^2)}\sin\theta_R$$

$$\equiv \mathscr{T}_L\mathscr{P}_L\sin\theta_R, \tag{2.39}$$

$$T_{\parallel(pSFTJ)}^{L\to R} = \frac{8\hbar^2}{m\eta_{\theta_R}}(k_R^{\downarrow}+k_R^{\uparrow})k_L\left[\frac{e^{-2\xi^{\uparrow}}q_L^{\uparrow}q_R^{\uparrow}(k_R^{\downarrow}k_R^{\uparrow}+q_R^{\downarrow 2})}{k_L^2+q_L^{\uparrow 2}} - \frac{e^{-2\xi^{\downarrow}}q_L^{\downarrow}q_R^{\downarrow}(k_R^{\downarrow}k_R^{\uparrow}+q_R^{\uparrow 2})}{k_L^2+q_L^{\downarrow 2}}\right]\sin\theta_R$$

$$\approx \frac{8\hbar^2}{m\eta_{\theta_R}}(k_R^{\downarrow}+k_R^{\uparrow})k_L\left[\frac{e^{-2\xi^{\uparrow}}q_L^{\uparrow}q_R^{\uparrow}(k_R^{\downarrow}k_R^{\uparrow}+q_R^{\downarrow 2})}{k_L^2+q_L^{\uparrow 2}}\right]\sin\theta_R. \tag{2.40}$$

For simplicity we have considered the contribution of electrons incident from the left layer only. $\mathscr{T}_L$ and $\mathscr{P}_L$, defined in Ref [60], are the transmissivity and effective Slonczewski polarization of the left layer, respectively. It is straightforward to notice from Eq. (2.39) that in MTJs the sign of $T_{\parallel}$ is determined by the sign of the polarization $\mathscr{P}_L \propto (k_L^{\downarrow}-k_L^{\uparrow})$ whereas in p-SFTJs, given in Eq. (2.40), $\mathscr{P}_L$ is absent and no sign reversal is expected since $T_{\parallel}$ is driven by the tunneling electrons that experience the lowest barrier height (majority electrons in Eq. 2.40).

2.3 Tight binding model based in Keldysh Formalism

Most of the existing theories of spin transfer torque in metallic spin-valves nanostructures use semiclassical approaches based on the generalization of the Valet-Fert theory for GMR [61] since the spin dependent transport in such structures is usually considered diffusive and quantum effects are not important. However, in tunnel junctions, a quantum treatment must be considered and, therefore, it is important to describe the system more realistically using quantum techniques. In the present, to describe spin filter tunnel junctions we use the tight binding (TB) model for a ballistic description of spin transport - based on an extension of the Keldysh formal-

ism [62] - to the case of non-collinear orientation of the magnetizations. Whereas the previous model, i.e., free electron model based in WKB approximation, is restricted to thick barriers with high barrier potentials, in this case we are allowed to consider thin barrier layers. Moreover, a tight binding analysis takes into account the atomic potentials in the system, which play a crucial role in the energy dispersion. In addition, Keldysh formalism is a powerful approach that provides means of calculating the density matrix through the Keldysh function, providing an exact description of the system even if the system does not have a well defined wavefunction, e.g., it allows to keep track of phase correlations between different points (or states) during non-equilibrium processes due to irreversible effects caused by inelastic interactions or due to applied fields that modify the distribution of the electrons inside the system.

2.3.1 Tight binding Hamiltonian in second quantization

For a single electron one dimensional problem, an operator $\hat{O}$, in second quantization, reads

$$\hat{O} = \sum_{j,j',\sigma,\sigma'} T_{j,j'}^{\sigma,\sigma'} \hat{c}_{j'}^{\dagger\sigma'} \hat{c}_{j}^{\sigma} = \sum_{j,j'} T_{j,j'}^{\uparrow,\uparrow} c_{j'}^{\dagger\uparrow} c_{j}^{\uparrow} + T_{j,j'}^{\uparrow,\downarrow} c_{j'}^{\dagger\downarrow} c_{j}^{\uparrow} + T_{j,j'}^{\downarrow,\uparrow} c_{j'}^{\dagger\uparrow} c_{j}^{\downarrow} + T_{j,j'}^{\downarrow,\downarrow} c_{j'}^{\dagger\downarrow} c_{j}^{\downarrow}. \tag{2.41}$$

$\hat{c}_{j'}^{\dagger\sigma'}(\hat{c}_{j}^{\sigma})$ is the creation (annihilation) operator on site j' (j) with spin index $\sigma'(\sigma)$ and $T_{j,j'}^{\sigma,\sigma'}$ is the matrix element defined as,

$$T_{j,j'}^{\sigma,\sigma'} = \langle j', \sigma' \mid \hat{O} \mid j, \sigma \rangle \tag{2.42}$$

Considering these definitions in a three dimensional case, we study a trilayer structure made of two semi-infinite ferromagnetic electrodes separated by a magnetic

insultating barrier. Transport is defined along the $y-$axis and the magnetization vector in each layer is restricted to the $xz-$plane, i.e., in spherical coordinates is defined by the angle θ. The Hamiltonian for each layer was defined in Eqs. (2.4)-(2.6). Notice however that in this case we will adopt a different convention, e.g., the Hamiltonian of the barrier reads,

$$\hat{H}_B = \frac{\hat{\boldsymbol{p}}^{\boldsymbol{2}}}{2m} + \Delta\hat{\boldsymbol{\sigma}} \cdot \boldsymbol{m}_B + \hat{V}, \tag{2.43}$$

where Δ is the exchange coupling parameter and $\hat{V}$ is the potential. Discretizing the problem, we have,

$$\frac{\hat{\boldsymbol{p}}^{\boldsymbol{2}}}{2m} = \sum_{ijk\sigma} \frac{-\hbar^2}{2ma^2}\Big[\hat{c}^{\dagger\sigma}_{i+1,jk}\hat{c}^{\sigma}_{ijk} - 3\hat{c}^{\dagger\sigma}_{ijk}\hat{c}^{\sigma}_{ijk} + \hat{c}^{\dagger\sigma}_{ij+1,k}\hat{c}^{\sigma}_{ijk} + \hat{c}^{\dagger\sigma}_{ij,k+1}\hat{c}^{\sigma}_{ijk} + h.c.\Big], \tag{2.44}$$

$$\Delta\hat{\boldsymbol{\sigma}} \cdot \boldsymbol{m}_B = \sum_{ijk} \Delta\Big[\cos\theta\hat{c}^{\uparrow\dagger}_{ijk}\hat{c}^{\uparrow}_{ijk} + \sin\theta\hat{c}^{\uparrow\dagger}_{ijk}\hat{c}^{\downarrow}_{ijk} + \sin\theta\hat{c}^{\downarrow\dagger}_{ijk}\hat{c}^{\uparrow}_{ijk} - \cos\theta\hat{c}^{\downarrow\dagger}_{ijk}\hat{c}^{\downarrow}_{ijk}\Big], \tag{2.45}$$

$$\hat{V} = \sum_{ijk} U(y)\Big[\hat{c}^{\dagger\uparrow}_{ijk}\hat{c}^{\uparrow}_{ijk} + \hat{c}^{\dagger\downarrow}_{ijk}\hat{c}^{\downarrow}_{ijk}\Big]. \tag{2.46}$$

Subindex i, j, and k refer to site enumeration along the x, y and z axis, respectively. $\hat{c}^{\dagger}_{ijk}(\hat{c}_{ijk})$ is the creation (annihilation) operator on site ijk, a is the lattice parameter, and $h.c.$ is the Hermitian conjugate. $U(y)$ is the potential in the barrier, $U(y) = 0$ otherwise. Considering $t = -\frac{\hbar^2}{2ma^2}$ and $\epsilon = \frac{6\hbar^2}{2ma^2} + U(y)$, the Hamiltonian for each layer becomes,

$$\hat{H}_\Omega = \sum_{\substack{j \\ (j\in\Omega)}} \left\{\epsilon_{\Omega,j}\hat{\boldsymbol{c}}^{\dagger}_j\hat{\boldsymbol{c}}_j + \Delta_\Omega\Big[\hat{\boldsymbol{c}}^{\dagger}_j\hat{\boldsymbol{\sigma}} \cdot \boldsymbol{m}\hat{\boldsymbol{c}}_j\Big]\right\} + t \sum_{\substack{ijk \\ (ijk\in\Omega)}} \Big[\hat{\boldsymbol{c}}^{\dagger}_{i+1}\hat{\boldsymbol{c}}_i + \hat{\boldsymbol{c}}^{\dagger}_{j+1}\hat{\boldsymbol{c}}_j + \hat{\boldsymbol{c}}^{\dagger}_{k+1}\hat{\boldsymbol{c}}_k + h.c.\Big], \tag{2.47}$$

where only the relevant subindex is considered as the system is conserved trans-

verse to the propagation direction. $\hat{\boldsymbol{c}}_j^\dagger = (\hat{c}_j^{\dagger\uparrow}, \hat{c}_j^{\dagger\downarrow})$ and $\hat{\boldsymbol{c}}_j = (\hat{c}_j^{\uparrow}, \hat{c}_j^{\downarrow})^t$. Ω represents the uncoupled left (L), right (R), or barrier (B) region. t is the hopping matrix element, which couples the orbital states and therefore allows the electron to hop from one site to one of its neighbors and ϵ is the on-site energy. Notice that we are assuming a spin-independent hopping matrix element. Considering $\epsilon^{\uparrow(\downarrow)} = \epsilon \mp \Delta$ the total on-site energy for majority (minority) carriers, then we define,

$$\epsilon^0 = \frac{\epsilon^\downarrow + \epsilon^\uparrow}{2}, \tag{2.48}$$

$$\Delta = \frac{\epsilon^\downarrow - \epsilon^\uparrow}{2}. \tag{2.49}$$

ϵ^0 is referred to as the averaged on-site energy. To couple the barrier layer with the electrodes we consider an interaction Hamiltonian; therefore, the total Hamiltonian reads,

$$\hat{H} = \hat{H}_L + \hat{H}_R + \hat{H}_B + \hat{H}_{int}. \tag{2.50}$$

The first three terms correspond to the isolated contribution and the last term define the coupling with the electrodes,

$$\hat{H}_{int} = t\Big[\hat{c}_a^{\uparrow\dagger}\hat{c}_\alpha^{\uparrow} + \hat{c}_a^{\downarrow\dagger}\hat{c}_\alpha^{\downarrow} + \hat{c}_b^{\uparrow\dagger}\hat{c}_{\alpha'}^{\uparrow} + \hat{c}_b^{\downarrow\dagger}\hat{c}_{\alpha'}^{\downarrow} + h.c.\Big]. \tag{2.51}$$

In Eq. (2.51), site $j = \alpha$ (α') in the left (right) electrode is next to site $j = a$ (b) in the insulating region, see Fig. 2.3(a). In Fig. 2.3(b) we show the potential profile of the system, describing the averaged on-site energies and the exchange-splittings. In the barrier, the on-site energy varies linearly with site number j as

$$\epsilon_{B_j}^\sigma = \epsilon_B^\sigma + eV\frac{j-1}{N-1}, \tag{2.52}$$

being $eV = \mu_R - \mu_L$, with μ_j the chemical potential in the lead, and N the number of atomic sites in the barrier. In the present setup, shown in Fig. 2.3(a), the magnetization of the barrier ($\mathbf{m_B}$) is defined along the $z-$axis ($\theta_B = 0$), and in the left (right) electrode it is rotated in the $xz-$ plane with angle θ_L (θ_R). The barrier is made up of 3-atomic sites numbered from 1 to 3. The right electrode is numbered from 4 to ∞ and the left electrode from $-\infty$ to -1.

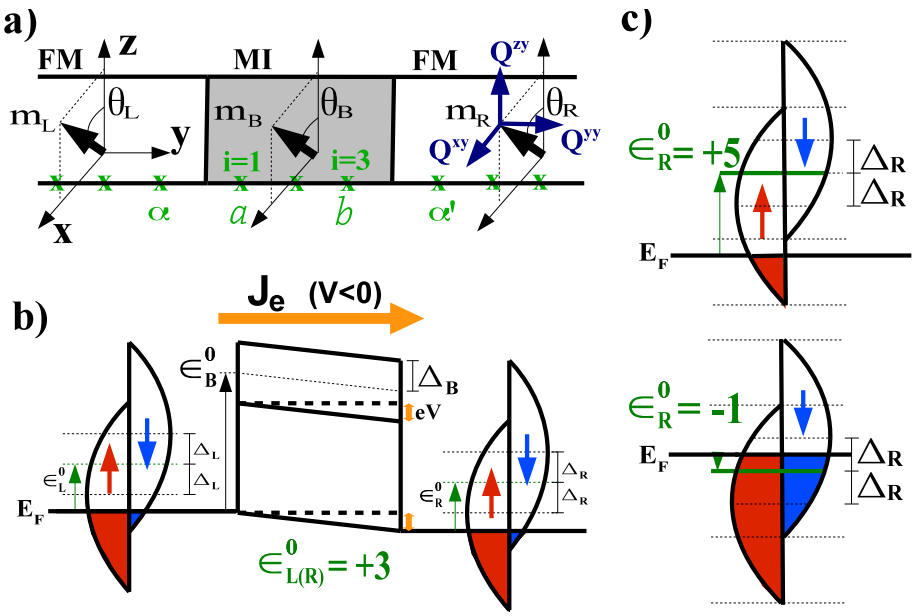

Figure 2.3: (Color online) a) Schematic structure of a SFTJ of the form FM/MI/FM. The magnetization vector on each layer is rotated by an angle θ in $xz-$plane. Subscripts L, R, and B stands for left, right, and barrier, respectively. The atomic layers, represented by green crosses, are enumerated from 1 to 3 in the barrier ($N_B = 3$). Subscripts next to left (right) interface are denoted a (b) in the barrier and α (α') in the lead. b) Potential profile describing the averaged on-site energies (ϵ^0_L, ϵ^0_B, and ϵ^0_R) and exchange-splittings (Δ_L, Δ_B, and Δ_R). eV $= \mu_R - \mu_L$, with μ the chemical potential in the lead. $E_F = 0$ eV refers to Fermi energy level. For negative bias, the electron flow density (J_e) goes from reference layer (left) to free layer (right). c) Density of states at zero bias for $\epsilon^0_R = +5$ eV and $\epsilon^0_R = -1$ eV cases.

Considering that transverse to $y-$axis, $\boldsymbol{k} = (k_x, k_y, k_z)$ is conserved then we can consider a solution of the form,

$$\mid \psi^{\sigma}_{k_x,k_z}\rangle = \frac{1}{\sqrt{N_x}}\frac{1}{\sqrt{N_z}}\sum_{\substack{l\in x\\ m\in z}} e^{ik_x a l}e^{ik_z a m} \mid l,m,\sigma\rangle, \tag{2.53}$$

$$\langle\psi^{\sigma'}_{k_x,k_z} \mid = \frac{1}{\sqrt{N_x}}\frac{1}{\sqrt{N_z}}\sum_{\substack{l'\in x\\ m'\in z}} e^{-ik_x a l'}e^{-ik_z a m'}\langle l',m',\sigma' \mid . \tag{2.54}$$

This is the usual Bloch wavefunction solution for a periodic potential in a tight binding model. $N_{x(z)}$ and l (m) represent the number of lattice points and site enumeration along x (z). If we consider in Eq. (2.47), $\hat{H}_{\boldsymbol{k}_{||}} = t\sum_{ik}\left[\hat{\boldsymbol{c}}^{\dagger}_{i+1}\hat{\boldsymbol{c}}_i + \hat{\boldsymbol{c}}^{\dagger}_{k+1}\hat{\boldsymbol{c}}_k + h.c.\right]$, then its matrix elements, in terms of Eqs. (2.53)-(2.54), are

$$\begin{aligned}\hat{H}^{\sigma,\sigma'}_{\boldsymbol{k}_{||}} &= \langle\psi^{\sigma'}_{k_x,k_z} \mid \hat{H}_{\boldsymbol{k}_{||}} \mid \psi^{\sigma}_{k_x,k_z}\rangle \\ &= \frac{1}{N_x N_z}\sum_{ll',mm'} e^{ik_x a(l-l')}e^{ik_z a(m-m')}\langle l',m',\sigma' \mid \hat{H}_{\boldsymbol{k}_{||}} \mid l,m\sigma\rangle.\end{aligned} \tag{2.55}$$

To solve Eq. (2.55) a simple cubic lattice in the nearest neighbor approximation is considered, which gives,

$$\hat{H}^{\uparrow,\uparrow}_{\boldsymbol{k}_{||}} = 2t(\cos k_x a + \cos k_z a), \tag{2.56}$$

$$\hat{H}^{\downarrow,\downarrow}_{\boldsymbol{k}_{||}} = 2t(\cos k_x a + \cos k_z a). \tag{2.57}$$

We define $\epsilon_{\boldsymbol{k}_{\|}} = 2t(\cos k_x a + \cos k_z a)$ as the in-plane energy and proceed to give a solution for the total wavefunction in the uncoupled region Ω (L, R, or B). We employ the Green's function formalism in Schrodinger's equation, i.e., $(E-H)\psi = 0 \rightarrow (E-H)G = I$, where G denotes the Green's function, H is given in Eq. (2.47), and E is the energy. Our final expression becomes,

$$\sum_{p_1}\left\{\left\{[(E-\epsilon_{\boldsymbol{k}_{||}})\delta_{pp_1}-\overline{H}_{pp_1}]\hat{I}-\delta H_{p,p_1}\begin{bmatrix}\cos\theta_\Omega & \sin\theta_\Omega\\ \sin\theta_\Omega & -\cos\theta_\Omega\end{bmatrix}\right\}\hat{g}_{p_1q}\right\}=\delta_{pq}\hat{I}. \quad (2.58)$$

p_1, p, and q denote atomic sites along $y-$axis. $\hat{I}$ is the 2×2 unit matrix operator, and θ_Ω is the angle of the magnetization with respect to the $z-$axis. $\overline{H}_{pq}=\epsilon^0_\Omega\delta_{pq}+t(\delta_{p,q+1}+\delta_{p,q-1})$ and $\delta H_{pq}=\Delta_\Omega\delta_{pq}$, where ϵ^0 and Δ are defined in Eqs. (2.48)-(2.49).

It is important to remark that in equilibrium Eqs. (2.53)-(2.54) can be extended to three dimensions and therefore for a simple cubic tight-binding model in nearest neighbor approximation we have,

$$\hat{H}^{\sigma,\sigma}_{\boldsymbol{k}_{||}}=2t(\cos k_x a+\cos k_y a+\cos k_z a), \quad (2.59)$$

which shows its maxima and minima at $6|t|$. Consequently, considering Eq. (2.47), the energy limits of the density of states (DOS) are given by $E^\sigma_{\min(\max)}=\epsilon^\sigma_\Omega\pm6t$, which brings different band filling values in the electrodes associated with the DOS at Fermi level ($E_F=0$ eV). Notice that we are choosing $t=-1.0$ eV. In the present work, four band filling cases are studied where $\Delta_\Omega=+2$ eV unless stated otherwise; therefore, for the parameters considered here, $\epsilon^0_{L(R)}=+5$ eV, given on Fig. 2.3(c) top-panel, defines the half metallic case which considers no states at E_F for minority carriers. $\epsilon^0_R=+3$ eV, in contrast, allows a small contribution of minority spin states at Fermi level, see Fig. 2.3(b). Both cases are referred to be in the *low band filling* regime which applies reasonably well to transition metals (Fe, Co, Ni) and their compounds. The tight-binding modeling of spin transfer torque in MgO-based tunnel junctions yields bias-dependences and magnitudes in semi-quantitative agreement with the experimental observations [63]. We additionally investigate the

cases $\epsilon_R^0 = +1$ eV and $\epsilon_R^0 = -1$ eV, where the population of minority carriers at Fermi level increases until it becomes larger than the population of the majority carriers; therefore, a polarization inversion is expected as the system moves towards the *high band filling* regime, see Fig. 2.3(c) bottom-panel.

Our model being limited to a single band, it does not capture the specific wave-function symmetries that would arise in crystalline junctions, such as Fe/MgO [64]. However, limiting this study to low bias voltage, this model provides a qualitative description of the spin transport in spin filter junctions.

2.3.2 Isolated Green's functions

We first proceed to give a solution for the isolated Green's functions. In the barrier, for $N = 3$, Eq. (2.58) in its matrix representation reads,

$$\begin{pmatrix} E-\epsilon_{B_1}^{\sigma} & -t & 0 \\ -t & E-\epsilon_{B_2}^{\sigma} & -t \\ 0 & -t & E-\epsilon_{B_3}^{\sigma} \end{pmatrix} \begin{pmatrix} \hat{g}_{11}^{\sigma} & \hat{g}_{12}^{\sigma} & \hat{g}_{13}^{\sigma} \\ \hat{g}_{21}^{\sigma} & \hat{g}_{22}^{\sigma} & \hat{g}_{23}^{\sigma} \\ \hat{g}_{31}^{\sigma} & \hat{g}_{32}^{\sigma} & \hat{g}_{33}^{\sigma} \end{pmatrix} = \begin{pmatrix} 1 & 0 & 0 \\ 0 & 1 & 0 \\ 0 & 0 & 1 \end{pmatrix}. \tag{2.60}$$

Notice that we are considering $\boldsymbol{m}_B = \boldsymbol{z}$; therefore, the 2×2 Green's function matrix $\hat{g}$ has off-diagonal terms equal to zero, i.e., $\hat{g}^{\uparrow\downarrow} = \hat{g}^{\downarrow\uparrow} = 0$, and the diagonal terms can be solved separately. For simplicity we consider $\hat{g}^{\uparrow\uparrow} = \hat{g}^{\downarrow\downarrow} = \hat{g}^{\sigma}$, with σ being either $\uparrow$ or $\downarrow$. In Eq. (2.60), $\epsilon_{B_j}^{\sigma}$ is defined in Eq. (2.52) and $E = E_0 - \epsilon_{\boldsymbol{k}_\parallel} + i\delta$, where E_0 is the energy and $i\delta$ is the imaginary term that appears in the definition of the retarded Green's function. Solving Eq. (2.60) we obtain our isolated retarded Green's functions, $\hat{g}^r$,

$$\hat{g}^{r,\sigma}_{11} = \hat{g}^{\sigma}_{aa} + t^2 \hat{g}^{\sigma}_{ab}\hat{g}^{\sigma}_{ba}\mathscr{D}^{\sigma}_3, \qquad \hat{g}^{r,\sigma}_{12} = \hat{g}^{\sigma}_{ab} + t^2 \hat{g}^{\sigma}_{ab}\hat{g}^{\sigma}_{bb}\mathscr{D}^{\sigma}_3, \qquad \hat{g}^{r,\sigma}_{13} = t\hat{g}^{r,\sigma}_{12}\mathscr{D}^{\sigma}_2, \quad (2.61)$$

$$\hat{g}^{r,\sigma}_{21} = \hat{g}^{\sigma}_{ba} + t^2 \hat{g}^{\sigma}_{bb}\hat{g}^{\sigma}_{ba}\mathscr{D}^{\sigma}_3, \qquad \hat{g}^{r,\sigma}_{22} = \hat{g}^{\sigma}_{bb} + t^2 \hat{g}^{\sigma}_{bb}\hat{g}^{\sigma}_{bb}\mathscr{D}^{\sigma}_3, \qquad \hat{g}^{r,\sigma}_{23} = t\hat{g}^{r,\sigma}_{22}\mathscr{D}^{\sigma}_2, \quad (2.62)$$

$$\hat{g}^{r,\sigma}_{31} = t\hat{g}^{r,\sigma}_{21}\mathscr{D}^{\sigma}_2, \qquad \hat{g}^{r,\sigma}_{32} = t\hat{g}^{r,\sigma}_{22}\mathscr{D}^{\sigma}_2, \qquad \hat{g}^{r,\sigma}_{33} = (1 + t\hat{g}^{r,\sigma}_{23})\mathscr{D}^{\sigma}_2, \quad (2.63)$$

with

$$\hat{g}^{\sigma}_{aa} = (E - \epsilon^{\sigma}_{B_2})\mathscr{D}^{\sigma}_1, \qquad \mathscr{D}^{\sigma}_1 = ((E - \epsilon^{\sigma}_{B_1})(E - \epsilon^{\sigma}_{B_2}) - t^2)^{-1}, \quad (2.64)$$

$$\hat{g}^{\sigma}_{bb} = (E - \epsilon^{\sigma}_{B_1})\mathscr{D}^{\sigma}_1, \qquad \mathscr{D}^{\sigma}_2 = (E - \epsilon^{\sigma}_{B_3})^{-1}, \quad (2.65)$$

$$\hat{g}^{\sigma}_{ab} = \hat{g}^{\sigma}_{ba} = t\mathscr{D}^{\sigma}_1, \qquad \mathscr{D}^{\sigma}_3 = (E - \epsilon^{\sigma}_{B_3} - t^2\hat{g}^{\sigma}_{bb})^{-1}. \quad (2.66)$$

To obtain solutions for the isolated Green's functions in the electrodes we directly solve Eq. (2.58), which turns into a system of 4 equations ($\hat{g}^{\uparrow\uparrow}_{pq}$, $\hat{g}^{\uparrow\downarrow}_{pq}$, $\hat{g}^{\downarrow\uparrow}_{pq}$, and $\hat{g}^{\downarrow\downarrow}_{pq}$). Considering nearest neighbors only, i.e., $\hat{g}_{p+1,q} = \hat{g}_{pq}e^{ika}$ and $\hat{g}_{p-1,q} = \hat{g}_{pq}e^{-ika}$, we have

$$\hat{g}^{\uparrow\uparrow(\downarrow\downarrow)}_{pq} = \frac{\delta_{pq}}{2}\left[\frac{1 \pm \cos\theta}{E - \epsilon^{\downarrow} - 2t\cos ka} + \frac{1 \mp \cos\theta}{E - \epsilon^{\uparrow} - 2t\cos ka}\right], \quad (2.67)$$

$$\hat{g}^{\downarrow\uparrow(\uparrow\downarrow)}_{pq} = \frac{\delta_{pq}}{2}\left[\frac{\sin\theta}{E - \epsilon^{\downarrow} - 2t\cos ka} - \frac{\sin\theta}{E - \epsilon^{\uparrow} - 2t\cos ka}\right], \quad (2.68)$$

Then, considering a Fourier transform in the first Brillouin zone and replacing $E \to E + i\delta$ to define the retarded Green's function we have,

$$\hat{g}^{r}(l, m, E) = \frac{a}{2\pi}\int_{-\pi/a}^{\pi/a} \hat{g}_{pq}e^{ika(l-m)}dk, \quad (2.69)$$

and consequently,

$$\hat{g}^{r,\uparrow\uparrow(\downarrow\downarrow)}(l,m;E) = -\frac{i}{2}\left[(1\pm\cos\theta)\frac{n^{\uparrow|l-m|}}{d^{\uparrow}} + (1\mp\cos\theta)\frac{n^{\downarrow|l-m|}}{d^{\downarrow}}\right], \tag{2.70}$$

$$\hat{g}^{r,\downarrow\uparrow(\uparrow\downarrow)}(l,m;E) = -\frac{i}{2}\left[\sin\theta\frac{n^{\uparrow|l-m|}}{d^{\uparrow}} - \sin\theta\frac{n^{\downarrow|l-m|}}{d^{\downarrow}}\right], \tag{2.71}$$

with

$$n^{\uparrow(\downarrow)} = \frac{E-\epsilon^{\uparrow(\downarrow)}}{2t} - i\sqrt{1-\left(\frac{E-\epsilon^{\uparrow(\downarrow)}}{2t}\right)^2}, \tag{2.72}$$

$$d^{\uparrow(\downarrow)} = \sqrt{4t^2-(E-\epsilon^{\uparrow(\downarrow)})^2}. \tag{2.73}$$

l and m represent atomic sites. Notice however that Eqs. (2.70)-(2.71) constitute our isolated retarded Green's functions for an infinite electrode. In the case of a semi-infinite system we need to consider the interaction at the interface, i.e., $\tilde{\hat{g}}_{\alpha\alpha} = \frac{\hat{g}_{\alpha\mu'}}{t\hat{g}_{\alpha'\mu'}}$, which appears as a result of Dyson's equation in a system made of two semi-infinite leads. $\tilde{\hat{g}}$ is the semi-infinite Green's function, $\hat{g}$ is the infinite Green's function, greek symbols represent the atomic sites, and (non-) prime symbols refer to one of the semi-infinite regions. Replacing $\mu' = \alpha+1 = \alpha'$ we get $\tilde{\hat{g}}_{\alpha\alpha} = \frac{\hat{g}_{\alpha,\alpha+1}}{t\hat{g}_{\alpha+1,\alpha+1}}$. Consequently, following a similar derivation, our semi-infinite retarded Green's functions become,

$$\hat{g}^{r,\uparrow\uparrow(\downarrow\downarrow)}(l,m;E) = -\frac{i}{2}\left[(1\pm\cos\theta)\frac{n^{\uparrow|l-m|}-n^{\uparrow(l+m)}}{d^{\uparrow}} + (1\mp\cos\theta)\frac{n^{\downarrow|l-m|}-n^{\downarrow(l+m)}}{d^{\downarrow}}\right], \tag{2.74}$$

$$\hat{g}^{r,\downarrow\uparrow(\uparrow\downarrow)}(l,m;E) = -\frac{i}{2}\left[\sin\theta\frac{n^{\uparrow|l-m|}}{d^{\uparrow}} - \sin\theta\frac{n^{\downarrow|l-m|}}{d^{\downarrow}} + \sin\theta\frac{n^{\downarrow(l+m)}}{d^{\downarrow}} - \sin\theta\frac{n^{\uparrow(l+m)}}{d^{\uparrow}}\right], \tag{2.75}$$

where we neglected the "˜" symbol for simplicity and considered l, m instead of α, μ.

2.3.3 Coupled Green's functions

For a barrier system in contact with two electrodes, the Hamiltonian given in Eq. (2.50) in its block form reads,

$$\hat{\boldsymbol{H}} = \begin{pmatrix} \hat{H}_L & \hat{H}_{LB} & 0 \\ \hat{H}_{LB}^{\dagger} & \hat{H}_B & \hat{H}_{RB}^{\dagger} \\ 0 & \hat{H}_{RB} & \hat{H}_R \end{pmatrix}, \tag{2.76}$$

where $\hat{H}_{LB}$ and $\hat{H}_{RB}$ are the two components of the interaction Hamiltonian given in Eq. (2.51). A schematic representation of Eq. (2.76) is given in Fig. 2.4.

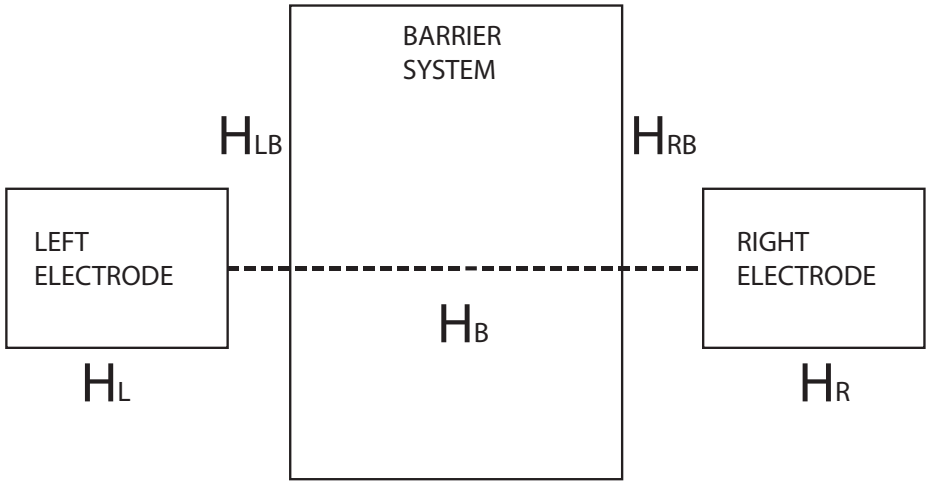

Figure 2.4: (Color online) Hamiltonian representation of a barrier system in contact with two electrodes. H_{LB} and H_{RB} are the components of the interaction Hamiltonian. H_Ω is the isolated Hamiltonian, $\Omega = L, R$ or B.

Solving Schrodinger's equation in the Green's function representation we have,

$$\begin{pmatrix} E-\hat{H}_L & -\hat{H}_{LB} & 0 \\ -\hat{H}_{LB}^\dagger & E-\hat{H}_B & -\hat{H}_{RB}^\dagger \\ 0 & -\hat{H}_{RB} & E-\hat{H}_R \end{pmatrix} \begin{pmatrix} \hat{G}_{LL} & \hat{G}_{LB} & 0 \\ \hat{G}_{BL} & \hat{G}_{BB} & \hat{G}_{BR} \\ 0 & \hat{G}_{RB} & \hat{G}_{RR} \end{pmatrix} = \hat{I}, \tag{2.77}$$

which gives rise to a solution of the form $(E-\hat{H}_B-\hat{\Sigma})\hat{G}_{BB}=\hat{I}$, with $\hat{\Sigma}=\hat{H}_{LB}^\dagger(E-\hat{H}_L)^{-1}\hat{H}_{LB}+\hat{H}_{RB}^\dagger(E-\hat{H}_R)^{-1}\hat{H}_{RB}$. Replacing Eq. (2.51) in the definition of $\hat{\Sigma}$ we have, $\hat{\Sigma}=t_{a\alpha}\hat{g}_{\alpha\alpha}t_{\alpha a}+t_{b\alpha'}\hat{g}_{\alpha'\alpha'}t_{\alpha' b}$, where site α (α') in the left (right) electrode is next to site a (b) in the insulating region, see Fig. 2.3(a). Notice that $\hat{g}_{\alpha\alpha(\alpha'\alpha')}$ is the 2×2 isolated semi-infinite retarded Green's function matrix derived in §2.3.2. In what follows, upper-index r is removed for simplicity. $\hat{\Sigma}$ describes the propagation of the electron across the interfaces and is referred to as the self energy term. It can be partitioned in two components,

$$\hat{\Sigma}_{aa}=t_{a\alpha}\hat{g}_{\alpha\alpha}t_{\alpha a}, \qquad\qquad \hat{\Sigma}_{bb}=t_{b\alpha'}\hat{g}_{\alpha'\alpha'}t_{\alpha' b}. \tag{2.78}$$

We now proceed to couple the full system made of semi-infinite electrodes and a barrier layer. For this we solve a system of Dyson's equations of the form

$$\hat{G}_{pq}=\hat{g}_{pq}+\hat{g}_{pa}\hat{\Sigma}_{aa}\hat{G}_{aq}+\hat{g}_{pb}\hat{\Sigma}_{bb}\hat{G}_{bq}, \tag{2.79}$$

where $\hat{G}$ ($\hat{g}$) is the 2×2 coupled (isolated) retarded Green's function matrix. p and q denote atomic sites in the barrier. Eq. (2.79) is self-consistent, which means that each coupled Green's function can be described in terms of isolated Green's functions. For example we have,

$$\hat{G}_{aq} = (I - \hat{g}_{aa}\hat{\Sigma}_{aa})^{-1}\hat{g}_{aq} + (I - \hat{g}_{aa}\hat{\Sigma}_{aa})^{-1}\hat{g}_{ab}\hat{\Sigma}_{bb}\hat{G}_{bq}, \tag{2.80}$$

$$\hat{G}_{bq} = (I - \hat{g}_{bb}\hat{\Sigma}_{bb})^{-1}\hat{g}_{bq} + (I - \hat{g}_{bb}\hat{\Sigma}_{bb})^{-1}\hat{g}_{ba}\hat{\Sigma}_{aa}\hat{G}_{aq}. \tag{2.81}$$

Replacing Eq. (2.81) in Eq. (2.80), we get,

$$\begin{aligned}\hat{G}_{aq} = (I - (I - \hat{g}_{aa}\hat{\Sigma}_{aa})^{-1}\hat{g}_{ab}\hat{\Sigma}_{bb}(I - \hat{g}_{bb}\hat{\Sigma}_{bb})^{-1}\hat{g}_{ba}\hat{\Sigma}_{aa})^{-1}(I - \hat{g}_{aa}\hat{\Sigma}_{aa})^{-1}\hat{g}_{aq} \\ + (I - (I - \hat{g}_{aa}\hat{\Sigma}_{aa})^{-1}\hat{g}_{ab}\hat{\Sigma}_{bb}(I - \hat{g}_{bb}\hat{\Sigma}_{bb})^{-1}\hat{g}_{ba}\hat{\Sigma}_{aa})^{-1}\hat{g}_{ab}\hat{\Sigma}_{bb}(I - \hat{g}_{bb}\hat{\Sigma}_{bb})^{-1}\hat{g}_{bq}.\end{aligned} \tag{2.82}$$

Similar calculations are performed for the advanced Green's functions, $\hat{G}^a_{pq}$, given as the Hermitian conjugate of $\hat{G}_{pq}$.

2.3.4 Quantum kinetic equation

The next step is to solve the quantum kinetic equation in the framework of Keldysh formalism. Here we need to consider other type of Green's functions. For systems in equilibrium or not far from equilibrium it is sufficient to consider the casual Green's function, $\hat{G}^c$, at zero temperature ($T = 0K$) or the Matsubara Green's function, $\hat{G}^M$, for $T > 0K$; as well as the retarded, $\hat{G}$, and advanced, $\hat{G}^a$, Green's functions, where the latter two describe the propagation of particles forward and backward in time, respectively. For systems far from equilibrium, Keldysh showed [62] that the system can be described considering additional Green's functions, i.e., the lesser, $\hat{G}^<$, the greater, $\hat{G}^>$, and the anticasual, $\hat{\tilde{G}}^c$, Green's functions. We therefore have,

$$\hat{G}^{c}_{pq}(t_1,t_2) = -i\langle 0 \mid \hat{T}\{\hat{c}_p(t_1)\hat{c}^{\dagger}_q(t_2)\} \mid 0\rangle, \tag{2.83}$$

$$\hat{G}^{<}(t_1,t_2) = +i\langle 0 \mid \hat{c}^{\dagger}_q(t_2)\hat{c}_p(t_1) \mid 0\rangle, \tag{2.84}$$

$$\hat{G}^{>}(t_1,t_2) = -i\langle 0 \mid \hat{c}_p(t_1)\hat{c}^{\dagger}_q(t_2) \mid 0\rangle, \tag{2.85}$$

$$\hat{\tilde{G}}^{c}(t_1,t_2) = -i\langle 0 \mid \tilde{T}\hat{c}_p(t_1)\hat{c}^{\dagger}_q(t_2) \mid 0\rangle, \tag{2.86}$$

where $\hat{c}_p$ and $\hat{c}^{\dagger}_p$ are the annihilation and creation operators. $\hat{T}$ denotes the time ordering operator from $-\infty$ to $+\infty$, $\tilde{T}$ denotes time ordering from $+\infty$ to $-\infty$, and the brackets, $\langle ... \rangle$, denote the averaging over some quantum state. For $T = 0K$, the average is performed over the ground state of $\hat{H}$, i.e., $\langle ... \rangle = \langle 0 \mid ... \mid 0 \rangle$. For major details of Keldysh contour and formalism refer to Ref. [62]. In the present thesis we focus instead on the quantum kinetic equation arising in Keldysh space. It is shown that a Dyson's equation may be written as,

$$\hat{\boldsymbol{G}}_{pq}(t_1,t_2) = \hat{\boldsymbol{g}}_{pq}(t_1,t_2) + \int \hat{\boldsymbol{g}}_{pm}(t_1,t)\hat{\boldsymbol{\Sigma}}_{mn}(t,t')\hat{\boldsymbol{G}}_{nq}(t',t_2)dtdt' \tag{2.87}$$

where,

$$\hat{\boldsymbol{G}} = \begin{pmatrix} \hat{G}^{c} & \hat{G}^{<} \\ \hat{G}^{>} & \hat{\tilde{G}}^{c} \end{pmatrix}, \qquad \hat{\boldsymbol{\Sigma}} = \begin{pmatrix} \hat{\Sigma}^{c} & \hat{\Sigma}^{<} \\ \hat{\Sigma}^{>} & \hat{\tilde{\Sigma}}^{c} \end{pmatrix}. \tag{2.88}$$

$\hat{\boldsymbol{G}}$ and $\hat{\boldsymbol{g}}$ are the Green's function matrices, in presence and absence of perturbations, respectively. $\hat{\boldsymbol{\Sigma}}$ is the self-energy matrix. Considering a canonical transformation, i.e., $(\frac{1-i\hat{\boldsymbol{\sigma}}_y}{2}\hat{\boldsymbol{G}}\frac{1+i\hat{\boldsymbol{\sigma}}_y}{2})$ [62], Eq. (2.87) becomes,

$$\begin{pmatrix} \hat{0} & \hat{G}^a \\ \hat{G} & \hat{G}^K \end{pmatrix} = \begin{pmatrix} \hat{0} & \hat{g}^a \\ \hat{g} & \hat{g}^K \end{pmatrix} + \begin{pmatrix} \hat{0} & \hat{g}^a \\ \hat{g} & \hat{g}^K \end{pmatrix} \begin{pmatrix} \hat{\Sigma}^K & \hat{\Sigma} \\ \hat{\Sigma}^a & 0 \end{pmatrix} \begin{pmatrix} \hat{0} & \hat{G}^a \\ \hat{G} & \hat{G}^K \end{pmatrix}, \tag{2.89}$$

where subscripts have been removed for simplicity and the following relationships hold,

$$\hat{G}^K = \hat{G}^c + \hat{\bar{G}}^c = \hat{G}^< + \hat{G}^>, \tag{2.90}$$

$$\hat{G} = \hat{G}^c - \hat{G}^< = -\hat{\bar{G}}^c + \hat{G}^>, \tag{2.91}$$

$$\hat{G}^a = \hat{G}^c - \hat{G}^> = -\hat{\bar{G}}^c + \hat{G}^<, \tag{2.92}$$

$$\hat{\Sigma}^K = \hat{\Sigma}^c + \hat{\bar{\Sigma}}^c = -(\hat{\Sigma}^< + \hat{\Sigma}^>), \tag{2.93}$$

$$\hat{\Sigma} = \hat{\Sigma}^c + \hat{\Sigma}^< = -(\hat{\bar{\Sigma}}^c + \hat{\Sigma}^>), \tag{2.94}$$

$$\hat{\Sigma}^a = \hat{\Sigma}^c + \hat{\Sigma}^> = -(\hat{\bar{\Sigma}}^c + \hat{\Sigma}^<). \tag{2.95}$$

Thus, from Eq. (2.89) we obtain a set of three equations, the off-diagonal terms are the usual Dyson's equations for the retarded and advanced Green's functions, whereas the diagonal term gives,

$$\hat{G}^K_{pq} = \hat{g}^K_{pq} + \hat{g}_{pq_1}\Sigma^K_{q_1q_2}\hat{G}^a_{q_2q} + \hat{g}_{pq_1}\hat{\Sigma}_{q_1q_2}\hat{G}^K_{q_2q} + \hat{g}^K_{pq_1}\hat{\Sigma}^a_{q_1q_2}\hat{G}^a_{q_2q} \tag{2.96}$$

$\hat{g}^K$ is the non-equilibrium 2×2 Green's function matrix for the uncoupled region, and the self energy takes the form

$$\hat{\Sigma}_{q_1q_2} = t\hat{I}(\delta_{q_1\alpha}\delta_{q_2a} + \delta_{q_1\alpha'}\delta_{q_2b}) + h.c. \tag{2.97}$$

Being the perturbation instantaneous, then $\hat{\Sigma} \equiv \hat{\Sigma}^a$ [62]. Therefore, considering Eqs. (2.93)-(2.95), we have $\Sigma^K = 0$ and the kinetic equation given in Eq. (2.96) reduces to,

$$\hat{G}^K_{pq} = \hat{g}^K_{pq} + \hat{g}_{pq_1}\hat{\Sigma}_{q_1q_2}\hat{G}^K_{q_2q} + \hat{g}^K_{pq_1}\hat{\Sigma}_{q_1q_2}\hat{G}^a_{q_2q}. \tag{2.98}$$

Replacing Eq. (2.97) in Eq. (2.98) we have,

$$\begin{aligned}\hat{G}^K_{pq} = \hat{g}^K_{pq} + \hat{g}_{p\alpha}t\hat{G}^K_{aq} + \hat{g}_{pa}t\hat{G}^K_{\alpha q} + \hat{g}^K_{p\alpha}t\hat{G}^a_{aq} + \hat{g}^K_{pa}t\hat{G}^a_{\alpha q} + \hat{g}_{pb}t'\hat{G}^K_{\alpha' q} + \hat{g}_{p\alpha'}t'\hat{G}^K_{bq} \\ + \hat{g}^K_{pb}t'\hat{G}^a_{\alpha' q} + \hat{g}^K_{p\alpha'}t'\hat{G}^a_{bq}.\end{aligned} \tag{2.99}$$

Since we are interested in evaluating the spin torque on the right interface. We solve for $\hat{G}^K_{b\alpha'(\alpha' b)}$. Because the various $\hat{G}^K s$ are coupled, once needs to write similar kinetic equations for additional terms. For $\hat{G}^K_{b\alpha'}$ the coupled system of equations, derived from Eq. (2.99), reads

$$\hat{G}^K_{b\alpha'} = \hat{g}_{ba}t\hat{G}^K_{\alpha\alpha'} + \hat{g}_{bb}t'\hat{G}^K_{\alpha'\alpha'}, \tag{2.100}$$

$$\hat{G}^K_{\alpha'\alpha'} = \hat{g}^K_{\alpha'\alpha'} + \hat{g}_{\alpha'\alpha'}t'\hat{G}^K_{b\alpha'} + \hat{g}^K_{\alpha'\alpha'}t'\hat{G}^a_{b\alpha'}, \tag{2.101}$$

$$\hat{G}^K_{\alpha\alpha'} = \hat{g}_{\alpha\alpha}t\hat{G}^K_{a\alpha'} + \hat{g}^K_{\alpha\alpha}t\hat{G}^a_{a\alpha'}, \tag{2.102}$$

$$\hat{G}^K_{a\alpha'} = \hat{g}_{aa}t\hat{G}^K_{\alpha\alpha'} + \hat{g}_{ab}t'\hat{G}^K_{\alpha'\alpha'}. \tag{2.103}$$

Considering $\hat{\Sigma}_R = t'\hat{g}_{\alpha'\alpha'}t'$ and $\hat{\Sigma}_L = t\hat{g}_{\alpha\alpha}t$, Eqs. (2.100)-(2.103) become,

$$(\hat{I} - \hat{g}_{bb}\hat{\Sigma}_R)\hat{G}^K_{b\alpha'} = \hat{g}_{ba}\hat{\Sigma}_L\hat{G}^K_{a\alpha'} + \hat{g}_{ba}t\hat{g}^K_{\alpha\alpha}t\hat{G}^a_{a\alpha'} + \hat{g}_{bb}t'\hat{g}^K_{\alpha'\alpha'} + \hat{g}_{bb}t'\hat{g}^K_{\alpha'\alpha'}t'\hat{G}^a_{b\alpha'}, \quad (2.104)$$

$$(\hat{I} - \hat{g}_{aa}\hat{\Sigma}_L)\hat{G}^K_{a\alpha'} = \hat{g}_{ab}t'\hat{g}^K_{\alpha'\alpha'} + \hat{g}_{ab}\hat{\Sigma}_R\hat{G}^K_{b\alpha'} + \hat{g}_{ab}t'\hat{g}^K_{\alpha'\alpha'}t'\hat{G}^a_{b\alpha'} + \hat{g}_{aa}t\hat{g}^K_{\alpha\alpha}t\hat{G}^a_{a\alpha'}. \quad (2.105)$$

Taking $\hat{A} = (\hat{I} - \hat{g}_{aa}\hat{\Sigma}_L)^{-1}$, $\hat{B} = (\hat{I} - \hat{g}_{bb}\hat{\Sigma}_R)^{-1}$, and $\hat{D} = (\hat{I} - \hat{B}\hat{g}_{ba}\hat{\Sigma}_L\hat{A}\hat{g}_{ab}\hat{\Sigma}_R)^{-1}$, Eqs. (2.104)-(2.105) simplify to $\hat{G}^K_{b\alpha'} = \hat{G}^{K,L}_{b\alpha'} + \hat{G}^{K,R}_{b\alpha'}$ with

$$\hat{G}^{K,L}_{b\alpha'} = t^2\hat{D}\hat{B}\hat{g}_{ba}\hat{g}^K_{\alpha\alpha}\hat{G}^a_{a\alpha'} + t^2\hat{D}\hat{B}\hat{g}_{ba}\hat{\Sigma}_L\hat{A}\hat{g}_{aa}\hat{g}^K_{\alpha\alpha}\hat{G}^a_{a\alpha'}, \quad (2.106)$$

$$\hat{G}^{K,R}_{b\alpha'} = t\hat{D}\hat{B}\hat{g}_{bb}\hat{g}^K_{\alpha'\alpha'}(\hat{I} + t\hat{G}^a_{b\alpha'}) + t\hat{D}\hat{B}\hat{g}_{ba}\hat{\Sigma}_L\hat{A}\hat{g}_{ab}\hat{g}^K_{\alpha'\alpha'}(\hat{I} + t\hat{G}^a_{b\alpha'}). \quad (2.107)$$

Similarly, for $\hat{G}^K_{\alpha'b}$ we have $\hat{G}^K_{\alpha'b} = \hat{G}^{K,L}_{\alpha'b} + \hat{G}^{K,R}_{\alpha'b}$ with

$$\hat{G}^{K,L}_{\alpha'b} = t\hat{L}\hat{N}\hat{\Sigma}_R\hat{g}_{ba}\hat{M}\hat{g}^K_{\alpha\alpha}\hat{G}^a_{ab}, \quad (2.108)$$

$$\hat{G}^{K,R}_{\alpha'b} = t'\hat{L}\hat{N}\hat{g}^K_{\alpha'\alpha'}\hat{G}^a_{bb}, \quad (2.109)$$

where $\hat{N} = (\hat{I} - \hat{\Sigma}_R\hat{g}_{bb})^{-1}$, $\hat{M} = (\hat{I} - \hat{\Sigma}_L\hat{g}_{aa})^{-1}$, and $\hat{L} = (\hat{I} - \hat{N}\hat{\Sigma}_R\hat{g}_{ba}\hat{M}\hat{\Sigma}_L\hat{g}_{ab})^{-1}$. Considering Eqs. (2.90)-(2.92) the following relationship holds,

$$\hat{G}^<_{pq} = \frac{1}{2}[\hat{G}^K_{pq} + \hat{G}^a_{pq} - \hat{G}_{pq}] \quad (2.110)$$

Moreover, by definition we have,

$$\hat{g}^< = i\hat{A}_\epsilon f_\Omega, \quad (2.111)$$

where $A_\epsilon = i[\hat{g} - \hat{g}^a]$ is the spectral function and f_Ω is the Fermi Dirac distribution given by,

$$f_L = \frac{1}{e^{(E-\mu_L)/k_BT} + 1}, \tag{2.112}$$

$$f_R = \frac{1}{e^{(E-\mu_R)/k_BT} + 1}. \tag{2.113}$$

Consequently,

$$g^K_{\alpha,\mu} = (1 - 2f_L)(\hat{g}_{\alpha,\mu} - \hat{g}^a_{\alpha,\mu}), \tag{2.114}$$

$$g^K_{\alpha'\mu'} = (1 - 2f_R)(\hat{g}_{\alpha',\mu'} - \hat{g}^a_{\alpha',\mu'}), \tag{2.115}$$

and the kinetic equation can easily be transformed in terms of lesser Green's functions. We therefore have,

$$\hat{G}^{<,L}_{b\alpha'} = t^2\hat{D}\hat{B}\hat{g}_{ba}\hat{g}^<_{\alpha\alpha}\hat{G}^a_{a\alpha'} + t^2\hat{D}\hat{B}\hat{g}_{ba}\hat{\Sigma}_L\hat{A}\hat{g}_{aa}\hat{g}^<_{\alpha\alpha}\hat{G}^a_{a\alpha'}, \tag{2.116}$$

$$\hat{G}^{<,R}_{b\alpha'} = t\hat{D}\hat{B}\hat{g}_{bb}\hat{g}^<_{\alpha'\alpha'}(\hat{I} + t\hat{G}^a_{b\alpha'}) + t\hat{D}\hat{B}\hat{g}_{ba}\hat{\Sigma}_L\hat{A}\hat{g}_{ab}\hat{g}^<_{\alpha'\alpha'}(\hat{I} + t\hat{G}^a_{b\alpha'}), \tag{2.117}$$

$$\hat{G}^{<,L}_{\alpha'b} = t\hat{L}\hat{N}\hat{\Sigma}_R\hat{g}_{ba}\hat{M}\hat{g}^<_{\alpha\alpha}\hat{G}^a_{ab}, \tag{2.118}$$

$$\hat{G}^{<,R}_{\alpha'b} = t'\hat{L}\hat{N}\hat{g}^<_{\alpha'\alpha'}\hat{G}^a_{bb}, \tag{2.119}$$

and

$$\hat{G}^<_{b\alpha'} = \hat{G}^{<,L}_{b\alpha'} + \hat{G}^{<,R}_{b\alpha'} \tag{2.120}$$

$$\hat{G}^<_{\alpha'b} = \hat{G}^{<,L}_{\alpha'b} + \hat{G}^{<,R}_{\alpha'b}. \tag{2.121}$$

2.3.5 Spin current densities and spin transfer torques

In the Heisenberg representation, the full quantum description of a system consisting of N particles is provided using the density matrix which is defined as,

$$\begin{aligned}\hat{\rho}^{\sigma\sigma'}(\boldsymbol{r}_1,\boldsymbol{r}_2,t) &= \frac{1}{N}\langle\hat{\Psi}_H^{\dagger\sigma'}(\boldsymbol{r}_2,t)\hat{\Psi}_H^{\sigma}(\boldsymbol{r}_1,t)\rangle \\ &= \mp\frac{i}{N}\hat{G}^{<\sigma,\sigma'}(\boldsymbol{r}_1,t;\boldsymbol{r}_2,t),\end{aligned} \tag{2.122}$$

being $\hat{\Psi}_H$ the field operator and $\hat{G}^<$ the lesser Green's function. If $\hat{O}^{\sigma\sigma'}$ is a single-particle operator of any physical observable then its average value in second quantization is given by

$$\begin{aligned}\langle O\rangle &= \sum_{\sigma\sigma'}\langle\hat{\Psi}_H^{\dagger\sigma'}(\boldsymbol{r},t)\hat{O}^{\sigma\sigma'}\hat{\Psi}_H^{\sigma}(\boldsymbol{r},t)\rangle d^3r, \\ &= N\sum_{\sigma\sigma'}\int[\hat{O}^{\sigma\sigma'}\hat{\rho}^{\sigma'\sigma}(\boldsymbol{r}_1,\boldsymbol{r}_2,t)]_{\boldsymbol{r}_2=\boldsymbol{r}_1=\boldsymbol{r}}d^3r, \\ &= \mp i\sum_{\sigma\sigma'}\int[\hat{O}^{\sigma\sigma'}\hat{G}^{<\sigma,\sigma'}(\boldsymbol{r}_1,t;\boldsymbol{r}_2,t)]_{\boldsymbol{r}_2=\boldsymbol{r}_1=\boldsymbol{r}}d^3r.\end{aligned} \tag{2.123}$$

Then, the average of any observable can be expressed in terms of the lesser Green's function. Similar to §2.2.3 we proceed to express the charge and spin (current) densities. The particle number (n) and spin density ($\boldsymbol{S}$) at a given point in second quantization are,

$$n(\boldsymbol{r},t) = \sum_{\sigma}\hat{\Psi}_H^{\dagger\sigma'}(\boldsymbol{r},t)\hat{\Psi}_H^{\dagger\sigma'}(\boldsymbol{r},t), \tag{2.124}$$

$$\boldsymbol{S}(\boldsymbol{r},t) = \sum_{\sigma}\hat{\Psi}_H^{\dagger\sigma'}(\boldsymbol{r},t)\hat{\boldsymbol{s}}^{\sigma\sigma'}\hat{\Psi}_H^{\dagger\sigma'}(\boldsymbol{r},t), \tag{2.125}$$

where $\hat{\boldsymbol{s}}^{\sigma\sigma'}$ is defined in §2.2.3. Therefore, considering Eq. (2.123), the average particle number, $\langle n(\boldsymbol{r},t)\rangle$, and average spin density, $\langle \boldsymbol{S}(\boldsymbol{r},t)\rangle$, become,

$$\langle n(\boldsymbol{r},t)\rangle = N\sum_{\sigma}\hat{\rho}^{\sigma\sigma}(\boldsymbol{r},\boldsymbol{r},t) = -i\sum_{\sigma}\hat{G}^{<\sigma,\sigma}(\boldsymbol{r},t;\boldsymbol{r},t), \tag{2.126}$$

$$\langle \boldsymbol{S}(\boldsymbol{r},t)\rangle = N\sum_{\sigma}\hat{\boldsymbol{s}}^{\sigma\sigma'}\hat{\rho}^{\sigma'\sigma}(\boldsymbol{r},\boldsymbol{r},t) = -i\sum_{\sigma'\sigma'}\hat{\boldsymbol{s}}^{\sigma\sigma'}\hat{G}^{<\sigma',\sigma}(\boldsymbol{r},t;\boldsymbol{r},t). \tag{2.127}$$

Similarly, the average charge, $\langle \boldsymbol{j}_e(\boldsymbol{r},t)\rangle$, and spin current densities, $\langle \boldsymbol{Q}(\boldsymbol{r},t)\rangle$, become,

$$\langle \boldsymbol{j}_e(\boldsymbol{r},t)\rangle = -\frac{e\hbar}{2m}\sum_{\sigma}[(\nabla_{\boldsymbol{r}}-\nabla_{\boldsymbol{r}'})\hat{G}^{<\sigma,\sigma}(\boldsymbol{r},t;\boldsymbol{r}',t)]_{\boldsymbol{r}'=\boldsymbol{r}}, \tag{2.128}$$

$$\langle \boldsymbol{Q}(\boldsymbol{r},t)\rangle = \frac{\hbar}{2m}\sum_{\sigma\sigma'}[\hat{\boldsymbol{s}}^{\sigma\sigma'}\otimes(\nabla_{\boldsymbol{r}}-\nabla_{\boldsymbol{r}'})\hat{G}^{<\sigma',\sigma}(\boldsymbol{r},t;\boldsymbol{r}',t)]_{\boldsymbol{r}'=\boldsymbol{r}}, \tag{2.129}$$

Discretizing the problem and integrating over E and $\boldsymbol{k}_{\parallel}$ we have,

$$\boldsymbol{j}_e = \frac{et}{2\pi\hbar}\int Tr[(\hat{G}^{<\sigma,\sigma'}_{p+1,p}-\hat{G}^{<\sigma,\sigma'}_{p,p+1})\hat{\boldsymbol{I}}]dEd\boldsymbol{k}_{\parallel}, \tag{2.130}$$

$$\boldsymbol{Q}^{xy}_{p,p+1} = \frac{t}{4\pi}\int Tr[(\hat{G}^{<\sigma,\sigma'}_{p+1,p}-\hat{G}^{<\sigma,\sigma'}_{p,p+1})\hat{\boldsymbol{\sigma}}_x]dEd\boldsymbol{k}_{\parallel}, \tag{2.131}$$

$$\boldsymbol{Q}^{yy}_{p,p+1} = \frac{t}{4\pi}\int Tr[(\hat{G}^{<\sigma,\sigma'}_{p+1,p}-\hat{G}^{<\sigma,\sigma'}_{p,p+1})\hat{\boldsymbol{\sigma}}_y]dEd\boldsymbol{k}_{\parallel}, \tag{2.132}$$

$$\boldsymbol{Q}^{zy}_{p,p+1} = \frac{t}{4\pi}\int Tr[(\hat{G}^{<\sigma,\sigma'}_{p+1,p}-\hat{G}^{<\sigma,\sigma'}_{p,p+1})\hat{\boldsymbol{\sigma}}_z]dEd\boldsymbol{k}_{\parallel}. \tag{2.133}$$

$\boldsymbol{j}_e$ is the charge current density and $\boldsymbol{Q}$ corresponds to the spin current density tensor, which is separated in its three components associated to the respective Pauli matrices, $\hat{\boldsymbol{\sigma}}$. Since the transverse spin current density is not conserved, the spin current lost at an atomic site p is transferred to its local magnetic moment, thereby exerting a local torque $\boldsymbol{T}_p$. In general we have

$$\boldsymbol{T}_p = -\nabla \cdot \boldsymbol{Q} = \boldsymbol{Q}_{p-1,p} - \boldsymbol{Q}_{p,p+1}, \tag{2.134}$$

where the second equality represents the discrete form of the divergence of the spin current density. To obtain the net torque in the right electrode we sum all the localized torque values, i.e., $\boldsymbol{T} = \sum_p^{\infty} \boldsymbol{T}_p$, where p refers to atomic sites in the right electrode. This eventually leads to a total torque given by the spin current density at the interface,

$$\boldsymbol{T}^R = \boldsymbol{Q}_{b\alpha'}. \tag{2.135}$$

The spin transfer torque can be separated in two components perpendicular to the magnetization direction. Then, considering that $\boldsymbol{m}_R$ rotates in the $xz-$plane, we have

$$\boldsymbol{T}_{\parallel}^R = \boldsymbol{Q}_{b\alpha'}^{xy} \cos\theta_R - \boldsymbol{Q}_{b\alpha'}^{zy} \sin\theta_R, \tag{2.136}$$

$$\boldsymbol{T}_{\perp}^R = \boldsymbol{Q}_{b\alpha'}^{yy}. \tag{2.137}$$

2.4 Results and discussion

First we investigate structures where insulating spacers needed to magnetically decouple the MI and FM layers are disregarded. Here we study the bias dependence of STT in partial SFTJs (§2.4.1) and the angular dependence of STT in junctions of the form FM/MI/FM (§2.4.2). The former is set considering $\theta_{R(B)} = \pi/2(0)$ and $\Delta_L = 0$, the latter takes into account $\theta_{L(R)} = \pi/2(0)$. In both cases $\epsilon_L^0 = \epsilon_R^0$ and the barrier height is set as close as possible to the Fermi level to guarantee large current densities. To avoid Fowler Nordheim effect [65], $\epsilon_B^0 = +9$ eV and $\Delta_B = +2$ eV are considered, which brings at zero-bias, $E_{min}^{\uparrow} = +1$ eV. In §2.4.3, we study the case where insulating spacers are inserted between FM and MI in order to decouple the two magnetic layers. Such an insertion is in principle expected to dramatically reduce both TMR and STT amplitudes. However, it has been shown experimentally that insertion of 0.8 nm-thick $SrTiO_3$ non-magnetic insulating spacer between FM electrode and magnetic insulating barrier in $La_{2/3}Sr_{1/3}MnO_3/(SrTiO_3)/NiFe_2O_4$/Au junctions, is efficient in decoupling the exchange interaction between the magnetic insulator and the electrode without substantially modifying the TMR ratio [39]. We show how the spin transfer torque components are modified when inserting the non-magnetic insulating spacer. The in-plane torque dramatically decreases in magnitude preserving its qualitative behavior as a function of bias. In contrast, the magnitude of the out-of-plane torque is only slightly reduced in both partial and symmetric SFTJs. Therefore, disregarding such spacers does not bring major changes in the out-of-plane component, which should be measurable experimentally.

2.4.1 Partial Spin Filter Tunnel Junction

As displayed in Figs. 2.5(a)(b), main panels, for the aforementioned band filling cases, it is found that a bilayer system of the form MI/FM is enough to dramatically

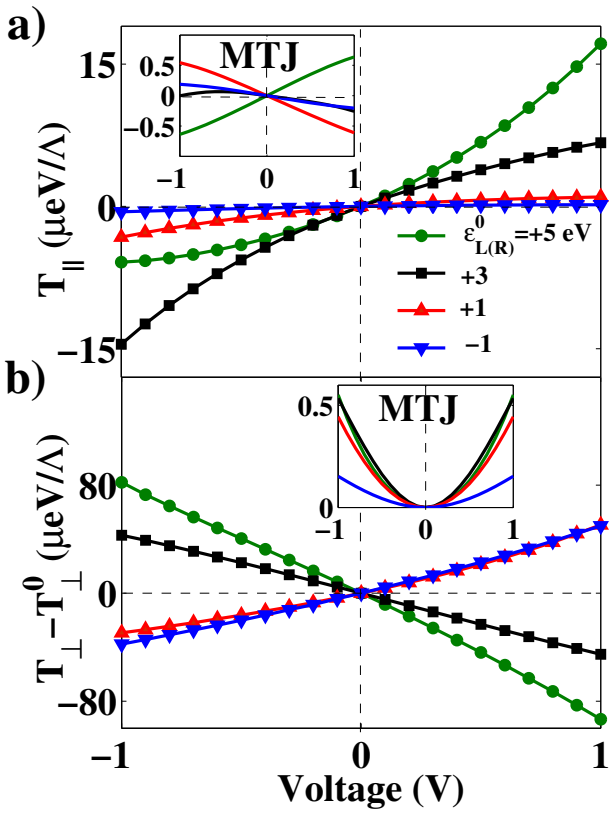

Figure 2.5: (Color online) Bias dependence of non-equilibrium (a) in-plane $T_\parallel$, and (b) out-of-plane, $T_\perp - T^0_\perp$, spin torque components, for NM/MI/FM (main panels) and FM/I/FM (insets) structures, with $\theta_R = \pi/2$, $\theta_{L(B)} = 0$ and $\epsilon^0_B = +9$ eV for different values of spin averaged on-site energies in the leads ($\epsilon^0_L = \epsilon^0_R$). $\Delta_L = 0$ and $\Delta_{R(B)} = +2$ eV in p-SFTJs (former). $\Delta_B = 0$ and $\Delta_{L(R)} = +2$ eV in MTJs (latter). $N_B = N_I = N_{MI} = 3$, and the hopping parameter is t = -1 eV. In all cases the magnitude of the torques are given in μeV/Λ where Λ denotes the interfacial unit area.

enhance the spin torque components compared to MTJs, displayed on insets. In Figs. 2.6(a)(b), the torque efficiencies are displayed as a function of band filling for V = −1.0 V. Whereas $T_\parallel/j_e$ magnitude remains in same order of MTJs, $(T_\perp - T^0_\perp)/j_e$ is increased by a factor of 10 in low band filling regions up to a factor of 100 as the system moves towards higher band filling values. Notice that the equilibrium interlayer exchange coupling (IEC) [60], i.e., the zero-bias value of $T_\perp$, $T^0_\perp$, has been subtracted.

The underlying mechanism of the out-of-plane torque is first understood in the

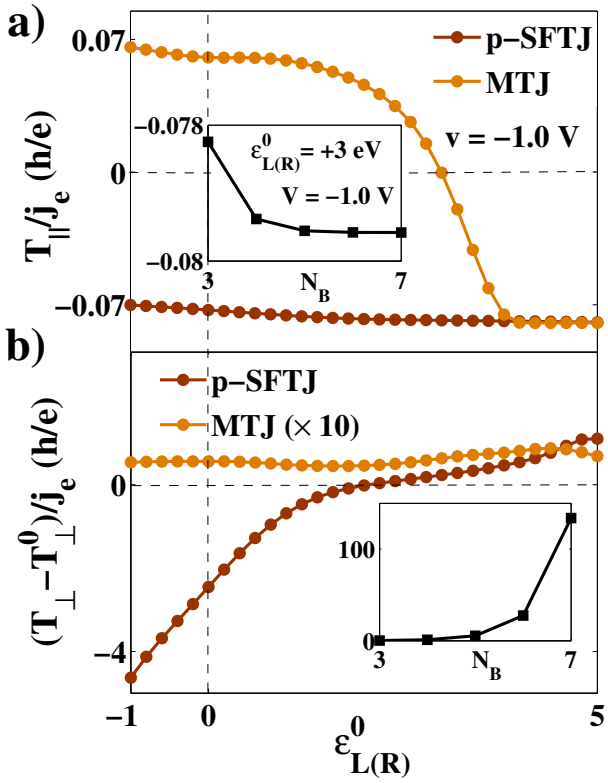

Figure 2.6: (Color online) MTJ and p-SFTJ efficiencies for the non-equilibrium (a) in-plane and (b) out-of-plane spin torque components as a function of $\epsilon^0_{L(R)}$ and V = −1.0 V. Similar parameters as in Fig. 2.5 are considered. In panel b) MTJ magnitude is multiplied by 10 to fit in the graph. Insets refer to the torque efficiencies of the p-SFTJ as a function of barrier thickness ($N_B = N_{MI}$), given in numbers of atomic layers, for V = −1.0 V and $\epsilon^0_{L(R)}$ = +3 eV. The magnitude of the torque efficiencies are given in units of h/e.

framework of free electron approach based in Wentzel-Kramers-Brillouin (WKB) approximation. As derived in §2.2.4, the out-of-plane torque is dominated by the spin-dependent reflection at MI/FM interface, depending strongly on $q^\uparrow_R - q^\downarrow_R$ and $k^\uparrow_R - k^\downarrow_R$ and being independent of the barrier width. This result is confirmed in the TB approach. For this, in Eqs. (2.120) and (2.121) we vanish $G^{<R}_{b\alpha'(\alpha' b)}$ ($G^{<L}_{b\alpha'(\alpha' b)}$) to describe the interaction arising from the left (right) layer only. It is found that even in the presence of a thin magnetic insulating barrier, for all band filling, the non-equilibrium out-of-plane torque, $T_\perp - T^0_\perp$, is driven by the spin-dependent reflection at MI/FM interface, and the contribution of the tunneling electrons ($L \to R$) becomes negligible

in high band filling regime. Meanwhile, the in-plane components, for electrons flowing from left to right and right to left, are both second order in barrier transmission, $\sim e^{-2d\kappa^{\uparrow(\downarrow)}}$ (not shown here), and strongly depend on the barrier width.

On insets in Figs. 2.6(a)(b), the torque efficiencies as a function of the barrier width for $\epsilon^0_{L(R)} = +3$ eV and V $= -1.0$ V are displayed. Whereas $\mathrm{T}_\parallel/j_e$ remains constant as a result of $\mathrm{T}_\parallel$ and j_e decaying at same rate, $(\mathrm{T}_\perp - \mathrm{T}^0_\perp)/j_e$ exponentially increases in agreement with Eq. (2.38). The torkances of the STT components, $\partial \boldsymbol{T}/\partial V$, as the system moves towards higher band filling, are of particular interest. First, in agreement with a recent work [43], due to the asymmetry of the junctions, the out-of-plane torque depends linearly as a function of bias voltage; however, as $\epsilon^0_{L(R)}$ decreases, $\partial(\mathrm{T}_\perp - \mathrm{T}^0_\perp)/\partial$V changes sign, see Fig. 2.5(b). The underlying mechanism is inferred from Eq. (2.38), $\mathrm{T}^{R\to L}_\perp \propto (k^\uparrow_R - k^\downarrow_R)$, where the torkance changes sign as a result of polarization inversion. Meanwhile, the in-plane STT component exhibits an important feature in contrast to MTJs. Whereas in MTJs $\partial \mathrm{T}_\parallel/\partial$V changes sign as $\epsilon^0_{L(R)}$ decreases [see inset in Fig. 2.5(a)], in p-SFTJs it does not [see main panel in Fig. 2.5(a)]. This behavior is understood considering WKB approximation. As given in §2.2.4, it is straightforward to notice from Eq. (2.39) that in MTJs the sign of $\mathrm{T}_\parallel$ is determined by the sign of the polarization $\mathscr{P}_L \propto (k^\downarrow_L - k^\uparrow_L)$ whereas in p-SFTJs, given in Eq. (2.40), $\mathscr{P}_L$ is absent and no sign reversal is expected since $\mathrm{T}_\parallel$ is driven by the tunneling electrons that experience the lowest barrier height (majority electrons in Eq. 2.40).

2.4.2 Symmetric Spin Filter Tunnel Junction

In §2.4.1, we have seen that a magnetic insulating barrier adjacent to a ferromagnetic layer dramatically enhances the torque amplitude compared to magnetic tunnel junctions. The out-of-plane torque is driven by the spin-dependent reflection at MI/FM interface, whereas the in-plane torque is dominated by the tunneling electrons that

experience the lowest barrier height. To exploit these important features, we propose a device of the form FM/MI/FM, referred to as symmetric spin filter tunnel junction, or s-SFTJ. The system now consists of two ferromagnets separated by a magnetic insulator, the left layer is referred to as the reference layer and the right layer is the free layer on which the torque is exerted. In this device, when the magnetization direction of the barrier is aligned on the magnetization of the free layer, the junction is expected to behave like a MTJ. In contrast, when the magnetization of the barrier is misaligned with respect to the magnetization of the free layer, the system behaves like the p-SFTJ discussed in §2.4.1. Therefore, the magnitude of the spin transfer torques can be tuned, depending on the relative angle between the magnetizations of the barrier and free layer. In Figs. 2.7(a)(b) we display the angular dependence of the STT components for V = +1.0 V. For this study, the magnetization of the barrier is rotated by an angle θ_B while the magnetization of the leads are kept perpendicular to each other, $\theta_{L(R)} = \pi/2(0)$, as sketched in Fig. 2.7(b). When the magnetization of the barrier is perpendicular to the magnetization of the free layer, the out-of-plane torque is driven by the spin-dependent reflection. Thus, as shown in Fig. 2.7(d) (bottom-right panel), where we have plotted the case $\epsilon^0_{L(R)} = +3$ eV and $\theta_B = 3\pi/2$ for s-SFTJ and p-SFTJ junctions, the out-of-plane torque is likely to be independent on the details of the electronic structure of the reference layer and therefore displays a bias dependence similar to partial SFTJs. In contrast, when the barrier is aligned or anti-aligned to the free layer, Eqs. (2.37) and (2.38) vanish; therefore, the contribution to the out-of-plane torque is driven by the leads, recovering MTJ bias characteristics, as shown in Fig. 2.7(d) (bottom-left panel) for the case $\theta_B = 0$, where the slight enhancement is due to the spin-filtering imposed by the magnetic insulating barrier. Similar outputs are found in other band filling cases. Consequently, at low voltage, the bias dependence of the non-equilibrium out-of-plane torque in s-SFTJs

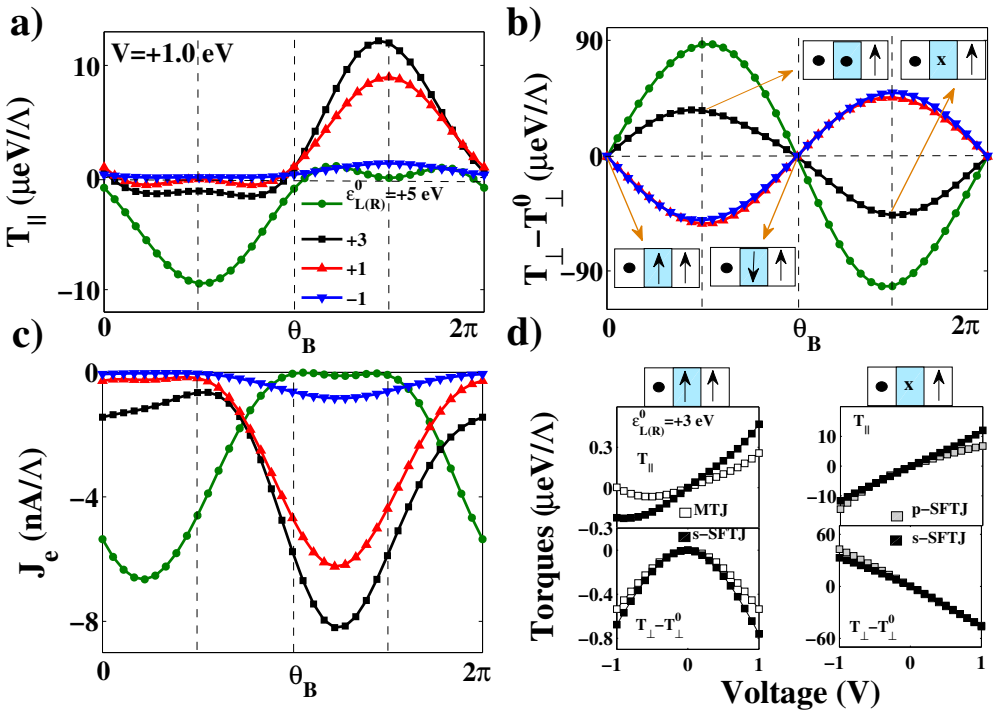

Figure 2.7: (Color online) Angular dependence of non-equilibrium (a) in-plane torque, (b) out-of-plane torque, and (c) electron flow density, for FM/MI/FM structure (s-SFTJ) with V=+1.0 V and four values of the spin-averaged on-site energy. (d) Bias dependence of the spin torque components for 1/4 band filling case ($\epsilon^0_{L(R)} = +3$ eV). Left- (Right-) hand insets compare the s-SFTJ solutions with a MTJ (p-SFTJ) structure with parameters similar to those given in Fig. 2. The magnetization of the barrier is rotated by an angle θ_B while the magnetization of the leads are kept perpendicular to each other, $\theta_{L(R)} = \pi/2(0)$. $\Delta_{L(R)(B)} = +2$ eV in s-SFTJ.

can be expressed as

$$\mathrm{T}_\perp - \mathrm{T}^0_\perp = b_{1(\theta_B)}\mathrm{V} + b_{2(\theta_B)}\mathrm{V}^2, \tag{2.138}$$

where the coefficients, in contrast to Eq. (1.2), depend on θ_B.

The in-plane STT component shows a more complex angular behavior which depends also on band filling regime and on the relative orientation of the magnetizations in the barrier and left layer. For the half metallic case, depicted by the filled green dots in Fig. 2.7, the reference layer filters the spin states. If these states are anti-aligned with the magnetization of the barrier ($\theta_B = 3\pi/2$), the electron flow density

exponentially drops, as shown in Fig. 2.7(c); therefore, $T_{\parallel}$ is dramatically reduced, see Fig. 2.7(a). However, if the spin states are aligned with the magnetization of the barrier ($\theta_B = \pi/2$), the enhanced electron tunneling results in a dramatic increase in the torque amplitude and in the electron flow density, see Figs. 2.7 (a)(c). Furthermore, when the magnetization of the barrier is aligned on the magnetization of the free layer ($\theta_B = 0$), the system behaves like a MTJ with an enhancement in the torque amplitude due to the magnetic nature of the insulating layer. This effect persists for higher band filling values, as displayed in Fig. 2.7(d), top-left panel, for the case $\epsilon^0_{L(R)} = +3$ eV. An important feature in non-half metallic cases appears when the magnetization of the barrier is antiparallel ($\theta_B = 3\pi/2$) or parallel ($\theta_B = \pi/2$) to the magnetization of the reference layer. In the former, given in Fig. 2.7(d) top-right panel, for $\epsilon^0_{L(R)} = +3$ eV, $T_{\parallel}$ behaves like in partial SFTJs, whereas in the latter, the magnitude is reduced, see Fig. 2.7(a). To understand these effects, we recall the discussion in the previous section, where we mentioned that $T_{\parallel}$ in p-SFTJs is driven by the tunneling electrons that experience the lowest barrier height, implying that when the polarization inversion is reached (high band filling regime), $J_{AP} > J_P$, being $J_{AP(P)}$ the charge current density in antiparallel (parallel) configuration, $\theta_B = 0$ and $\theta_R = \pi(0)$. Similarly, in s-SFTJ for the antiparallel alignment between the magnetization of the barrier and the magnetization of the reference layer, polarization inversion allows higher current densities, which results in larger torque amplitudes compared to the parallel configuration, see Figs. 2.7(a)(c).

2.4.3 Spin Filter Tunnel Junctions with insulating spacers

In §2.4.1 the bias dependence of partial spin filter tunnel junctions (NM/MI/FM) was studied. A dramatic enhancement of the spin torque components compared to magnetic tunnel junctions was uncovered, as well as a domination of the out-of-plane term compared to the in-plane torque ($T_{\perp} > T_{\parallel}$). It was additionally found

that the efficiency of $T_{\parallel}$ remains in same order as in MTJs, whilst the efficiency of $T_{\perp}$ is dramatically enhanced. In §2.4.2 the angular dependence of symmetric structures of the form FM/MI/FM was studied, and we showed that depending on the relative orientation of the magnetizations in the barrier and free layer the system behaves like a MTJ or partial-SFTJ. These results may be put under debate since realistic structures require additional spacers to break the exchange interaction of the

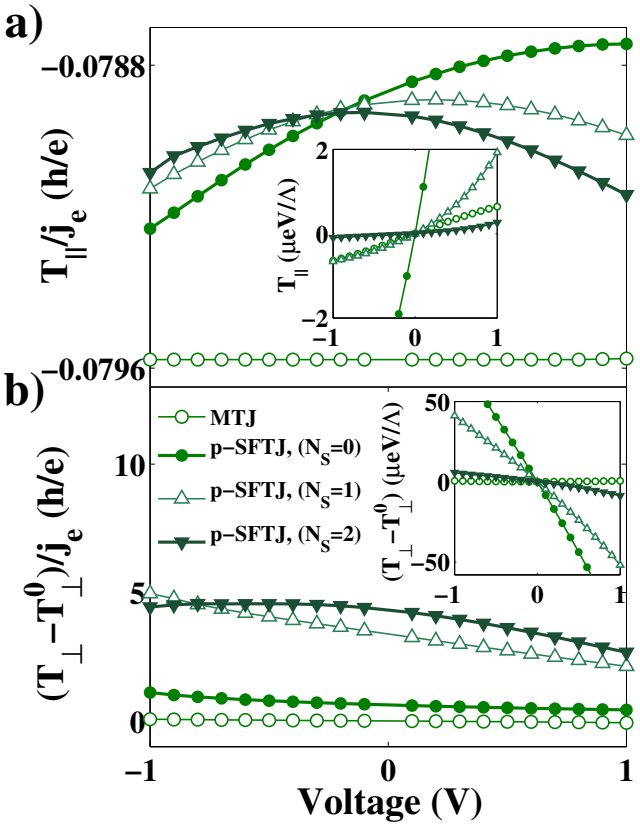

Figure 2.8: (Color online) MTJ and p-SFTJ efficiencies for the non-equilibrium (a) in-plane and (b) out-of-plane spin torque components as a function of bias. Three p-SFTJ structures of the form NM/MI/S/FM are studied, where the thickness of MI is fixed to $N_{MI} = 3$ and of S to $N_S = 0, 1$, or 2 monolayers. The barrier thickness of the MTJ is set to $N_I = 3$. Insets refer to the bias dependence of the non-equilibrium (top) in-plane and (bottom) out-of-plane torque. In all cases $\epsilon^0_{L(R)} = +5$ eV, $\epsilon^0_B = +9$ eV, $\theta_R = \pi/2$, $\theta_{L(B)} = 0$, and t= -1 eV. $\epsilon^0_S = +7$ eV, $\Delta_{R(B)} = +2$ eV, and $\Delta_{L(S)} = 0$ in p-SFTJs. $\Delta_{L(R)} = +2$ eV and $\Delta_B = 0$ in MTJs.

magnetic insulator and the ferromagnetic electrode; for this reason we study here two architectures, a partial SFTJ of the form NM/MI/S/FM, and a symmetric junction

of the form FM/S/MI/S/FM, where S stands for the insulating spacer defined by N_S atomic layers. The barrier height of the spacer is set to $\epsilon_S^0 = +7$ eV and $\Delta_S = 0$, which guarantees large current densities without reaching the resonant regime. We also set $\epsilon_B^0 = +9$ eV and $\Delta_B = +2$ eV and fix the other parameters as in the previous sections. It is found that insertion of insulating spacers does not qualitatively change our conclusions. In Fig. 2.8 main panels (insets) we display the bias dependence of the spin torque efficiencies (components) for a MTJ with $N_I = 3$ and p-SFTJs with $N_{MI} = 3$ and $N_S = 0, 1$ and 2. Only the half metallic case is given, but similar results are obtained in other band filling cases. Whereas in MTJs, the insertion of a spacer between the barrier and free layer modifies the quadratic profile of the out-of-plane torque by inducing a linear term in V, in p-SFTJs, spacers do not affect the linear profile reported in Fig. 2.5(b); moreover, because the torque is driven by the spin-dependent reflection, its amplitude exhibits a small decrease, which for $N_S = 2$ remains still higher than MTJs, see inset in Fig. 2.8(b).

In contrast, the in-plane torque being driven by the tunneling electrons that experience the lowest barrier height, this component dramatically decreases with the insertion of an insulating spacer (inset of Fig. 2.8(a)). These results are confirmed by considering the torque efficiencies, displayed in main panels. Whereas the efficiency of the in-plane torque, $T_\parallel/j_e$, remains unaffected by the insertion of the spacer (~ -0.079), the efficiency of the perpendicular torque, $(T_\perp - T_\perp^0)/j_e$, increases; consequently, $T_\perp \gg T_\parallel$ when insulating spacers are taken into consideration. Indeed, the dramatic enhancement of the spin torque magnitudes in p-SFTJs is reduced in the presence of insulating spacers; however, when considering thin spacers the predicted spin torque is still higher than in MTJs.

We have extended this study to the case of a symmetric spin filter tunnel junction of the form FM/S/MI/S/FM with $N_{MI} = 3$ and $N_S = 1$. The barrier heights are set to $\epsilon_B^0 = +9$ eV and $\epsilon_S^0 = +7$ eV for the magnetic insulator and the spacers, respectively.

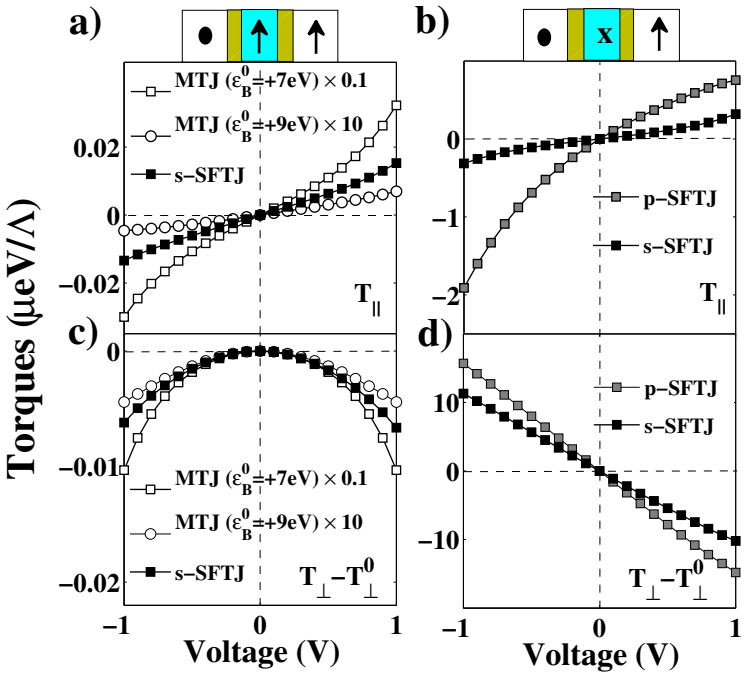

Figure 2.9: (Color online) Bias dependence of the spin torque components for 1/4 band filling case ($\epsilon^0_{L(R)} = +3$ eV). Left (Right) panels compare the s-SFTJ system of the form FM/S/MI/S/FM with a MTJ (p-SFTJ) structure of the form FM/I/FM (NM/MI/S/FM), where the thicknesses of I, MI, and S are fixed to $N_{I(MI)(S)} = 5(3)(1)$. Top (Bottom) panels refer to the non-equilibrium in-plane (out-of-plane) spin torque component. The magnetization of the leads are kept perpendicular to each other, $\theta_{L(R)} = \pi/2(0)$. Left (Right) panels refer to the configuration where $\theta_B = 0(3\pi/2)$. Two MTJ structures are displayed on left panels, $\epsilon^0_B = +7$ eV and $\epsilon^0_B = +9$ eV. To fit in the graph, the former has been multiplied by 0.1 and the latter by 10. Other parameters are similar to previous Figs.

We found that the angular dependence of the torque becomes qualitatively similar to the case discussed in §2.4.2, where insulating spacers are neglected (not shown). In Fig. 2.9 the STT bias dependence of this symmetric junction in the low band filling regime ($\epsilon^0_{L(R)} = +3$ eV) is displayed for two configurations, $\theta_B = 0$ and $\theta_B = 3\pi/2$. The leads are set to $\theta_{L(R)} = \pi/2(0)$, see top sketches in Fig. 2.9. The former case ($\theta_B = 0$) defines a symmetric SFTJ with MTJ-like characteristics. Here we compare our solutions with two types of MTJs with similar barrier thicknesses, $N_I = 5$, and different barrier heights, $\epsilon^0_B = +7$ eV and +9 eV. When the barrier height is closer to the Fermi level, the torque amplitudes are much larger; therefore, the

MTJ with $\epsilon_B^0 = +7$ eV ($\epsilon_B^0 = +9$ eV) shows much larger (lower) amplitudes than the symmetric SFTJ, as given in Figs 2.9(a)(c). If a MTJ of the form FM/S/I/S/FM is considered with similar parameters as the symmetric SFTJ, the latter will show torque amplitudes slightly enhanced due to the spin filtering imposed by the magnetic insulator (not show), in clear agreement with the ideal case given in Fig. 2.7(d) left-panels. The latter case ($\theta_B = 3\pi/2$), which defines a symmetric SFTJ with p-SFTJ-like characteristics becomes more interesting. Here, the in-plane torque amplitude in the symmetric structure is lowered with respect to partial SFTJs of the form NM/MI/S/FM with $N_{MI} = 3$ and $N_S = 1$, in contrast to the ideal case given in Fig. 2.7(d) top right-panel where both, symmetric and partial junctions showed similar amplitudes. This is due to the extra spacer added between the reference and barrier layers which contributes to an exponential decay of the electrons tunneling. Despite this decay, the magnitude is still larger than in MTJs with $N_I = 3$, see Fig. 2.9(b) and inset in Fig. 2.5(a). Meanwhile, the out-of-plane torque amplitude remains much larger than in MTJs and similar to partial SFTJs of the form NM/MI/S/FM because the contribution of electrons incident from the free layer (right to left) dominates; consequently, even if thick spacers are considered to decouple the reference and barrier layers, the torque magnitude shall not decrease significantly, see Fig. 2.9(d).

2.5 Conclusion

To conclude, using a free-electron model based in WKB approximation and a tight-binding model based in Keldysh formalism, we have theoretically studied the spin transfer torque mechanism in junctions involving a magnetic insulating barrier. In the case of partial spin filter tunnel junction, composed of a magnetic tunnel barrier adjacent to a metallic ferromagnet, NM/MI/FM, we have shown a strong enhancement of the torque amplitudes compared to conventional MTJs. When insu-

lating spacer is added to decouple the exchange interaction between MI and FM, i.e., NM/MI/S/FM, we have shown that for thin spacers made of 1 or 2 monolayers, the torque amplitudes remain larger than conventional MTJs. The out-of-plane torque strongly depends on the spin-dependent reflection at MI/FM interface. Meanwhile, the in-plane torque is driven by the tunneling electrons that experience the lowest barrier height. To exploit these important features and those of conventional MTJs, a hybrid device has been proposed, referred to as symmetric spin filter tunnel junction, and composed of two ferromagnetic electrodes separated by a magnetic tunneling barrier, FM/(S)/MI/(S)/FM. In such structure, we have shown that the STT components can be tuned from conventional MTJ-like to partial SFTJ-like behavior just by rotating the magnetization of the insulating layer. This offers the possibility of fabricating a device that is able to retrieve bias characteristics of both systems, partial SFTJ and conventional MTJ, which opens novel avenues in the future developments of STT-MRAM technologies, i.e., current-induced-magnetization-reversal and -excitation devices.

Chapter 3

Rashba Torque in Ferromagnetic Films

3.1 Introduction

In contrast to the conventional spin transfer torque mechanism, discussed in Chap. 2 for non collinear magnetization structures such as spin filter tunnel junctions [66], in-plane current induced spin-orbit torques (SOT) are present even in collinear homogeneous ferromagnetic layers [44] offering novel avenues in magnetic memory technology. Referred to as SOT-MRAM, this new approach, in contrast to conventional STT-MRAM, offers lower switching currents and lower density.

Two mechanisms for the spin-orbit torques have been proposed in ferromagnet/heavy metal bilayers: i) the bulk spin Hall effect generated in the heavy metal and acting in the ferromagnet [50], ii) the interfacial spin-orbit coupling effect referred to as the Rashba effect [48, 46]. It has been shown that both effects contribute to the in-plane and out-of-plane spin-orbit torque components; therefore, substantial efforts to qualitatively and quantitatively determine the contribution of each effect has been under discussion in recent years (to the date of publication of this thesis) [67]. Here we study the so called Rashba effect at the interface of a ferromagnet and heavy metal and provide a qualitative description of the Rashba torque. For this, in §3.2

we develop a set of drift diffusion equations that provides a coherent description to the diffusive spin dynamics. This model, based in Keldysh formalism under Wigner expansion, captures quantum effects that are usually neglected in semiclassical approaches [68]; therefore, it provides a complete picture of the system. In §3.3 the characteristics of the spin torque and its implication on magnetization dynamics are discussed for a wide range of relative strength between Rashba spin-orbit induced energy splitting and the ferromagnetic exchange. Of particular interest is the strong dependence of the spin torque components on magnetization direction, a behavior to be referred to as angular dependence. Comparing the experimental results of the angular dependence [69, 70] with our calculated results provides clues to the mechanism of the spin-orbit torque. In §3.4 we summarize the major conclusions.

3.2 Quantum kinetic equation

In this section, considering a diffusive model based on Keldysh formalism under Wigner expansion, we develop analytical expressions for the in-plane and out-of-plane spin-orbit torque components in ferromagnets in the presence of Rashba spin-orbit coupling. The typical system we have in mind is a magnetic trilayer such as, but not limited to, Pt/Co/AlOx. Although the charge transport in such a system is three dimensional, for the sake of simplicity we model this system by a two dimensional electron that accommodates both magnetism and Rashba spin-orbit interaction.

3.2.1 Kinetic equation in Keldysh space

In Keldysh formalism the left- and right-hand Dyson's equations read,

$$(\hat{\boldsymbol{G}}_{\mathbf{0}}^{-\mathbf{1}} - \hat{\boldsymbol{\Sigma}}) \otimes \hat{\boldsymbol{G}} = \hat{I}, \tag{3.1}$$

$$\hat{\boldsymbol{G}} \otimes (\hat{\boldsymbol{G}}_{\mathbf{0}}^{-\mathbf{1}} - \hat{\boldsymbol{\Sigma}}) = \hat{I}. \tag{3.2}$$

Each term is defined in Keldysh space and is represented by the advanced $(\hat{G}^A, \hat{\Sigma}^A)$, retarded $(\hat{G}^R, \hat{\Sigma}^R)$, and Keldysh $(\hat{G}^K, \hat{\Sigma}^K)$ functions. In §2.3.4 the Green's function, $\hat{\boldsymbol{G}}$, and self-energy, $\hat{\boldsymbol{\Sigma}}$, matrices were defined according to Ref. [62]. Here we perform a different canonical transformation [71] that gives rise to a set of matrices of the form,

$$\hat{\boldsymbol{G}} = \begin{pmatrix} \hat{G}^R & \hat{G}^K \\ 0 & \hat{G}^A \end{pmatrix}, \qquad \hat{\boldsymbol{G}}_{\mathbf{0}}^{-\mathbf{1}} = \begin{pmatrix} [\hat{G}_0^R]^{-1} & 0 \\ 0 & [\hat{G}_0^A]^{-1} \end{pmatrix}, \qquad \hat{\boldsymbol{\Sigma}} = \begin{pmatrix} \hat{\Sigma}^R & \hat{\Sigma}^K \\ 0 & \hat{\Sigma}^A \end{pmatrix}. \tag{3.3}$$

It is important to distinguish between the Green's functions in absence $(\hat{G}_0)$ and presence $(\hat{G})$ of perturbations. The former is given by $\hat{G}_0^{R(A)} = \frac{1}{E - H_0 \pm i\delta}$ and the latter by $\hat{G}^{R(A)} = \frac{1}{E - H_0 - \Sigma^{R(A)}}$. $\hat{H}_0$ is the unperturbed Hamiltonian, E is the energy, and $\hat{\Sigma}$ takes into account the perturbation. Therefore, the following relation holds, $[\hat{G}^{R(A)}]^{-1} = [\hat{G}_0^{R(A)}]^{-1} - \Sigma^{R(A)}$. Eqs. (3.1)-(3.2) simplify to,

$$\begin{pmatrix} [\hat{G}^R]^{-1} & -\hat{\Sigma}^K \\ 0 & [\hat{G}^A]^{-1} \end{pmatrix} \begin{pmatrix} \hat{G}^R & \hat{G}^K \\ 0 & \hat{G}^A \end{pmatrix} = \begin{pmatrix} \hat{G}^R & \hat{G}^K \\ 0 & \hat{G}^A \end{pmatrix} \begin{pmatrix} [\hat{G}^R]^{-1} & -\hat{\Sigma}^K \\ 0 & [\hat{G}^A]^{-1} \end{pmatrix}, \tag{3.4}$$

where the off-diagonal term gives rise to a quantum kinetic equation of the form,

$$[\hat{G}^R]^{-1} \otimes \hat{G}^K - \hat{G}^K \otimes [\hat{G}^A]^{-1} = \hat{\Sigma}^K \otimes \hat{G}^A - \hat{G}^R \otimes \hat{\Sigma}^K. \tag{3.5}$$

$\otimes$ refers to a convolution product. We proceed now to study our system which is defined as a quasi-two-dimensional ferromagnetic metal layer rolled out in the xy plane. Two asymmetric interfaces provide a confinement in the z direction, along which the potential gradient generates a Rashba spin-orbit coupling. Therefore a single particle Hamiltonian for an electron of momentum $\hat{\boldsymbol{k}}$ is ($\hbar = 1$ is assumed throughout)

$$\hat{H} = \frac{\hat{\boldsymbol{k}}^2}{2m} + \alpha\hat{\boldsymbol{\sigma}} \cdot (\hat{\boldsymbol{k}} \times \hat{\boldsymbol{z}}) + \frac{1}{2}\Delta_{xc}\hat{\boldsymbol{\sigma}} \cdot \boldsymbol{m} + \hat{H}^i \tag{3.6}$$

where $\hat{\boldsymbol{\sigma}}$ is the Pauli matrix, m the effective mass, and $\boldsymbol{m}$ the magnetization direction. The ferromagnetic exchange splitting is given by Δ_{xc} and α represents the Rashba constant (parameter). The Hamiltonian $\hat{H}^i = \sum_{j=1}^{N} V(\boldsymbol{r} - \boldsymbol{R}_j)$ sums the contribution of the non-magnetic impurity scattering potential $V(\boldsymbol{r})$ localized at $\boldsymbol{R}_j$. The importance of the impurity potential will be discussed in Chap. 4 where we consider spin-orbit coupled impurities.

To derive a diffusion equation for the non-equilibrium charge and spin densities, Eq. (3.5) is considered [72], where all Green's functions are full functions with interactions taken care of by the self-energies $\hat{\Sigma}^{R,A,K}$. The retarded (advanced) Green's function in momentum and energy space is

$$\hat{G}^{R(A)}(\boldsymbol{k}, \epsilon) = \frac{1}{\epsilon - \epsilon_{\boldsymbol{k}} - \hat{\boldsymbol{\sigma}} \cdot \boldsymbol{\eta}(\boldsymbol{k}) - \hat{\Sigma}^{R(A)}(\boldsymbol{k}, \epsilon)}, \tag{3.7}$$

where $\epsilon_{\boldsymbol{k}} = \boldsymbol{k}^2/(2m)$ is the single particle energy. We have introduced a $\boldsymbol{k}$-dependent total effective field $\boldsymbol{\eta}(\boldsymbol{k}) = \Delta_{xc}\boldsymbol{m}/2 + \alpha(\boldsymbol{k} \times \boldsymbol{z})$ with magnitude $\eta_k = |\Delta_{xc}\boldsymbol{m}/2 + \alpha(\boldsymbol{k} \times \boldsymbol{z})|$ and the direction $\hat{\boldsymbol{\eta}} = \boldsymbol{\eta}(\boldsymbol{k})/\eta_k$.

Neglecting localization effects and electron-electron interactions, we assume a short-range δ-function type impurity scattering potential, i.e., $V(\boldsymbol{r}) = V_0\delta(\boldsymbol{r} - \boldsymbol{R}_j)$, where V_0 is the potential magnitude. At a low impurity concentration and a weak

electron-impurity coupling we assume a spin-independent momentum relaxation, i.e., independent of exchange splitting and spin-orbit interaction [73]. Therefore, in the first Born approximation the self-energy, in $\boldsymbol{k}-$space, reads

$$\hat{\Sigma}^{R,A,K} = n_i V_0^2 \int \frac{d^2\boldsymbol{k'}}{(2\pi)^2} G_0^{R,A,K} \tag{3.8}$$

and the momentum relaxation, τ, becomes,

$$\frac{1}{\tau} \approx 2\pi n_i V_0^2 \int \frac{d^2\boldsymbol{k'}}{(2\pi)^2} \delta(E - E_{\boldsymbol{k'}}). \tag{3.9}$$

$\mp\frac{i}{2\hat{\tau}} = \hat{\Sigma}^{R(A)}$ and n_i is the impurity concentration. Notice that in order to obtain macroscopic values, the potential had been averaged over the possible positions which the impurities may have in the solid. In Chap. 4 we discuss in detail the momentum relaxation and self-energy derivations without neglecting the spin-dependent contribution. Here we address the results directly.

3.2.2 Wigner expansion

The Keldysh formalism is a general powerful approach which provides a means to calculate the density matrix through the Keldysh function, providing an exact description of the system. Therefore, the equation of motion of $\hat{G}^K$, given in Eq. (3.5), constitutes the quantum-kinetic equation. To solve it and derive a set of transport equations in the diffusive limit, we introduce the ingredients of the gradient expansion scheme, known as Wigner expansion. The Green's functions in general are given by $\hat{G}^j = \hat{G}^j(\mathbf{r_1}, t_1, \mathbf{r_2}, t_2)$, where 1 and 2 denote two points in real space ($\mathbf{r}$) and real time (t), and $j = R, A, K$. We consider now a new set of coordinates and define $\mathbf{R} = (\mathbf{r_1} + \mathbf{r_2})/2$, $T = (t_1 + t_2)/2$, $\mathbf{r} = (\mathbf{r_1} - \mathbf{r_2})$, and $t = (t_1 - t_2)$. The first two are the

center of mass coordinates and the last two are the relative ones. The separation in this manner is aiming at distinguishing the microscopic variable $(\mathbf{r}, t)$ describing the quantum character of the system and the macroscopic one $(\mathbf{R}, T)$ that represents the non-equilibrium semiclassical response of the system under an external disturbance, such as the presence of an applied field. As mentioned in §3.2.1, the product, $\otimes$, in the quantum kinetic equation is a convolution product, this means,

$$C(\mathbf{r_1}, t_1, \mathbf{r_2}, t_2) = [\hat{A} \otimes \hat{B}](\mathbf{r_1}, t_1, \mathbf{r_2}, t_2) = \int d\mathbf{r}' dt' \hat{A}(\mathbf{r_1}, t_1; \mathbf{r}', t')\hat{B}(\mathbf{r}', t'; \mathbf{r_2}, t_2), \tag{3.10}$$

where C is the convolution operator and $\hat{A}$ and $\hat{B}$ represent any of the terms given in Eq. (3.5). The same convolution product can be described in terms of new coordinates, such as,

$$\begin{aligned} C(\mathbf{R} + \mathbf{r}/2, T + t/2, &\mathbf{R} - \mathbf{r}/2, T - t/2) = [\hat{A} \otimes \hat{B}](\mathbf{R} + \mathbf{r}/2, T + t/2, \mathbf{R} - \mathbf{r}/2, T - t/2) \\ &= \int d\mathbf{r}' dt' [\hat{A}(\mathbf{R} + \mathbf{r}/2, T + t/2; \mathbf{r}', t')\hat{B}(\mathbf{r}', t'; \mathbf{R} - \mathbf{r}/2, T - t/2). \end{aligned} \tag{3.11}$$

Notice that Eq. (3.11) is exactly the same as Eq. (3.10). We define a new convolution operator of the form,

$$\overline{C}(\mathbf{R}, T, \mathbf{r}, t) = C(\mathbf{R} + \mathbf{r}/2, T + t/2, \mathbf{R} - \mathbf{r}/2, T - t/2) \tag{3.12}$$

Therefore, in this new representation we have,

$$\overline{\hat{A}}(\frac{\mathbf{R}+\mathbf{r}/2+\mathbf{r}'}{2},\frac{T+t/2+t'}{2};\mathbf{R}+\mathbf{r}/2-\mathbf{r}',T+t/2-t')=\hat{A}(\mathbf{R}+\mathbf{r}/2,T+t/2;\mathbf{r}',t'), \tag{3.13}$$

$$\overline{\hat{B}}(\frac{\mathbf{R}-\mathbf{r}/2+\mathbf{r}'}{2},\frac{T-t/2+t'}{2};\mathbf{r}'-\mathbf{R}+\mathbf{r}/2,t'-T+t/2)=\hat{B}(\mathbf{r}',t';\mathbf{R}-\mathbf{r}/2,T-t/2). \tag{3.14}$$

Consequently, the new convolution operator reads,

$$\overline{C}(\mathbf{R},T,\mathbf{r},t)=\int d\mathbf{r}'dt'\overline{\hat{A}}(...)\overline{\hat{B}}(...). \tag{3.15}$$

Since the intergral is only for variables $\mathbf{r}'$ and t', we make a shift $(\mathbf{r}',t')\rightarrow(\mathbf{r}'+\mathbf{R}-\mathbf{r}/2,t'+T-t/2)$, after which Eq. (3.15) becomes,

$$\overline{C}=\int d\mathbf{r}'dt'\overline{\hat{A}}(\mathbf{R}+\mathbf{r}'/2,T+t'/2;\mathbf{r}-\mathbf{r}',t-t')\overline{\hat{B}}(\mathbf{R}-\mathbf{r}/2+\mathbf{r}'/2,T-t/2+t'/2;\mathbf{r}',t'). \tag{3.16}$$

Notice that $\overline{C}\equiv\overline{C}(\mathbf{R},T,\mathbf{r},t)$. In Eq. (3.16) we Fourier transform the convolution operator to remove the relative coordinates, $C(\mathbf{R},T,\mathbf{k},\omega)=\int d\mathbf{r}dte^{-i(\mathbf{kr}-\omega t)}\overline{C}(\mathbf{R},T,\mathbf{r},t)$, then

$$\begin{aligned}C=&\int d\mathbf{r}dte^{-i(\mathbf{kr}-\omega t)}\int d\mathbf{r}'dt'\int\frac{d\omega'}{2\pi}\frac{d^3\mathbf{k}'}{(2\pi)^3}e^{i\mathbf{k}'(\mathbf{r}-\mathbf{r}')-i\omega'(t-t')}\hat{A}(\mathbf{R}+\mathbf{r}'/2,T+t'/2;\mathbf{k}',\omega')\\&\int\frac{d\omega''}{2\pi}\frac{d^3\mathbf{k}''}{(2\pi)^3}e^{i\mathbf{k}''\mathbf{r}'-i\omega''t'}\hat{B}(\mathbf{R}-\mathbf{r}/2+\mathbf{r}'/2,T-t/2+t'/2;\mathbf{k}'',\omega'').\end{aligned} \tag{3.17}$$

Notice that we have removed the overline symbol for simplicity and $C\equiv C(\mathbf{R},T,\mathbf{k},\omega)$.

Now we perform a two dimensional Taylor expansion on $\hat{A}$ and $\hat{B}$ with respect to the variables $\mathbf{R}$ and T. To the first order in the Taylor expansion we have,

$$\begin{aligned}
&\hat{A}(\mathbf{R}+\mathbf{r}'/2, T+t'/2; \mathbf{k}', \omega') \\
&\quad = \hat{A}(\mathbf{R}, T; \mathbf{k}', \omega') + \frac{\mathbf{r}'}{2}\frac{\partial \hat{A}}{\partial \mathbf{R}}(\mathbf{R}, T; \mathbf{k}', \omega') + \frac{\mathbf{t}'}{2}\frac{\partial \hat{A}}{\partial \mathbf{T}}(\mathbf{R}, T; \mathbf{k}', \omega'), \qquad (3.18) \\
&\hat{B}(\mathbf{R}-\mathbf{r}/2+\mathbf{r}'/2, T-t/2+t'/2; \mathbf{k}'', \omega'') \\
&\quad = \hat{B}(\mathbf{R}, T; \mathbf{k}'', \omega'') + \frac{\mathbf{r}'-\mathbf{r}}{2}\frac{\partial \hat{B}}{\partial \mathbf{R}}(\mathbf{R}, T; \mathbf{k}'', \omega'') + \frac{t'-t}{2}\frac{\partial \hat{B}}{\partial T}(\mathbf{R}, T; \mathbf{k}'', \omega''). \qquad (3.19)
\end{aligned}$$

Therefore to the first order in gradient expansion we have,

$$\begin{aligned}
&\hat{A}(\mathbf{R}+\mathbf{r}'/2, T+t'/2; \mathbf{k}', \omega')\hat{B}(\mathbf{R}-\mathbf{r}/2+\mathbf{r}'/2, T-t/2+t'/2; \mathbf{k}'', \omega'') \\
&\quad \approx \hat{A}(...)\hat{B}(...) + \frac{\mathbf{r}'-\mathbf{r}}{2}\hat{A}(...)\frac{\partial \hat{B}}{\partial \mathbf{R}}(...) + \frac{\mathbf{t}'-\mathbf{t}}{2}\hat{A}(...)\frac{\partial \hat{B}}{\partial T}(...) \\
&\quad + \frac{\mathbf{r}'}{2}\hat{B}(...)\frac{\partial \hat{A}}{\partial \mathbf{R}}(...) + \frac{t'}{2}\hat{B}(...)\frac{\partial \hat{A}}{\partial T}(...), \qquad (3.20)
\end{aligned}$$

where $\hat{A}$ and $\hat{B}$ on the right hand side depend on $(\mathbf{R}, T; \mathbf{k}', \omega')$ and $(\mathbf{R}, T; \mathbf{k}'', \omega'')$, respectively. The first term in Eq.(3.20) is at zeroth-order in gradient expansion whereas the other terms are given at first order. We now proceed to solve Eq. (3.17) considering each of the terms derived in Eq.(3.20). The zeroth order term simplifies to $\hat{A}(\mathbf{R}, T; \mathbf{k}, \omega)\hat{B}(\mathbf{R}, T; \mathbf{k}, \omega)$, where we have considered the following properties of delta functions,

$$\delta(k-k_0) = \int e^{i(k-k_0)x} dx \qquad (3.21)$$

$$\delta(x) = \delta(-x) \qquad (3.22)$$

The second and third terms in Eq. (3.20) are a bit more tricky to solve. For these terms we notice that,

$$\begin{aligned} \frac{i}{2}\frac{\partial}{\partial \mathbf{k}'}[e^{i\mathbf{k}'(\mathbf{r}-\mathbf{r}')}] &= \frac{\mathbf{r}'-\mathbf{r}}{2}e^{i\mathbf{k}'(\mathbf{r}-\mathbf{r}')}, \\ -\frac{i}{2}\frac{\partial}{\partial \omega'}[e^{-i\omega'(t-t')}] &= \frac{t'-t}{2}e^{-i\omega'(t-t')}. \end{aligned} \tag{3.23}$$

Replacing (3.23) in Eq. (3.17) we have,

$$= \int \left[\frac{i}{2}\frac{\partial}{\partial \mathbf{k}'}[e^{i\mathbf{k}'(\mathbf{r}-\mathbf{r}')}]A(...)\frac{\partial \hat{B}}{\partial \mathbf{R}}(...) - \frac{i}{2}\frac{\partial}{\partial \omega'}[e^{-i\omega'(t-t')}]\hat{A}(...)\frac{\partial \hat{B}}{\partial T}(...)\right], \tag{3.24}$$

where $\int \equiv \int d\mathbf{r}dte^{-i(\mathbf{kr}-\omega t)} \int d\mathbf{r}'dt' \int \frac{d\omega'}{2\pi}\frac{d^3\mathbf{k}'}{(2\pi)^3}e^{-i\omega'(t-t')} \int \frac{d\omega''}{2\pi}\frac{d^3\mathbf{k}''}{(2\pi)^3}e^{i\mathbf{k}''\mathbf{r}'-i\omega''t'}$. Considering a partial integration over $\mathbf{k}'$ and ω' and the properties given in (3.21)-(3.22), Eq. (3.24) becomes, $-\frac{i}{2}\frac{\partial A}{\partial \mathbf{k}}(\mathbf{R},T;\mathbf{k},\omega)\frac{\partial \hat{B}}{\partial \mathbf{R}}(\mathbf{R},T;\mathbf{k},\omega) + \frac{i}{2}\frac{\partial \hat{A}}{\partial \omega}(\mathbf{R},T;\mathbf{k},\omega)\frac{\partial \hat{B}}{\partial T}(\mathbf{R},T;\mathbf{k},\omega)$.

Similarly, for the fourth and fifth terms in Eq. (3.20), we consider the following relations,

$$\begin{aligned} -\frac{i}{2}\frac{\partial}{\partial \mathbf{k}''}[e^{i\mathbf{k}''\mathbf{r}'}] &= \frac{\mathbf{r}'}{2}e^{i\mathbf{k}''\mathbf{r}'} \\ \frac{i}{2}\frac{\partial}{\partial \omega''}[e^{-i\omega''t'}] &= \frac{t'}{2}e^{-i\omega''t'}, \end{aligned} \tag{3.25}$$

which gives rise to $\frac{i}{2}\frac{\partial A}{\partial \mathbf{R}}(\mathbf{R},T;\mathbf{k},\omega)\frac{\partial \hat{B}}{\partial \mathbf{k}}(\mathbf{R},T;\mathbf{k},\omega) - \frac{i}{2}\frac{\partial \hat{A}}{\partial T}(\mathbf{R},T;\mathbf{k},\omega)\frac{\partial \hat{B}}{\partial \omega}(\mathbf{R},T;\mathbf{k},\omega)$.

In total, the convolution operation, given in Eq. (3.17), becomes

$$C(\mathbf{R},T;\mathbf{k},\omega)=\hat{A}(\mathbf{R},T;\mathbf{k},\omega)\hat{B}(\mathbf{R},T;\mathbf{k},\omega)-\frac{i}{2}\frac{\partial\hat{A}}{\partial\mathbf{k}}(\mathbf{R},T;\mathbf{k},\omega)\frac{\partial\hat{B}}{\partial\mathbf{R}}(\mathbf{R},T;\mathbf{k},\omega)$$
$$+\frac{i}{2}\frac{\partial\hat{A}}{\partial\omega}(\mathbf{R},T;\mathbf{k},\omega)\frac{\partial\hat{B}}{\partial T}(\mathbf{R},T;\mathbf{k},\omega)+\frac{i}{2}\frac{\partial\hat{A}}{\partial\mathbf{R}}(\mathbf{R},T;\mathbf{k},\omega)\frac{\partial\hat{B}}{\partial\mathbf{k}}(\mathbf{R},T;\mathbf{k},\omega)$$
$$-\frac{i}{2}\frac{\partial\hat{A}}{\partial T}(\mathbf{R},T;\mathbf{k},\omega)\frac{\partial\hat{B}}{\partial\omega}(\mathbf{R},T;\mathbf{k},\omega), \tag{3.26}$$

or in a more compact form is given by,

$$C(\mathbf{R},T;\mathbf{k},\omega)=\hat{A}\hat{B}+\frac{1}{2i}(\frac{\partial\hat{A}}{\partial\mathbf{k}}\frac{\partial\hat{B}}{\partial\mathbf{R}}-\frac{\partial\hat{A}}{\partial\omega}\frac{\partial\hat{B}}{\partial T}-\frac{\partial\hat{A}}{\partial\mathbf{R}}\frac{\partial\hat{B}}{\partial\mathbf{k}}+\frac{\partial\hat{A}}{\partial T}\frac{\partial\hat{B}}{\partial\omega}). \tag{3.27}$$

Eqs. (3.27) is referred to as the Wigner expansion. Consequently, by inspection, the terms of our quantum kinetic equation, given in Eq. (3.5), can be expressed in the new representation as follow,

$$[\hat{G}^R]^{-1}\otimes\hat{G}^K\approx[E-(E_k+\hat{\boldsymbol{\sigma}}\cdot\boldsymbol{\eta})-\hat{\Sigma}^R]\hat{G}^K(\mathbf{R},T;\mathbf{k},E)$$
$$+\frac{i}{2}\Big(\frac{\partial}{\partial\mathbf{k}}(E_k+\hat{\boldsymbol{\sigma}}\cdot\boldsymbol{\eta})\frac{\partial\hat{G}^K}{\partial\mathbf{R}}(\mathbf{R},T;\mathbf{k},E)+\frac{\partial\hat{G}^K}{\partial T}(\mathbf{R},T;\mathbf{k},E)\Big), \tag{3.28}$$
$$\hat{G}^K\otimes[\hat{G}^A]^{-1}\approx\hat{G}^K(\mathbf{R},T;\mathbf{k},E)[E-(E_k+\hat{\boldsymbol{\sigma}}\cdot\boldsymbol{\eta})-\hat{\Sigma}^A]$$
$$-\frac{i}{2}\Big(\frac{\partial\hat{G}^K}{\partial\mathbf{R}}(\mathbf{R},T;\mathbf{k},E)\frac{\partial}{\partial\mathbf{k}}(E_k+\hat{\boldsymbol{\sigma}}\cdot\boldsymbol{\eta})+\frac{\partial\hat{G}^K}{\partial T}(\mathbf{R},T;\mathbf{k},E)\Big), \tag{3.29}$$
$$\hat{\Sigma}^K\otimes\hat{G}^A\approx\Sigma^K(\mathbf{R},T;\mathbf{k},E)\hat{G}^A(\mathbf{R},T;\mathbf{k},E), \tag{3.30}$$
$$\hat{G}^R\otimes\hat{\Sigma}^K\approx\hat{G}^R(\mathbf{R},T;\mathbf{k},E)\hat{\Sigma}^K(\mathbf{R},T;\mathbf{k},E), \tag{3.31}$$

where we have considered the definition given in Eq. (3.7) and $E\equiv\hbar\omega$, with $\hbar=1$. For simplicity we consider $\hat{g}=\hat{G}^K(\mathbf{R},T;\mathbf{k},E)$, then the kinetic equation becomes,

$$[\hat{g}, \hat{\boldsymbol{\sigma}} \cdot \boldsymbol{\eta}(\boldsymbol{k})] + \frac{i}{\tau}\hat{g} + i\frac{\partial \hat{g}}{\partial T} + \frac{i}{2}\left\{\frac{\boldsymbol{k}}{m} + \alpha(\hat{\boldsymbol{z}} \times \hat{\boldsymbol{\sigma}}), \nabla_{\boldsymbol{R}}\hat{g}\right\} = \hat{\Sigma}^K\hat{G}^A - \hat{G}^R\hat{\Sigma}^K, \quad (3.32)$$

where $[\cdot,\cdot]$ and $\{\cdot,\cdot\}$ are the conmutator and anticommutator, respectively.

3.2.3 Density matrix

The relaxation time approximation indulges the right hand side of Eq.(3.5) as

$$\hat{\Sigma}^K\hat{G}^A - \hat{G}^R\hat{\Sigma}^K \approx \frac{1}{\tau}\left[\hat{\rho}(\epsilon, T, \boldsymbol{R})\hat{G}^A(\boldsymbol{k}, \epsilon) - \hat{G}^R(\boldsymbol{k}, \epsilon)\hat{\rho}(\epsilon, T, \boldsymbol{R})\right] \quad (3.33)$$

where we have introduced the density matrix by integrating out $\boldsymbol{k}'$ in $\hat{g}$, i.e.,

$$\hat{\rho}(E, T, \boldsymbol{R}) = \frac{1}{2\pi N_0}\int \frac{d^2\boldsymbol{k}'}{(2\pi)^2}\hat{g}_{\boldsymbol{k}',\epsilon}(T, \boldsymbol{R}), \quad (3.34)$$

For the convenience of discussion, the time variable is changed from T to t. At this stage, we have a kinetic equation depending on $\hat{\rho}$ and $\hat{g}$,

$$i[\hat{\boldsymbol{\sigma}} \cdot \boldsymbol{\eta}(\boldsymbol{k}), \hat{g}] + \frac{1}{\tau}\hat{g} + \frac{\partial \hat{g}}{\partial t} + \frac{1}{2}\left\{\frac{\boldsymbol{k}}{m} + \alpha(\hat{\boldsymbol{z}} \times \hat{\boldsymbol{\sigma}}), \nabla_{\boldsymbol{R}}\hat{g}\right\} = \frac{i}{\tau}\left[\hat{G}^R(\boldsymbol{k}, \epsilon)\hat{\rho}(\epsilon) - \hat{\rho}(\epsilon)\hat{G}^A(\boldsymbol{k}, \epsilon)\right]. \quad (3.35)$$

A Fourier transformation

$$\hat{g}(t) = \int \frac{d\omega}{2\pi}e^{-i\omega t}\hat{g}(\omega), \quad (3.36)$$

$$\hat{\rho}(t) = \int \frac{d\omega}{2\pi}e^{-i\omega t}\hat{\rho}(\omega), \quad (3.37)$$

leads to,

$$(\omega+\frac{i}{\tau})\hat{g}-\eta_k[\hat{U}_k,\hat{g}]=-\frac{i}{2}\left\{\frac{\boldsymbol{k}}{m}+\alpha(\hat{\boldsymbol{z}}\times\hat{\boldsymbol{\sigma}}),\nabla_{\boldsymbol{R}}\hat{g}\right\}-\frac{1}{\tau}\left[\hat{G}^R(\boldsymbol{k},\epsilon)\hat{\rho}(\epsilon)-\hat{\rho}(\epsilon)\hat{G}^A(\boldsymbol{k},\epsilon)\right]. \tag{3.38}$$

Simplifying the notation we have,

$$\Omega\hat{g}-\eta_k[\hat{U}_k,\hat{g}]=i\hat{K}, \tag{3.39}$$

where $\Omega=\omega+i/\tau$ and the operator $\hat{U}_k\equiv\hat{\boldsymbol{\sigma}}\cdot\hat{\boldsymbol{\eta}}$ satisfies $\hat{U}_k\hat{U}_k=1$. The right hand side of Eq.(3.39) is partitioned according to

$$\hat{K}=\underbrace{-\frac{1}{2}\left\{\frac{\boldsymbol{k}}{m}+\alpha(\hat{\boldsymbol{z}}\times\hat{\boldsymbol{\sigma}}),\nabla_{\boldsymbol{R}}\hat{g}\right\}}_{\hat{K}^{(1)}}+\underbrace{\frac{i}{\tau}\left[\hat{G}^R(\boldsymbol{k},\epsilon)\hat{\rho}(\epsilon)-\hat{\rho}(\epsilon)\hat{G}^A(\boldsymbol{k},\epsilon)\right]}_{\hat{K}^{(0)}}. \tag{3.40}$$

The equilibrium part is denoted by $\hat{K}^{(0)}$ and the gradient term $\hat{K}^{(1)}$ is treated as perturbation. Functions $\hat{g}$ and $\hat{\rho}$ are both in frequency domain.

We solve Eq. (3.39) formally to find a solution to $\hat{g}$

$$\hat{g}=i\frac{(2b_k^2-\Omega^2)\hat{K}+2b_k^2\hat{U}_k\hat{K}\hat{U}_k-\Omega b_k[\hat{U}_k,\hat{K}]}{\Omega(4b_k^2-\Omega^2)}\equiv\mathscr{L}[\hat{K}]. \tag{3.41}$$

An iteration procedure to solve Eq.(3.41) has been outlined in Ref. [73]. We adopt the procedure here: according to the partition scheme of $\hat{K}$, we use $\hat{K}^{(0)}$ to obtain the zeroth order approximation given by $\hat{g}^{(0)}\equiv\mathscr{L}[\hat{K}^{(0)}(\hat{\rho})]$ which replaces $\hat{g}$ in $\hat{K}^{(1)}$ to generate a correction due to the gradient term, i.e., $\hat{K}^{(1)}(\hat{g}^{(0)})$; we further insert $\hat{K}^{(1)}(\hat{g}^{(0)})$ back to Eq.(3.41) to obtain a correction $\mathscr{L}[\hat{K}^{(1)}(\hat{g}^{(0)})]$, then we have the

first order approximation to the quasiclassical distribution function,

$$\hat{g}^{(1)} = \hat{g}^{(0)} + \mathscr{L}[\hat{K}^{(1)}(\hat{g}^{(0)})]. \tag{3.42}$$

The above procedure is repeated to desired orders using

$$\hat{g}^{(n)} = \hat{g}^{(n-1)} + \mathscr{L}[\hat{K}^{(1)}(\hat{g}^{(n-1)})]. \tag{3.43}$$

In this work, the second order approximation is sufficient. The full expression of the second order approximation for $\hat{g}$ is tedious thus to be excluded in the following.

3.2.4 Diffusion equations

The diffusion equation is derived by an angle averaging in momentum space, which allows all terms that are of odd order in k_i $(i = x, y)$ to vanish while the combinations such as $k_i k_j$ contribute to the averaging by a factor $k_F^2 \delta_{ij}$ [74].

Furthermore, a Fourier transform from frequency domain back to the real time brings a diffusion-like equation for the density matrix,

$$\begin{aligned}\frac{\partial}{\partial t}\hat{\rho}(t) =& D\nabla^2\hat{\rho} - \frac{1}{\tau_{DP}}\hat{\rho} + \frac{1}{2\tau_{DP}}(\hat{\boldsymbol{z}}\times\hat{\boldsymbol{\sigma}})\cdot\hat{\rho}(\hat{\boldsymbol{z}}\times\hat{\boldsymbol{\sigma}}) + iC\left[\hat{\boldsymbol{z}}\times\hat{\boldsymbol{\sigma}}, \boldsymbol{\nabla}\hat{\rho}\right] - B\left\{\hat{\boldsymbol{z}}\times\hat{\boldsymbol{\sigma}}, \boldsymbol{\nabla}\hat{\rho}\right\} \\ &+ \Gamma\left[(\boldsymbol{m}\times\boldsymbol{\nabla})_z\hat{\rho} - \hat{\boldsymbol{\sigma}}\cdot\boldsymbol{m}\boldsymbol{\nabla}\hat{\rho}\cdot(\hat{\boldsymbol{z}}\times\hat{\boldsymbol{\sigma}}) - (\hat{\boldsymbol{z}}\times\hat{\boldsymbol{\sigma}})\cdot\boldsymbol{\nabla}\hat{\rho}\hat{\boldsymbol{\sigma}}\cdot\boldsymbol{m}\right] \\ &+ \frac{1}{2\tau_\phi}\left(\hat{\boldsymbol{\sigma}}\cdot\boldsymbol{m}\hat{\rho}\hat{\boldsymbol{\sigma}}\cdot\boldsymbol{m} - \hat{\rho}\right) - i\tilde{\Delta}_{xc}[\hat{\boldsymbol{\sigma}}\cdot\boldsymbol{m}, \hat{\rho}] - 2R\left\{\hat{\boldsymbol{\sigma}}\cdot\boldsymbol{m}, (\boldsymbol{m}\times\boldsymbol{\nabla})_z\hat{\rho}\right\},\end{aligned} \tag{3.44}$$

where all quantities are evaluated at Fermi energy ϵ_F. In a two-dimensional system, the diffusion constant $D = \tau v_F^2/2$ is given in terms of Fermi velocity v_F and momentum relaxation time τ. The renormalized exchange splitting reads $\tilde{\Delta}_{xc} =$

$(\Delta_{xc}/2)/(4\xi^2+1)$ where $\xi^2=(\Delta_{xc}^2/4+\alpha^2k_F^2)\tau^2$. The other parameters are given by

$$\begin{aligned} C =&\frac{\alpha k_F v_F\tau}{(4\xi^2+1)^2},\ \Gamma=\frac{\alpha\Delta_{xc}v_Fk_F\tau^2}{2(4\xi^2+1)^2},\\ R =&\frac{\alpha\Delta_{xc}^2\tau^2}{2(4\xi^2+1)},\ B=\frac{2\alpha^3k_F^2\tau^2}{4\xi^2+1},\\ \frac{1}{\tau_{DP}} =&\frac{2\alpha^2k_F^2\tau}{4\xi^2+1},\ \frac{1}{\tau_\phi}=\frac{\Delta_{xc}^2\tau}{4\xi^2+1}. \end{aligned}$$

τ_{DP} is the relaxation time due to the D'yakonov-Perel mechanism [75]. Equation (3.44) is valid in the dirty limit $\xi\ll 1$, which enables the approximation $1+4\xi^2\approx 1$. Charge density n and the nonequilibrium spin density $\boldsymbol{S}$ are introduced by the vector decomposition of the density matrix $\hat{\rho}=n/2+\boldsymbol{S}\cdot\hat{\boldsymbol{\sigma}}$. In real experiments [46], spin transport in a ferromagnetic film suffers from random magnetic scatterers, for which we introduce, phenomenologically, an isotropic spin-flip relaxation $\boldsymbol{S}/\tau_{sf}$.

Eventually, we obtain a set of diffusion equations for the charge and spin densities of the form [48],

$$\frac{\partial n}{\partial t}=D\nabla^2 n+B\boldsymbol{\nabla}_z\cdot\boldsymbol{S}+\Gamma\boldsymbol{\nabla}_z\cdot\boldsymbol{m}n+R\boldsymbol{\nabla}_z\cdot\boldsymbol{m}(\boldsymbol{S}\cdot\boldsymbol{m}), \tag{3.45}$$

and

$$\begin{aligned} \frac{\partial\boldsymbol{S}}{\partial t}=&D\nabla^2\boldsymbol{S}-\frac{\boldsymbol{S}_\parallel}{\tau_\parallel}-\frac{\boldsymbol{S}_\perp}{\tau_\perp}-\Delta_{xc}\boldsymbol{S}\times\boldsymbol{m}-\frac{\boldsymbol{m}\times(\boldsymbol{S}\times\boldsymbol{m})}{\tau_\phi}+B\boldsymbol{\nabla}_z n+2C\boldsymbol{\nabla}_z\times\boldsymbol{S}\\ &+2R(\boldsymbol{m}\cdot\boldsymbol{\nabla}_z n)\boldsymbol{m}+\Gamma\left[\boldsymbol{m}\times(\boldsymbol{\nabla}_z\times\boldsymbol{S})+\boldsymbol{\nabla}_z\times(\boldsymbol{m}\times\boldsymbol{S})\right], \end{aligned} \tag{3.46}$$

where $\boldsymbol{\nabla}_z\equiv\hat{\boldsymbol{z}}\times\boldsymbol{\nabla}$. The spin density $\boldsymbol{S}_\parallel\equiv S_x\hat{\boldsymbol{x}}+S_y\hat{\boldsymbol{y}}$ is relaxed at a rate $1/\tau_\parallel\equiv 1/\tau_{DP}+1/\tau_{sf}$ while $\boldsymbol{S}_\perp\equiv S_z\hat{\boldsymbol{z}}$ has a rate $1/\tau_\perp\equiv 2/\tau_{DP}+1/\tau_{sf}$.

For a broad range of the relative strength between the spin-orbit coupling and the exchange splitting, i.e., $\alpha k_F/\Delta_{xc}$, Eq.(3.45) and Eq.(3.46) describe the spin dynamics in a ferromagnetic film. When the magnetism vanishes ($\Delta_{xc}=0$), the B term provides

a source that generates spin density electrically [76, 73]. On the other hand, when the Rashba spin-orbit coupling is absent ($\alpha = 0$), the first two lines in Eq.(3.46) describe a diffusive motion of spin density in a ferromagnetic metal, which agrees excellently with early results [77]. The C term describes the coherent precession of the spin density around the effective Rashba field. The precession of the spin density (induced by the Rashba field) around the exchange field is described by the Γ term, is thus at a higher order (compared to C) in the dirty limit for $\Gamma = \Delta_{xc}\tau C/2$. The R term contributes to the magnetization renormalization, and τ_ϕ is the dephasing term [78].

3.2.5 Spin-orbit torques

The spin torque exerted on the local magnetization by the nonequilibrium spin density is given by

$$\boldsymbol{T} = \Delta_{xc}\boldsymbol{S} \times \hat{\boldsymbol{m}} + \frac{1}{\tau_\phi}\hat{\boldsymbol{m}} \times (\boldsymbol{S} \times \hat{\boldsymbol{m}}), \tag{3.47}$$

which takes into account a fieldlike spin precession (first term) and dephasing of the transverse component (second term). At a stationary state $\partial \boldsymbol{S}/\partial t = 0$, Eq. (3.46), in the weak Rashba regime ($\alpha k_F < \Delta_{xc}$) leads to

$$\boldsymbol{T} = T_\parallel \boldsymbol{m} \times (\hat{\boldsymbol{y}} \times \boldsymbol{m}) + T_\perp \hat{\boldsymbol{y}} \times \boldsymbol{m}, \tag{3.48}$$

where $\boldsymbol{m}$ is the magnetization direction and $\hat{\boldsymbol{y}}$ is the directional unit vector, see Fig. 3.1(a). Two components in Eq.(3.48) are usually referred to as *in-plane* ($T_\parallel$) and *out-of-plane* ($T_\perp$) torques, which is in agreement with experiments and theories reported initially [46, 48, 47]. In the following section we will show that in the strong Rashba regime ($\alpha k_F > \Delta_{xc}$) anisotropic spin relaxation rates driven by the Rashba spin-orbit coupling assign the spin torque a general expression $\boldsymbol{T} = T_\parallel^y(\theta)\boldsymbol{m} \times (\hat{\boldsymbol{y}} \times \boldsymbol{m}) + T_\perp^y(\theta)\hat{\boldsymbol{y}} \times \boldsymbol{m} + T_\parallel^z(\theta)\boldsymbol{m} \times (\hat{\boldsymbol{z}} \times \boldsymbol{m}) + T_\perp^z(\theta)\hat{\boldsymbol{z}} \times \boldsymbol{m}$, where the coefficients $T_{\parallel,\perp}^{y,z}$

depend on the magnetization direction.

3.3 Results and discussion

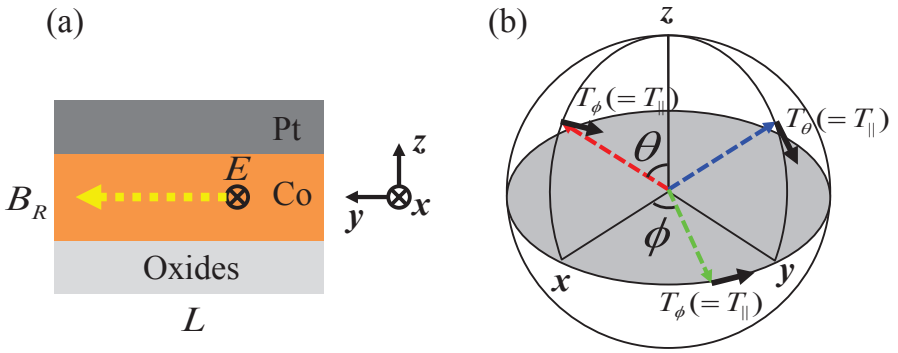

Figure 3.1: (Color online)(a) Schematic view the device cross section. A charge current is flowing along the x direction, generating an effective Rashba field $\boldsymbol{B}_R$ (dotted yellow line) that is pointing to y. L is the size of the lateral dimensions. (b) Spin torque components $\boldsymbol{T}_{\boldsymbol{\phi}}$ and $\boldsymbol{T}_{\boldsymbol{\theta}}$ in a spherical coordinate, with θ and ϕ being the azimuthal and the in-plane angle, respectively. Dashed lines show the magnetization directions.

A schematic view of the device is shown in Fig. 3.1(a). The inversion asymmetry across the interfaces generates a Rashba type spin-orbit coupling from the potential gradient along the $\hat{\boldsymbol{z}}$ direction. In this quasi-two-dimensional system, the diffusive dynamics of nonequilibrium spin density $\boldsymbol{S}$ and charge density n are described by Eqs. (3.45) and (3.46). First, we numerically solve these equations to demonstrate that they provide a coherent framework to describe the spin-dynamics in the diffusive regime for a wide range of parameters. Here, we consider an in-plane magnetization that lies along the $\hat{\boldsymbol{x}}$ direction. Using finite element methods in COMSOL, for a two-dimensional electron system we adopt the following boundary conditions: (i) vanishing spin accumulation at the edges along the transverse direction i.e., $\mathcal{S}(y = 0, L) = 0$; (ii) an electric field is implemented along the $\hat{\boldsymbol{x}}$ direction therefore we set the charge densities at two ends of the propagation direction to be constant $n_L = n_R = n_F$. Equivalently, one can use a voltage drop (along the transport

direction) instead of the explicit inclusion of an electric field. The first boundary condition implies a strong spin-flip scattering at the edges, which is consistent with the experimental observations in spin-Hall effect [79]. The second boundary condition sets the charge density at the Fermi level.

The numerical results of nonequilibrium spin densities are summarized in Fig. 3.2. When viewing from the top panels (i.e., (a) and (b)) to the lower ones (i.e., (c) and (d)), for a fixed value of exchange splitting, we are moving across from the regime of a weak spin-orbit coupling (i.e., *weak coupling*) to the opposite limit of a strong spin-orbit coupling (i.e., *strong coupling*). It is rather clear from, for example panel (c), that in the strong coupling regime, the spin-Hall signature emerges, i.e., the S_z is peaked at boundaries while S_y is robust in the bulk.

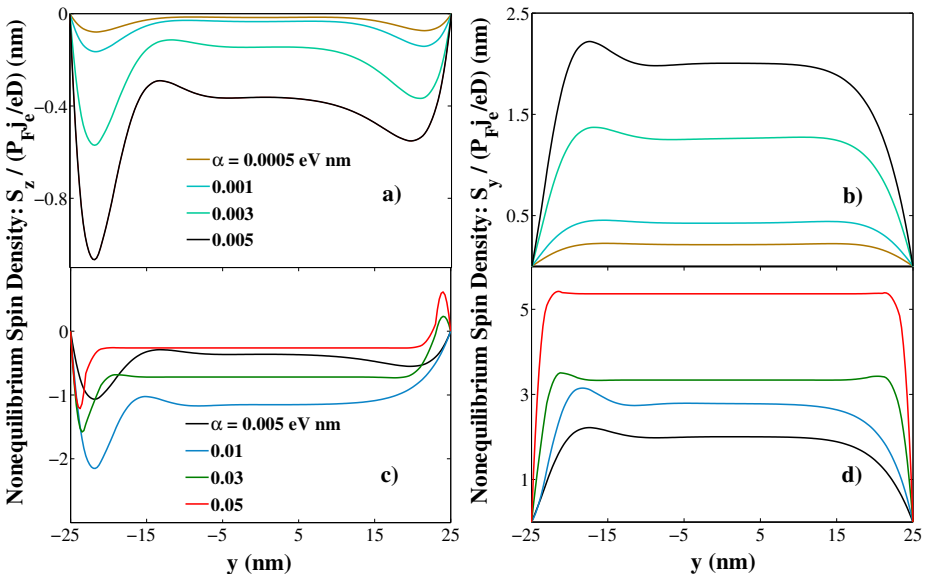

Figure 3.2: (color online). Spatial profile of the nonequilibrium spin density S_z (a),(c) and S_y (b),(d) for various values of the Rashba constant. The width of the wire is $L = 50$ nm. The magnetization direction is along the $\hat{\boldsymbol{x}}$ axis. Other parameters are: momentum relaxation time $\tau = 10^{-15}$ s, exchange splitting $\Delta_{xc} = 0.01$ eV, spin relaxation time $\tau_{sf} = 10^{-12}$ s, and the Fermi vector $k_F = 4.3$ nm^{-1}.

The symmetry distortion is a manifestation of the competition of the Rashba and exchange fields. In the weak coupling regime, the total field is dominated by the exchange field pointing at the $\hat{\boldsymbol{x}}$ direction, around which yields a spin accumula-

tion profile that is symmetric. This is reflected by the curves with small α in Figs. 3.2(a)(b). As the spin-orbit coupling increases, the total field is tilted towards the $\hat{\boldsymbol{y}}$ axis, then the spin projection along $+y$ and $-y$ is no longer symmetric, as indicted by curves with intermediate α values in Figs. 3.2(a)(b). When the system is ruled by a large α over the exchange field, the antisymmetric profile in S_z and the symmetric one of S_y follow naturally from the spin-Hall effect induce by a Rashba spin-orbit coupling.

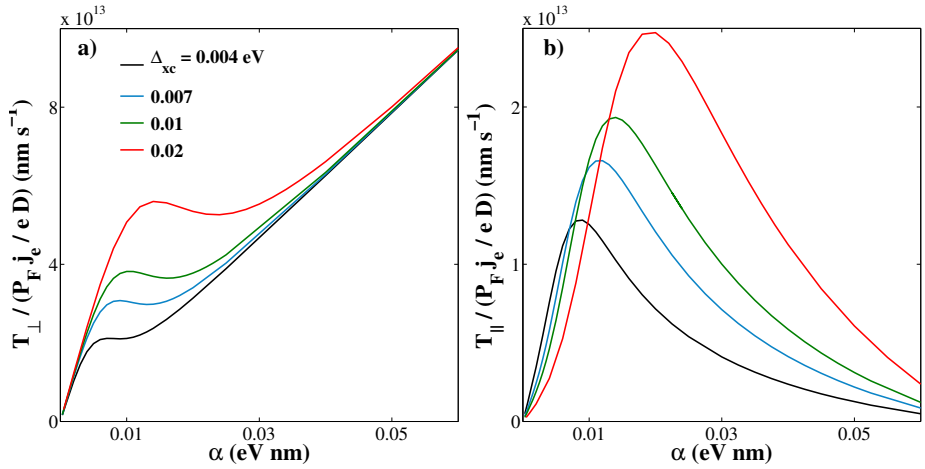

Figure 3.3: (color online). The magnitude of the out-of-plane torque $T_\perp$ (a) and in-plane torque $T_\parallel$ (b) as a function of Rashba constant for various exchange splitting. Other parameters are the same as in Fig. 3.2.

The out-of-plane and in-plane torques, given in Eq. (3.47) are plotted in Fig. 3.3 as functions of the Rashba constant for various exchange splitting. The transition regions are of particular interest. During the transition from the weak to strong coupling, the out-of-plane torque $T_\perp$ (see Fig. 3.3(a)) first experience a decrease in the magnitude then rises again as the α increases. In the large α limit, though the magnitude of the torque increases with α, the torque efficiency defined as $dT_\perp/d\alpha$ is actually smaller than it is in the weak coupling. The in-plane torque $T_\parallel$ behaves differently. In the strong coupling limit, $T_\parallel$ is proportional to $1/\alpha$ due to the large D'yakonov-Perel spin relaxation rate that is of the order α^2. Therefore a stronger spin-orbit coupling means a decrease in the torque magnitude. In fact, the transition

suggests that the optimal magnitude of the in-plane torque is achieved when the exchange energy is about the same order of magnitude of the Rashba splitting αk_F.

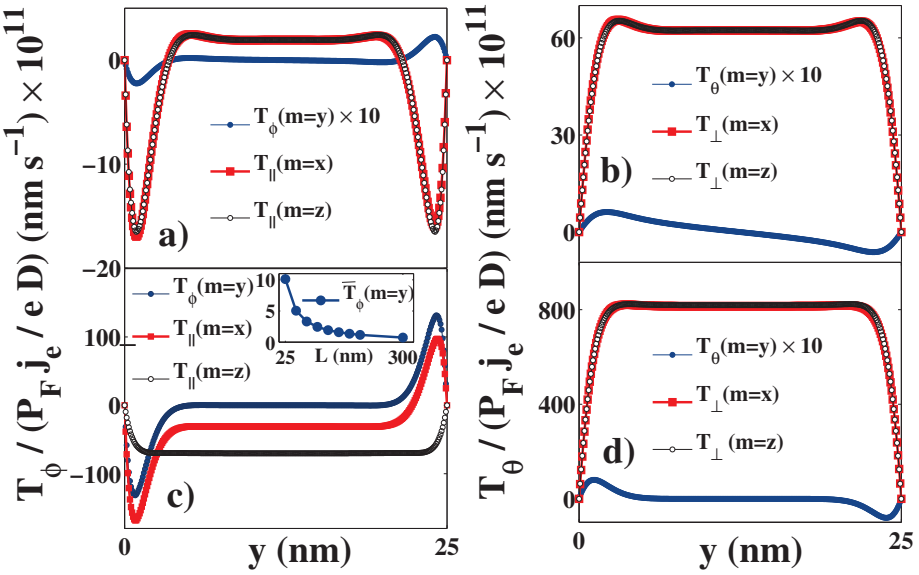

Figure 3.4: (Color online) Spatial distribution of the Rashba torque along the y axis in a $yz-$ plane located at the center of the device of size $L = 25$ nm. Panels (a) and (c) refer to the *in-plane* component (here $T_{\parallel} \equiv T_{\phi}$). Panels (b) and (d) are for the *out-of-plane* component ($T_{\perp} \equiv T_{\theta}$). Panels (a) and (b): weak Rashba regime ($\alpha = 0.001$ eV nm, $\Delta_{xc} = 0.1$ eV). Panels (c) and (d): strong coupling ($\alpha = 0.05$ eV nm, $\Delta_{xc} = 0.01$ eV). The inset in panel (c) displays: $\overline{T}_{\phi(m=y)} = (1/L)\int_{y=L/2}^{y=L} T_{\phi(m=y)} dy$ for different widths. In panels (a),(b) and (d), $T_{\phi(m=y)}$ is multiplied by a factor 10. The Fermi energy is $E_F = 0.7$ eV, $k_F = 4.3$ nm^{-1} and $v_F = 5 \times 10^{14}$ nm s^{-1}. $\tau = 10^{-15}$ s and $\tau_{sf} = 10^{-12}$ s.

We now discuss the symmetries and the angular dependence of the Rashba torque. Here we argue that reducing the size of the device further changes the *symmetry* of the torque. To support our argument, we plot in Fig. 3.4 the spatial distribution of the spin torque density along the y axis in the $yz-$plane, for various magnetization directions in both weak ($\Delta_{xc} \gg \alpha k_F$) and strong ($\Delta_{xc} \ll \alpha k_F$) coupling regimes. In Fig. 3.1(b), the spin torque density $\boldsymbol{T} = T_{\phi}\hat{\boldsymbol{e}}_{\phi} + T_{\theta}\hat{\boldsymbol{e}}_{\theta}$ is in a spherical coordinate that is more general than Eq. (3.48). On the right column of Fig. 3.4, T_{θ} is robust in the bulk, resulting from a robust nonequilibrium spin density S_y driven by the spin-galvanic effect discussed by Edelstein [76]. This effect disappears towards the boundaries, as

imposed by the boundary conditions [79]. An important feature in Fig. 3.4 appears to be the nonvanishing spin torque at the edges even when the magnetization $\boldsymbol{m}$ is parallel to $\boldsymbol{B}_R$, see the deep blue curves. In general, as the angle between the exchange field $\boldsymbol{m}$ and $\boldsymbol{B}_R$ closes, the spin torque amplitude decreases. For a strong spin-orbit coupling, the spin-Hall effect drives oppositely polarized spin densities S_z accumulating at opposite edges [49]. In our finite-size device, within the distance of spin-flip relaxation length from the edges, the spin density S_z distributed along the y direction generates a nonvanishing local spin torque at the edges even when $\boldsymbol{m}$ is aligned parallel to $\boldsymbol{B}_R$. As the spin-orbit coupling weakens, torques at $\boldsymbol{m} \parallel \boldsymbol{B}_R$ driven by the spin-Hall effect become negligible, see Fig. 3.4(a). Meanwhile, as the sample size increases $L \gg \lambda_{sf}$, the expression $\overline{T}_{\phi(m=y)} = (1/L)\int_{y=L/2}^{y=L} T_{\phi(m=y)} dy$ decreases, see inset in Fig. 3.4(c). Another feature is the inhomogeneous profile of T_ϕ, which is driven by the competition between the spin-Hall effect and spin precession around the total field. The spin-Hall effect (precession around the total field) is dominant in the strong (weak) Rashba regime. When $\boldsymbol{m} = \hat{\boldsymbol{z}}$, spin density S_z does not contribute to the spin-Hall induced torque and the in-plane torque becomes homogeneous, as confirmed by the solid black line in Fig. 3.4(c). In a finite-size device, these effects contribute to the angular dependence discussed in the following.

First, in an infinite system with a weak Rashba spin-orbit coupling, once the anisotropy in spin relaxation rates due to the D'yakonov-Perel mechanism is quenched, Eq. (3.46) gives rise to a torque described by Eq. (3.48) [48]. However, as the spin relaxation rate becomes anisotropic, the torque assumes a complex angular dependence. By setting $\boldsymbol{\nabla}_{xy} = \hat{\boldsymbol{z}} \times eE\partial_\epsilon \hat{\boldsymbol{x}}$, Eq. (3.46) reduces to

$$\frac{1}{\tau_\Delta}\boldsymbol{S} \times \boldsymbol{m} + \frac{1}{\tau_\varphi}\boldsymbol{m} \times (\boldsymbol{S} \times \boldsymbol{m}) + \frac{1}{\tau_{xy}} S_x \boldsymbol{x} + \frac{1}{\tau_{xy}} S_y \hat{\boldsymbol{y}} + \frac{1}{\tau_z} S_z \hat{\boldsymbol{z}} = \boldsymbol{X}, \tag{3.49}$$

where $\tau_\Delta = 1/\Delta_{xc}$ and last three terms on the left hand side subscribe to both the D'yakonov-Perel mechanism and spin relaxation induced by random magnetic impurities: $\tau_{xy}^{-1} = \tau_{DP}^{-1} + \tau_{sf}^{-1}$ and $\tau_z^{-1} = 2\tau_{DP}^{-1} + \tau_{sf}^{-1}$. On the right hand side,

$$\begin{aligned}\boldsymbol{X} \equiv \frac{neE}{\epsilon_F}(&B\hat{\boldsymbol{y}} + \Gamma P_F \boldsymbol{m} \times \hat{\boldsymbol{y}} \times \boldsymbol{m} \\ &+ 2CP_F \hat{\boldsymbol{y}} \times \boldsymbol{m} + 2Rm_y \boldsymbol{m}),\end{aligned} \tag{3.50}$$

where P_F is the spin polarization at Fermi energy ϵ_F. Analytical solutions to Eq. (3.49) in the strong coupling limit ($B, C \gg \Gamma, R$) gives rise to a spin torque of the form

$$\begin{aligned}\boldsymbol{T} =& \frac{neE}{\epsilon_F}\epsilon_\theta[(\tilde{C}\kappa + B\tilde{\beta})\hat{\boldsymbol{y}} \times \boldsymbol{m} + (B\kappa - \tilde{C}\tilde{\beta})\boldsymbol{m} \times \hat{\boldsymbol{y}} \times \boldsymbol{m} \\ &- \alpha_\theta((B\kappa - \tilde{C}\tilde{\beta})m_y m_z + B\tilde{\beta}m_x)\boldsymbol{m} \times \hat{\boldsymbol{z}} \times \boldsymbol{m} \\ &+ \tilde{\beta}\alpha_\theta(-(\tilde{C}\delta + B)m_y m_z + B\delta m_x)\hat{\boldsymbol{z}} \times \boldsymbol{m}],\end{aligned} \tag{3.51}$$

where $\tilde{C} = 2CP_F$, $\epsilon_\theta = \frac{1}{1+\xi\tilde{\beta}\alpha_\theta \sin^2\theta}$, $\alpha_\theta = \frac{\chi}{\beta+\chi\cos^2\theta}$, $\xi = \frac{\tau_\Delta}{\tau_\varphi} + \frac{\tau_\Delta}{\tau_{xy}}$, $\beta = \frac{\tau_\Delta}{\tau_{xy}}$, $\chi = \frac{\tau_\Delta}{\tau_z} - \frac{\tau_\Delta}{\tau_{xy}} = \frac{\tau_\Delta}{\tau_{DP}}$, $\tilde{\beta} = \frac{\beta}{1+\xi^2}$, $\kappa = 1 - \xi\tilde{\beta}$, and $\delta = \xi - \beta$.

Equation (3.51) comprises one of the major results in this letter. The spin torque in Eq. (3.51) consists of both odd and even components with respect to the inversion of magnetization direction $\boldsymbol{m}$, which agrees with Eqs. (9) and (10) proposed by Garello *et al* in Ref. [69]. In particular, in Eq. (3.51) the first term (out-of-plane torque) is a direct consequence of the spin-galvanic effect [44, 76] meeting magnetism and the second term (in-plane torque) originates from the Slonczewski-Berger type spin-transfer torque accounting spin-dephasing. The last two terms arise from the anisotropic spin relaxation that allows for the generation of spin density components perpendicular to both $\boldsymbol{m}$ and $\boldsymbol{B}_R$ [80]. It is worthy pointing out that the relative

magnitude of the torque components is material-dependent and their complex angular dependence is determined by the anisotropy in spin-relaxation times. By setting $\tau_z \approx \tau_{xy}$ ($\chi \ll 1$) to suppress the anisotropy, the complex angular dependence vanishes and the torque reduces to

$$\boldsymbol{T} = \frac{neE}{\epsilon_F}\left(A_\perp \hat{\boldsymbol{y}} \times \boldsymbol{m} + A_\parallel \boldsymbol{m} \times \hat{\boldsymbol{y}} \times \boldsymbol{m}\right), \tag{3.52}$$

where $A_\perp = \tilde{C}\kappa + B\tilde{\beta}$ and $A_\parallel = B\kappa - \tilde{C}\tilde{\beta}$. In our model, this anisotropic spin relaxation is driven by the D'yakonov-Perel mechanism in the presence of a Rashba spin-orbit coupling [75]. We note here that Eq. (3.51) is obtained in a sample of infinite size.

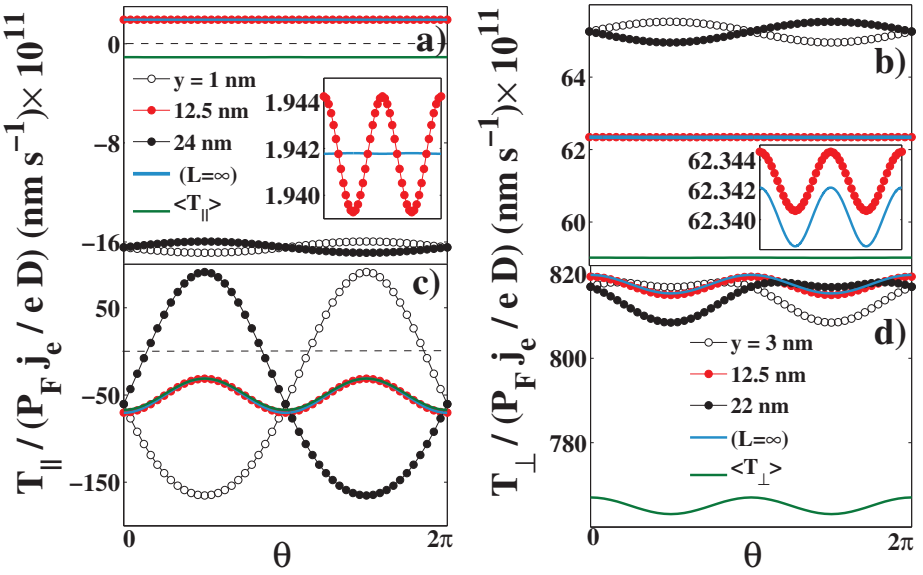

Figure 3.5: (Color online) Angular dependence of spin torque as $\boldsymbol{m}$ varies in the $xz-$plane in a system with $L = 25$ nm. Panels (a) and (c): in-plane torque; panels (b) and (d): out-of-plane component. Panels (a) and (b): weak Rashba regime; panels (c) and (d): strong Rashba regime. Solid red curves are taken at the center of the device. Empty and solid black dots are taken at positions near two edges along the y direction. Insets in panels (a) and (b) refer to the zoom in of solid red and solid cyan curves ($L = \infty$). Solid green lines display the magnitude of the average spin torque, defined as $\langle T_{\parallel(\perp)}\rangle = (1/L)\int_0^L T_{\parallel(\perp)} dy$, for $L = 25$ nm.

We show in Fig. 3.5 that the angular dependence of the Rashba torque also

exists in a *finite*-size device. In addition, we also explain in Fig. 3.5 the symmetry properties of the spin torque at sample edges and analyze the angular dependence for various $\boldsymbol{m}$ in the $xz-$plane at three particular locations in the device: in the center at $x, y = 12.5$ nm to highlight the *bulk* values, and two other locations near the edges along y at $x = 12.5$ nm.

In the weak Rashba regime, when $\boldsymbol{m}$ is along $\hat{\boldsymbol{z}}$, the spin density components that contribute to the torque show a symmetric profile [48]. As $\boldsymbol{m}$ moves towards the $\hat{\boldsymbol{x}}$ direction, the spin density generated perpendicular to $(\boldsymbol{m}, \boldsymbol{B}_R)$ points to the $\hat{\boldsymbol{z}}$ direction. In contrast to the case when $\boldsymbol{m} = \hat{\boldsymbol{z}}$, the faint presence of spin-Hall effect, however, renders the profile on one edge more negative than the other, which contributes to the angular dependence at the device edge, as depicted by the open and filled black dots in Fig. 3.5(a)(b). In the strong Rashba regime, the spin-Hall effect is dominating, producing a more pronounced angular dependence, as shown by the open and filled black dots in Fig. 3.5(c)(d).

To illustrate the above effects when the magnetization is in the $xz-$ plane, we study the angular dependence in the bulk for different device sizes (in Fig. 3.5, $L = 25$ nm and $L = \infty$, only). In the strong Rashba regime, D'yakonov-Perel spin relaxation rules, the angular dependence is pronounced and insensitive to the change in device size, which shall eventually approach the limit characterized by Eq. (3.51). In contrast, in the weak Rashba regime the relaxation rate is mostly isotropic, which results in a weak angular dependence vanishing as the size increases. These numerical results are consistent with the argument that the angular dependence of spin torque in the bulk is driven by the anisotropy in spin relaxation rate. Furthermore, in a finite system with isotropic spin relaxation rates, oscillations may arise due to edge effects diffusing towards the center and such a phenomenon is better seen in the weak Rashba regime depicted in the inset in Fig. 3.5(a).

We summarize in Fig. 3.6 the angular dependence of the spin torque density in

the bulk as $\boldsymbol{m}$ rotates in the $xz-$, $xy-$ and $yz-$ planes. First we describe the strong Rashba regime where a general trend emerges: the in-plane component $T_{\parallel}$ has a more pronounced angular dependence than $T_{\perp}$, see Figs. 3.6(c)(d). For the parameters used here ($\tau_{DP} \ll \tau_{sf}, \tau_{\phi}$), we reduce the expressions by taking $\epsilon_{\theta} \approx (1+\cos^2\theta)/2$, and obtain

$$T_{\parallel}^{xy(xz)} \approx \frac{neE}{\epsilon_F}\frac{A_{\parallel}}{2}(1+\cos^2\theta), \quad T_{\parallel}^{yz} \approx \frac{neE}{\epsilon_F}A_{\parallel}, \tag{3.53}$$

$$T_{\perp}^{xy(xz)(yz)} \approx \frac{neE}{\epsilon_F}\left(\tilde{\beta}B + \tilde{C}\kappa\frac{\cos^2\theta}{2}\right), \tag{3.54}$$

which indicates that the angular dependence is determined by $A_{\parallel}$ and $A_{\perp}$ components, respectively. In the weak Rashba regime ($B \sim 0$) the angular dependence is driven by higher order terms, i.e. the variation of the in-plane torque in the $yz-$ plane is much more significant due to the $R-$term contribution, see Fig. 3.6(a).

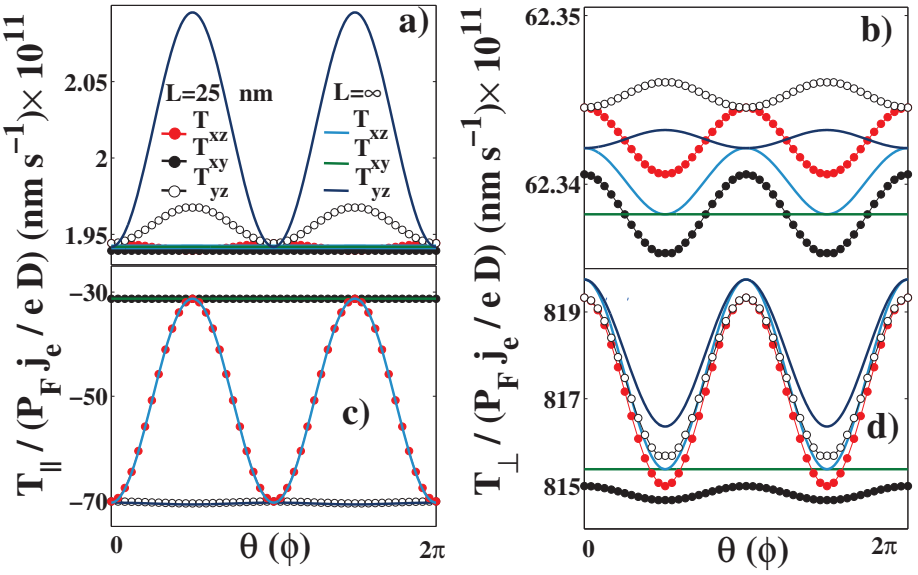

Figure 3.6: (Color online) Angular dependence in the bulk as $\boldsymbol{m}$ varies in the xz, xy and yz planes for $L = 25$ nm and $L = \infty$. The horizontal axis is defined as ϕ (θ) for the xy (xz and yz) case(s). Panels (a) and (c): in-plane torque; panels (b) and (d): out-of-plane torque. Panels (a) and (b): weak Rashba regime; panels (c) and (d): strong Rashba regime. T_{ij} refers to the spin torque when $\boldsymbol{m}$ is in the $ij-$ plane.

3.4 Conclusions

Using Keldysh technique, in the presence of both magnetism and a Rashba spin-orbit coupling, we derived a spin diffusion equation that provides a coherent description to the diffusive spin dynamics. In particular, we have derived a general expression for the Rashba torque in the bulk of a ferromagnetic metal layer, at both weak and strong Rashba limits. We found that the magnetization dynamics driven by the Rashba torque presents several interesting similarities to that induced by SHE torque [50]. We have shown also that the spin torque is nonvanishing at the edges of the sample even when the magnetization and the effective Rashba field are parallel, due to the spin-Hall effect. Furthermore, the symmetry and angular dependence of the spin torque are in general complex and consisting of more than the commonly accepted in-plane and out-of-plane components. In an infinite system, we have obtained an analytical expression for the spin-orbit torque that shows both odd and even components against magnetization inversion and agrees favorably with the empirical expression derived from experiments. We expect that results presented in this chapter not only provide a better understanding to the key mechanisms behind the experimental observations but also shed light on the design of realistic spin-orbit torque devices.

Chapter 4

Spin Swapping and Spin Hall Effect in Ferromagnetic Films

4.1 Introduction

The exploitation of spin-orbit coupling to probe and control the magnetization of nanodevices has been extensively studied, uncovering many physical properties and phenomena such as, but not limited to, anomalous Hall effect [81], spin Hall effect [82], tunneling anisotropic magnetoresistance [83], electrically controlled perpendicular magnetic anisotropy [84], and spin orbit torques (refer to §1.4). The latter, observed in multilayers comprising ferromagnets and heavy metals displayed both, spin orbit torques induced by interfacial inverse spin galvanic effect [46] and spin transfer torques induced by spin Hall effect [50]. In Chap. 3 we discussed the so called Rashba spin-orbit torque, which arises in the presence of intrinsic spin-orbit coupling and gives rise to an interfacial inverse spin galvanic effect [68, 85]. In this chapter we study a new kind of spin-orbit torque, recently discovered in normal metals (to the date of publication of this thesis) in the presence of extrinsic spin-orbit coupling [55]. Referred to as spin swapping torque, this torque acts in a similar way to the spin transfer torque induced by spin Hall effect. In this case however, the transverse spin current generated appears as a result of spin-spin conversion (refer to

§1.4 for major details). We discuss spin swapping torque in single layer ferromagnets in the presence of spin orbit coupled impurities, which may offer potential advantages in device design in contrast to normal metals and may open novel avenues in SOT-MRAM technology. To do so, we develop in §4.2 a set of drift-diffusion equations in systems involving spin-orbit coupled impurities and exchange interaction. The theory is developed considering quantum kinetic equations within Keldysh formalism and performing a Wigner expansion. In §4.3 we show that the interplay between spin swapping, spin Hall effect, and spin precession around the magnetization results in a rich spatial profile of the spin accumulation that can be exploited to generate spin torques. Of particular interest is the role of the geometry to control magnetization switching, an approach that is capturing more attention as it may lead to new ways of nucleating and propagating magnetic domain walls [97]. We show that a diamond-like structure may contribute to magnetization switching through the spin swapping-induced spin accumulation.

4.2 Quantum kinetic equation

In this section, considering a diffusive model based on Keldysh formalism under Wigner expansion, we develop analytical expressions for the spin and charge dynamics in ferromagnets in the presence of spin-orbit coupled impurities.

4.2.1 Unperturbed Green's function

The Hamiltonian of an unperturbed ferromagnet is given by,

$$H_0 = \frac{\mathbf{k^2}}{2m} + J\hat{\boldsymbol{\sigma}} \cdot \mathbf{m} \tag{4.1}$$

The first term in Eq. (4.1) represents the kinetic part, where $\mathbf{p} = \hbar\mathbf{k}$ is the momentum and m is the mass of the electron. Notice that throughout this chapter

we are going to consider $\hbar = 1$ and remove the "$\hat{}$" symbol in the operators. The second term is the s-d exchange interaction. J is the exchange coupling parameter, $\mathbf{m} = (m_x, m_y, m_z)$ is the magnetization unit vector, and $\hat{\boldsymbol{\sigma}} = (\sigma_x, \sigma_y, \sigma_z)$ is the Pauli matrix vector. This expression is similar to the one described in §2.2.1, where the sign difference is only a matter of convention. We first proceed to derive the unperturbed retarded (R) and advanced (A) Green's functions (G_0), defined as,

$$G^{R(A)}_{0,\mathbf{k}} = \frac{1}{\epsilon - H_0 \pm iO^+} = \frac{\sum_s \mid \psi\rangle^s \langle\psi \mid^s}{\epsilon - \epsilon_{\mathbf{k},\mathbf{s}} \pm iO^+}. \tag{4.2}$$

$\epsilon_{\mathbf{k}',s} = \frac{\mathbf{k'^2}}{2m} + sJ$ is the eigenenergy and $\mid \psi\rangle^s$ is the eigenstate of H_0, where index $s = \pm 1$ refers to the spin. Notice from Eq. (4.2) that in order to define a proper Green's function we first need to calculate the eigenstate $\mid \psi\rangle^s$. The analysis here is similar to §2.2.1, we therefore address directly the result,

$$\mid \psi\rangle^s = \begin{bmatrix} se^{-i\phi}\sqrt{\frac{1+s\cos\theta}{2}} \\ \sqrt{\frac{1-s\cos\theta}{2}} \end{bmatrix}. \tag{4.3}$$

Replacing Eq. (4.3) in Eq. (4.2), our unperturbed Green's functions become,

$$G^{R(A)}_{0,\mathbf{k}} = \frac{1}{2}\frac{\sum_s (I + s\hat{\boldsymbol{\sigma}} \cdot \boldsymbol{m})}{\epsilon - \epsilon_{\mathbf{k},\mathbf{s}} \pm iO^+}. \tag{4.4}$$

Using the Sokhatsky-Weierstrass theorem, for a small imaginary part the above equation simplifies to

$$G^{R(A)}_{0,\mathbf{k}} = \frac{1}{2}\sum_s (I + s\hat{\boldsymbol{\sigma}} \cdot \boldsymbol{m})\Big[\text{p.v.}(\frac{1}{\epsilon - \epsilon_{\mathbf{k},\mathbf{s}}}) \mp i\pi\delta(\epsilon - \epsilon_{\mathbf{k},s})\Big], \tag{4.5}$$

where the principal value (p.v.) only contributes to an energy shift that can be neglected by selecting an energy reference. Therefore,

$$G^{R(A)}_{0,\mathbf{k}} = \frac{1}{2}\sum_{s}(I + s\hat{\boldsymbol{\sigma}}\cdot\boldsymbol{m})\Big[\mp i\pi\delta(\epsilon - \epsilon_{\mathbf{k},s})\Big]. \tag{4.6}$$

Eq. (4.6) corresponds to the unperturbed Green's function of a ferromagnetic metal.

4.2.2 Spin orbit coupled impurities

We consider now a ferromagnet in the presence of spin-orbit coupled impurities. The Hamiltonian in real space is given by,

$$H = \frac{\mathbf{p}^2}{2m} + J\hat{\boldsymbol{\sigma}}\cdot\mathbf{m} + V(\mathbf{r}). \tag{4.7}$$

The first two terms are described in §4.2.1. The third term is the impurity potential which, for random distributed impurities, is defined as

$$V(\mathbf{r}) = \sum_{j}^{N}\Big[V_{\text{imp}}(\mathbf{r} - \mathbf{R_j}) + \xi\hat{\boldsymbol{\sigma}}\cdot(\nabla V_{\text{imp}}(\mathbf{r} - \mathbf{R_j})\times\mathbf{p})\Big]. \tag{4.8}$$

N is the number of impurities and V_{imp} is a general function that depends on the positions of the electron, $\mathbf{r}$, and of the random distributed impurities, $\mathbf{R}_j$. In Eq. (4.8), the second term appears in the presence of spin-orbit coupling only, where ξ is the spin-orbit coupling parameter, assumed independent of momentum and position. In reciprocal space we have,

$$V_{\mathbf{k},\mathbf{k}'} \equiv \langle\mathbf{k}|\hat{V}|\mathbf{k}'\rangle \equiv \int_V u^*_{\mathbf{k}}(\mathbf{r})V(\mathbf{r})u_{\mathbf{k}'}(\mathbf{r})d\mathbf{r}, \tag{4.9}$$

Eq. (4.9) represents the matrix element of V. If we consider a plane wave solution for the unperturbed problem, then the wave function is given by $u_{\mathbf{k}}(\mathbf{r}) = \frac{1}{\sqrt{\Omega}}e^{i\mathbf{kr}}$, where Ω is the volume of the sample. Therefore,

$$V_{\mathbf{k},\mathbf{k}'} = \frac{1}{\Omega}\sum_{j}^{N}\int_{V}\Big[e^{-i\mathbf{kr}}V_{\text{imp}}(\mathbf{r}-\mathbf{R_j})e^{i\mathbf{k}'\mathbf{r}} + e^{-i\mathbf{kr}}\xi\hat{\boldsymbol{\sigma}}\cdot(\nabla V_{\text{imp}}(\mathbf{r}-\mathbf{R_j})\times\mathbf{p})e^{i\mathbf{k}'\mathbf{r}}\Big]. \tag{4.10}$$

Considering short-range impurity scattering then $V_{\text{imp}}(\mathbf{r}-\mathbf{R_j}) = V_0\delta(\mathbf{r}-\mathbf{R_j})$, where V_0 is the magnitude, assumed constant and positive for all impurities. Eq. (4.10) simplifies to,

$$V_{\mathbf{k},\mathbf{k}'} = \frac{V_0}{\Omega}\sum_{j}^{N}\int_{V}\Big[e^{-i(\mathbf{k}-\mathbf{k}')\mathbf{r}}\delta(\mathbf{r}-\mathbf{R_j}) + e^{-i\mathbf{kr}}\xi\hat{\boldsymbol{\sigma}}\cdot(\nabla\delta(\mathbf{r}-\mathbf{R_j})\times\mathbf{k}')e^{i\mathbf{k}'\mathbf{r}}\Big]. \tag{4.11}$$

where we have replaced $\mathbf{p} = -i\frac{\partial}{\partial_{\mathbf{r}}}$ and noticed that this momentum operator acts in $e^{i\mathbf{k}'\mathbf{r}}$, i.e., $-i\frac{\partial e^{i\mathbf{k}'\mathbf{r}}}{\partial_{\mathbf{r}}} = \mathbf{k}'e^{i\mathbf{k}'\mathbf{r}}$. To solve Eq. (4.11) we consider the following properties of delta functions,

$$\int_{V} f(\mathbf{r})\delta(\mathbf{r}-\mathbf{r}_0) = f(\mathbf{r}_0), \tag{4.12}$$

$$\int_{V} f(\mathbf{r})[\nabla\delta(\mathbf{r}-\mathbf{r}_0)] = -\int_{V}\nabla f(\mathbf{r})[\delta(\mathbf{r}-\mathbf{r}_0)], \tag{4.13}$$

therefore,

$$V_{\mathbf{k},\mathbf{k}'} = \frac{V_0}{\Omega}\sum_{j}^{N} e^{-i(\mathbf{k}-\mathbf{k}')\mathbf{R}_j}u_{\mathbf{k},\mathbf{k}'}, \tag{4.14}$$

where $u_{\mathbf{k},\mathbf{k}'} = [1 - i\xi\hat{\boldsymbol{\sigma}}\cdot\boldsymbol{n}]$ and $\boldsymbol{n} = \mathbf{k}'\times\mathbf{k}$. In order to obtain macroscopic values, the potential must be averaged over the possible positions that the impurities may have in the solid. This was derived by Kohn and Luttinger in 1957 [86]. They

assumed the impurities to be identical, and therefore the averaging only involved the phase factor $\sum_j^N e^{-i\mathbf{k}\mathbf{R_j}}$. It was obtained for instance,

$$\Big\langle \sum_j^N e^{-i\mathbf{k}\mathbf{R_j}} \Big\rangle = N\delta_{\mathbf{k},0}, \tag{4.15}$$

where $\langle \dots \rangle$ denotes ensemble averaging, N is the number of impurities, and $\delta_{\mathbf{k},0}$ is Kronecker's delta. Eq. (4.15) is non-zero only when $\mathbf{k} = 0$, this is because in any other case the summation cancels out after averaging over the possible impurity positions. It was obtained also,

$$\begin{aligned}\Big\langle \sum_j^N e^{-i\mathbf{k}_1\mathbf{R_j}} \sum_l^N e^{-i\mathbf{k}_2\mathbf{R_l}} \Big\rangle &= \Big\langle \sum_{j\neq l}^N e^{-i\mathbf{k}_1\mathbf{R_j}} e^{-i\mathbf{k}_2\mathbf{R_l}} + \sum_{j=l}^N e^{-i(\mathbf{k}_1+\mathbf{k}_2)\mathbf{R_j}} \Big\rangle \\ &= N(N-1)\delta_{\mathbf{k}_1,0}\delta_{\mathbf{k}_2,0} + N\delta_{\mathbf{k}_1+\mathbf{k}_2,0} \\ &\approx N^2\delta_{\mathbf{k}_1,0}\delta_{\mathbf{k}_2,0} + N\delta_{\mathbf{k}_1+\mathbf{k}_2,0} \end{aligned} \tag{4.16}$$

4.2.3 Self-energy

The self-energy terms read,

$$\Sigma^{R,A,} = n_i V_0^2 \int \frac{d^3\boldsymbol{k'}}{(2\pi)^3} [1 - i\xi\hat{\boldsymbol{\sigma}}\cdot\boldsymbol{n}] G^{R,A}_{\boldsymbol{k'}} [1 + i\xi\hat{\boldsymbol{\sigma}}\cdot\boldsymbol{n}], \tag{4.17}$$

$$\begin{aligned}\Sigma^{K} = n_i V_0^2 \int \frac{d^3\boldsymbol{k'}}{(2\pi)^3} \Bigg\{ &[1 - i\xi\hat{\boldsymbol{\sigma}}\cdot\boldsymbol{n}] g^K_{\boldsymbol{k'},E}(\boldsymbol{R},T)[1 + i\xi\hat{\boldsymbol{\sigma}}\cdot\boldsymbol{n}] \\ &+ \frac{\xi}{2}\{\boldsymbol{\sigma}\times(\boldsymbol{k}-\boldsymbol{k'}), \nabla_{\boldsymbol{R}} g^K_{\boldsymbol{k'},E}(\boldsymbol{R},T)\}\Bigg\}, \end{aligned} \tag{4.18}$$

4.2.4 Momentum relaxation

The imaginary part of the retarded (advanced) self-energy is related to the damping of the particle [87], i.e.,

$$\mp\frac{i}{2\hat{\boldsymbol{\tau}}} = \hat{\Sigma}^{R(A)}. \tag{4.19}$$

$\hat{\boldsymbol{\tau}}$ is the momentum relaxation and $\hat{\Sigma}^{R(A)} = \mp i\hat{\Sigma}$, given in Eq. (4.17), is the self-energy term. Replacing Eq. (4.17) in Eq. (4.19), we have

$$\frac{1}{\hat{\boldsymbol{\tau}}} = \pi u_{1B}\int\frac{d^3\mathbf{k}'}{(2\pi)^3}\Big[1 - i\xi\hat{\boldsymbol{\sigma}}\cdot\mathbf{n}\Big]\sum_s(I + s\hat{\boldsymbol{\sigma}}\cdot\mathbf{m})\Big[1 + i\xi\hat{\boldsymbol{\sigma}}\cdot\mathbf{n}\Big]\Big[\delta(\epsilon - \epsilon_{\mathbf{k}',s})\Big]. \tag{4.20}$$

To simplify the above expression we make use of the following properties,

$$\int\frac{k^2 dk sin\theta d\theta d\phi}{(2\pi)^3}k_j = 0, \qquad \int_{j\neq l}\frac{k^2 dk sin\theta d\theta d\phi}{(2\pi)^3}k_j k_l = 0, \tag{4.21}$$

which states that terms linear in k_j vanish after $\mathbf{k}$ integration. Notice that in spherical coordinates $d^3\mathbf{k}' = k'^2 dk' sin\theta d\theta d\phi$. Consequently the expression reduces to,

$$\frac{1}{\hat{\boldsymbol{\tau}}} = \pi u_{1B}\sum_s\int\frac{d^3\mathbf{k}'}{(2\pi)^3}\Big(1 + s\hat{\boldsymbol{\sigma}}\cdot\mathbf{m} + \xi^2\hat{\boldsymbol{\sigma}}\cdot\mathbf{n}\hat{\boldsymbol{\sigma}}\cdot\mathbf{n} + \xi^2 s\hat{\boldsymbol{\sigma}}\cdot\mathbf{n}\hat{\boldsymbol{\sigma}}\cdot\mathbf{m}\hat{\boldsymbol{\sigma}}\cdot\mathbf{n}\Big)\delta(\epsilon - \epsilon_{\mathbf{k}',s}). \tag{4.22}$$

To simplify Eq. (4.22) we consider the following properties of vectorial products,

$$(\hat{\boldsymbol{\sigma}}\cdot\mathbf{a})(\hat{\boldsymbol{\sigma}}\cdot\mathbf{a}) = \mathbf{a}^2 I, \tag{4.23}$$

$$(\hat{\boldsymbol{\sigma}}\cdot\mathbf{a})(\hat{\boldsymbol{\sigma}}\cdot\mathbf{b}) = \mathbf{ab}I + i\hat{\boldsymbol{\sigma}}\cdot(\mathbf{a}\times\mathbf{b}), \tag{4.24}$$

$$\mathbf{a}\times(\mathbf{b}\times\mathbf{c}) = \mathbf{b}(\mathbf{ac}) - \mathbf{c}(\mathbf{ab}), \tag{4.25}$$

$$(\hat{\boldsymbol{\sigma}}\cdot\mathbf{a})(\hat{\boldsymbol{\sigma}}\cdot\mathbf{b})(\hat{\boldsymbol{\sigma}}\cdot\mathbf{a}) = \hat{\boldsymbol{\sigma}}\cdot(2\mathbf{a}(\mathbf{ba}) - \mathbf{ba}^2), \tag{4.26}$$

and the following relation of delta functions,

$$\delta(\epsilon - \epsilon_{\mathbf{k}',\pm}) = \frac{\delta(k' - {k'}_{0,\pm})}{\frac{{k'}_{0,\pm}\hbar^2}{m}}. \tag{4.27}$$

Consequently,

$$\begin{aligned}\frac{1}{\hat{\boldsymbol{\tau}}} = \pi u_{1B}\int\frac{d^3\mathbf{k}'}{(2\pi)^3}(1+\xi^2\mathbf{n}^2)\Big[\frac{\delta(k'-{k'}_{0,+})}{\frac{{k'}_{0,+}\hbar^2}{m}} + \frac{\delta(k'-{k'}_{0,-})}{\frac{{k'}_{0,-}\hbar^2}{m}}\Big] \\ + (\hat{\boldsymbol{\sigma}}\cdot\mathbf{m} + \xi^2\hat{\boldsymbol{\sigma}}\cdot(2\mathbf{n}(\mathbf{mn}) - \mathbf{mn}^2)\Big[\frac{\delta(k'-{k'}_{0,+})}{\frac{{k'}_{0,+}\hbar^2}{m}} - \frac{\delta(k'-{k'}_{0,-})}{\frac{{k'}_{0,-}\hbar^2}{m}}\Big].\end{aligned} \tag{4.28}$$

Notice that we have reconsidered $\hbar$ to give a proper definition to the momentum relaxation. Eq. (4.27) is a direct consequence of the property $\delta(f(x)) = (x - x_0)/|f'(x_0)|$, where x_0 is the root of function f. In this case we took $f(x) \equiv \epsilon - \epsilon_{\mathbf{k}',\pm} = \epsilon_F - \frac{\hbar^2\mathbf{k'^2}}{2m} \mp J$, with ϵ_F being the energy at Fermi level (see §4.2.1) and $x_0 \equiv {k'}_{0,\pm} = \sqrt{(\epsilon_F \mp J)2m/\hbar^2}$. To simplify Eq. (4.28) the following properties are considered,

$$\int \frac{d^3\mathbf{k}'}{(2\pi)^3} k'_j \Big[\frac{\delta(k'-k'_{0,+})}{\frac{k'_{0,+}\hbar^2}{m}} \pm \frac{\delta(k'-k'_{0,-})}{\frac{k'_{0,-}\hbar^2}{m}} \Big] = 0, \tag{4.29}$$

$$\int \frac{d^3\mathbf{k}'}{(2\pi)^3} k'_i k'_j \Big[\frac{\delta(k'-k'_{0,+})}{\frac{k'_{0,+}\hbar^2}{m}} \pm \frac{\delta(k'-k'_{0,-})}{\frac{k'_{0,-}\hbar^2}{m}} \Big] = 0, \tag{4.30}$$

$$\int \frac{d^3\mathbf{k}'}{(2\pi)^3} k'^2_j \Big[\frac{\delta(k'-k'_{0,+})}{\frac{k'_{0,+}\hbar^2}{m}} \pm \frac{\delta(k'-k'_{0,-})}{\frac{k'_{0,-}\hbar^2}{m}} \Big] = \int \frac{d^3\mathbf{k}'}{(2\pi)^3} k'^2_i \Big[\frac{\delta(k'-k'_{0,+})}{\frac{k'_{0,+}\hbar^2}{m}} \pm \frac{\delta(k'-k'_{0,-})}{\frac{k'_{0,-}\hbar^2}{m}} \Big], \tag{4.31}$$

$$\int \frac{d^3\mathbf{k}'}{(2\pi)^3} \mathbf{n^2} = \int \frac{d^3\mathbf{k}'}{(2\pi)^3} 2k^2 k'^2_j, \tag{4.32}$$

where $i \neq j$; therefore,

$$\begin{aligned} \frac{1}{\hat{\boldsymbol{\tau}}} = \pi u_{1B} \int \frac{d^3\mathbf{k}'}{(2\pi)^3} (1 + \xi^2 2k^2 k'^2_j) \Big[\frac{\delta(k'-k'_{0,+})}{\frac{k'_{0,+}\hbar^2}{m}} + \frac{\delta(k'-k'_{0,-})}{\frac{k'_{0,-}\hbar^2}{m}} \Big] \\ + (\hat{\boldsymbol{\sigma}} \cdot \mathbf{m} + \xi^2 \hat{\boldsymbol{\sigma}} \cdot (-2k'^2_j \mathbf{k}(\mathbf{k} \cdot \mathbf{m})) \Big[\frac{\delta(k'-k'_{0,+})}{\frac{k'_{0,+}\hbar^2}{m}} - \frac{\delta(k'-k'_{0,-})}{\frac{k'_{0,-}\hbar^2}{m}} \Big]. \end{aligned} \tag{4.33}$$

Integrating out $\mathbf{k}'$ we get,

$$\begin{aligned} \frac{1}{\hat{\boldsymbol{\tau}}} = \pi u_{1B} \Big[\frac{(k_{0,+} + k_{0,-})m}{2\hbar^2\pi^2} + 2\xi^2 k^2 \frac{(k^3_{0,+} + k^3_{0,-})m}{6\hbar^2\pi^2} + \hat{\boldsymbol{\sigma}} \cdot \mathbf{m} \frac{(k_{0,+} - k_{0,-})m}{2\hbar^2\pi^2} \\ - 2\xi^2 \hat{\boldsymbol{\sigma}} \cdot \mathbf{k}(\mathbf{k} \cdot \mathbf{m}) \frac{(k^3_{0,+} - k^3_{0,-})m}{6\hbar^2\pi^2} \Big]. \end{aligned} \tag{4.34}$$

Because k_0 depends on J, we perform a Taylor expansion to second order in exchange coupling; then,

$$\frac{1}{\hat{\boldsymbol{\tau}}} = \frac{1}{\tau_0}\Big[1 - \frac{\beta^2}{2} + \frac{2}{3}\xi^2 k^2 k_F^2 + \xi^2 k^2 k_F^2 \beta^2 - \beta\hat{\boldsymbol{\sigma}}\cdot\mathbf{m} + 2\xi^2 k_F^2 \beta\hat{\boldsymbol{\sigma}}\cdot\mathbf{k}(\mathbf{k}\cdot\mathbf{m})\Big]. \quad (4.35)$$

$\epsilon_F = \frac{\hbar^2 k_F^2}{2m}$, $\frac{1}{\tau_0} = \frac{u_{1B} m\sqrt{2\epsilon_F m}}{\hbar^3\pi} = \frac{u_{1B} m k_F}{\hbar^2\pi} = \frac{u_{1B} m(k_F^{\uparrow}+k_F^{\downarrow})}{2\hbar^2\pi} = \pi u_{1B}(N^{\uparrow}+N^{\downarrow})$, and $\beta = \frac{J}{2\epsilon_F}$. τ_0 is the spin-independent momentum relaxation term and β is the polarization factor. Neglecting terms at higher order in exchange and spin-orbit coupling, Eq. (4.35) simplifies to,

$$\frac{1}{\hat{\boldsymbol{\tau}}} = \frac{1}{\tau_0}\Big[1 + \frac{2}{3}\xi^2 k^2 k_F^2 - \beta\hat{\boldsymbol{\sigma}}\cdot\mathbf{m}\Big]. \quad (4.36)$$

4.2.5 Kinetic equation

The Hamiltonian describing a ferromagnetic layer in the presence of spin-orbit coupled impurities is given in Eq. (4.7). In reciprocal space it reads,

$$H_{\boldsymbol{k}\boldsymbol{k}'} = \frac{\boldsymbol{k}^2}{2m} + J\hat{\boldsymbol{\sigma}}\cdot\boldsymbol{m} + V_{\boldsymbol{k}\boldsymbol{k}'}, \quad (4.37)$$

where $V_{\boldsymbol{k}\boldsymbol{k}'}$ is defined in §4.2.2. In §3.2.1 we derived the quantum kinetic equation in Keldysh space [88], which reads,

$$[G^R]^{-1}\otimes G^K - G^K\otimes[G^A]^{-1} = \Sigma^K\otimes G^A - G^R\otimes\Sigma^K. \quad (4.38)$$

$G^i = G^i(\boldsymbol{r},t;\boldsymbol{r}',t')$ with $i = K, A, R$ represent the real space real time Keldysh, advanced, and retarded Green's functions, respectively. All G's are supposed to be full functions which account all interactions through the self-energy term, Σ. Eq.

(4.38) is then expanded to the first order in spatio-temporal gradient using Wigner expansion method. This method was derived in §3.2.2 and has been used in various contexts such as spin-orbit coupled transport in normal metals [56], non-magnetic and magnetic Rashba gases [89], and topological insulators [90]. Similar to the derivation of Eq. (3.32) given in §3.2.2, in this case our kinetic equation becomes,

$$[g^K, J\hat{\boldsymbol{\sigma}}\cdot\boldsymbol{m}] + i\frac{\partial g^K}{\partial T} + \frac{i}{2}\{\frac{\partial g^K}{\partial \boldsymbol{R}}, \frac{\partial H_{\boldsymbol{k}\boldsymbol{k}'}}{\partial \boldsymbol{k}}\} = \Sigma^K G^A - G^R\Sigma^K - i\{g^K, \Sigma\}, \tag{4.39}$$

where g^K is the Fourier transform of the Keldysh function, i.e.,

$$G^K(\boldsymbol{r}, t; \boldsymbol{r}', t') = \int \frac{dE}{2\pi}\frac{d^2\boldsymbol{k}}{(2\pi)^2} e^{i\boldsymbol{k}\cdot(\boldsymbol{r}-\boldsymbol{r}')-iE(t-t')} g^K_{\boldsymbol{k},E}(T, \boldsymbol{R}), \tag{4.40}$$

with $\boldsymbol{R} = (\boldsymbol{r}+\boldsymbol{r}')/2$ and $T = (t+t')/2$. Notice that Eq. (4.39) no longer depends on the relative spatial $(\boldsymbol{r}-\boldsymbol{r}')$ and temporal $(t-t')$ coordinates but instead in the center of mass coordinates, $\boldsymbol{R}$ and T. To remove the energy dependence in Eq. (4.39) we consider a function $h_{\boldsymbol{k}}(\boldsymbol{R}, t)$ that satisfies,

$$\int \frac{dE}{2\pi} g^K_{\boldsymbol{k},E}(t, \boldsymbol{R}) = -ih_{\boldsymbol{k}}(t, \boldsymbol{R}). \tag{4.41}$$

Then

$$-i[h_{\boldsymbol{k}}, J\hat{\boldsymbol{\sigma}}\cdot\boldsymbol{m}] + \frac{\partial h_{\boldsymbol{k}}}{\partial T} + \frac{1}{2}\{\frac{\partial h_{\boldsymbol{k}}}{\partial \boldsymbol{R}}, \frac{\partial H_{\boldsymbol{k}\boldsymbol{k}'}}{\partial \boldsymbol{k}}\} = -\{h_{\boldsymbol{k}}, \frac{1}{2\hat{\boldsymbol{\tau}}}\} + \int \frac{dE}{2\pi}(\Sigma^K G^A - G^R\Sigma^K), \tag{4.42}$$

where we have considered Eq. (4.19) to express the self-energy in terms of the momentum relaxation. The left-hand side is the *coherent term* that appears in ab-

sence of perturbations, whereas the right-hand side, referred to as the *collision term* in analogy to semiclassical Boltzmann transport equations, takes into account the scattering events and relaxation. Eq. (4.41) is satisfied through the anzat relation,

$$g^K_{k',E}(t,\boldsymbol{R}) = G^R_{k',E} h_{k'}(t,\boldsymbol{R}) - h_{k'}(t,\boldsymbol{R}) G^A_{k',E}. \tag{4.43}$$

First we study the right-hand side of Eq. (4.42). Considering Eq. (4.18) we have,

$$\begin{aligned}\Sigma^K G^A = u_{1B}\int \frac{d^3\boldsymbol{k'}}{(2\pi)^3}\left[g^K_{\boldsymbol{k'}}G^A_{\boldsymbol{k}} + i\xi(g^K_{\boldsymbol{k'}}\hat{\boldsymbol{\sigma}}\cdot\boldsymbol{n}G^A_{\boldsymbol{k}} - \hat{\boldsymbol{\sigma}}\cdot\boldsymbol{n}g^K_{\boldsymbol{k'}}G^A_{\boldsymbol{k}}) + \xi^2\hat{\boldsymbol{\sigma}}\cdot\boldsymbol{n}g^K_{\boldsymbol{k'}}\hat{\boldsymbol{\sigma}}\cdot\boldsymbol{n}G^A_{\boldsymbol{k}}\right] \\ + u_{1B}\int\frac{d^3\boldsymbol{k'}}{(2\pi)^3}\frac{\xi}{2}\left[\boldsymbol{\sigma}\times(\boldsymbol{k}-\boldsymbol{k'})(\nabla_{\boldsymbol{R}}g^K_{\boldsymbol{k'}}) + (\nabla_{\boldsymbol{R}}g^K_{\boldsymbol{k'}})\boldsymbol{\sigma}\times(\boldsymbol{k}-\boldsymbol{k'})\right]G^A_{\boldsymbol{k}}, \end{aligned}\tag{4.44}$$

$$\begin{aligned}G^R\Sigma^K = u_{1B}\int \frac{d^3\boldsymbol{k'}}{(2\pi)^3}\left[G^R_k g^K_{k'} + i\xi(G^R_k g^K_{k'}\hat{\boldsymbol{\sigma}}\cdot\boldsymbol{n} - G^R_k\hat{\boldsymbol{\sigma}}\cdot\boldsymbol{n}g^K_{k'}) + \xi^2 G^R_k\hat{\boldsymbol{\sigma}}\cdot\boldsymbol{n}g^K_{k'}\hat{\boldsymbol{\sigma}}\cdot\boldsymbol{n}\right] \\ + u_{1B}\int\frac{d^3\boldsymbol{k'}}{(2\pi)^3}\frac{\xi}{2}G^R_k[\boldsymbol{\sigma}\times(\boldsymbol{k}-\boldsymbol{k'})(\nabla_{\boldsymbol{R}}g^K_{\boldsymbol{k'}}) + (\nabla_{\boldsymbol{R}}g^K_{\boldsymbol{k'}})\boldsymbol{\sigma}\times(\boldsymbol{k}-\boldsymbol{k'})].\end{aligned}\tag{4.45}$$

Injecting Eq. (4.43) in Eqs. (4.44)-(4.45), and considering $\int \frac{dE}{2\pi}G^{R(A)}_{k',E}G^{R(A)}_{k,E} = 0$, we have

$$\begin{aligned}\int\frac{dE}{2\pi}\Sigma^K G^A = u_{1B}\int\frac{dE}{2\pi}\int\frac{d^3\boldsymbol{k'}}{(2\pi)^3}\Big[G^R_{k'}h_{k'}G^A_k + i\xi(G^R_{k'}h_{k'}\hat{\boldsymbol{\sigma}}\cdot\boldsymbol{n}G^A_k - \hat{\boldsymbol{\sigma}}\cdot\boldsymbol{n}G^R_{k'}h_{k'}G^A_k) \\ + \xi^2\hat{\boldsymbol{\sigma}}\cdot\boldsymbol{n}G^R_{k'}h_{k'}\hat{\boldsymbol{\sigma}}\cdot\boldsymbol{n}G^A_k + \frac{\xi}{2}\left[\boldsymbol{\sigma}\times(\boldsymbol{k}-\boldsymbol{k'})G^R_{\boldsymbol{k'}}(\nabla_{\boldsymbol{R}}h_{\boldsymbol{k'}}) + G^R_{\boldsymbol{k'}}(\nabla_{\boldsymbol{R}}h_{\boldsymbol{k'}})\boldsymbol{\sigma}\times(\boldsymbol{k}-\boldsymbol{k'})\right]G^A_{\boldsymbol{k}}\Big]\end{aligned}\tag{4.46}$$

$$\begin{aligned}\int\frac{dE}{2\pi}G^R\Sigma^K = u_{1B}\int\frac{dE}{2\pi}\int\frac{d^3\boldsymbol{k'}}{(2\pi)^3}\Big[-G^R_k h_{k'}G^A_{k'} - i\xi(G^R_k h_{k'}G^A_{k'}\hat{\boldsymbol{\sigma}}\cdot\boldsymbol{n} - G^R_k\hat{\boldsymbol{\sigma}}\cdot\boldsymbol{n}h_{k'}G^A_{k'}) \\ - \xi^2 G^R_k\hat{\boldsymbol{\sigma}}\cdot\boldsymbol{n}h_{k'}G^A_{k'}\hat{\boldsymbol{\sigma}}\cdot\boldsymbol{n} - \frac{\xi}{2}G^R_k[\boldsymbol{\sigma}\times(\boldsymbol{k}-\boldsymbol{k'})(\nabla_{\boldsymbol{R}}h_{\boldsymbol{k'}})G^A_{\boldsymbol{k'}} + (\nabla_{\boldsymbol{R}}h_{\boldsymbol{k'}})G^A_{\boldsymbol{k'}}\boldsymbol{\sigma}\times(\boldsymbol{k}-\boldsymbol{k'})]\Big].\end{aligned}\tag{4.47}$$

In Eqs. (4.46)-(4.47), the energy integral is transformed into a complex integral, e.g.,

$$\int \frac{dE}{2\pi} G^R_k h_{k'} G^A_{k'} = \frac{\pi}{4} \sum_{s,s'} \delta(E_{\boldsymbol{k'},s'} - E_{\boldsymbol{k},s})(1 + s\hat{\boldsymbol{\sigma}} \cdot \boldsymbol{m}) h_{\boldsymbol{k'}} (1 + s'\hat{\boldsymbol{\sigma}} \cdot \boldsymbol{m}), \tag{4.48}$$

$$\int \frac{dE}{2\pi} G^R_{k'} h_{k'} G^A_{k} = \frac{\pi}{4} \sum_{s,s'} \delta(E_{\boldsymbol{k'},s'} - E_{\boldsymbol{k},s})(1 + s'\hat{\boldsymbol{\sigma}} \cdot \boldsymbol{m}) h_{\boldsymbol{k'}} (1 + s\hat{\boldsymbol{\sigma}} \cdot \boldsymbol{m}) \tag{4.49}$$

where $\delta(E_{\boldsymbol{k'},s'} - E_{\boldsymbol{k},s})$ acquires the following values,

$$\begin{aligned}
\delta(E_{k',+} - E_{k,+}) &= \delta(E_{k'} - E_k), \\
\delta(E_{k',+} - E_{k,-}) &= \delta(E_{k'} - E_k + 2J), \\
\delta(E_{k',-} - E_{k,+}) &= \delta(E_{k'} - E_k - 2J), \\
\delta(E_{k',-} - E_{k,-}) &= \delta(E_{k'} - E_k).
\end{aligned} \tag{4.50}$$

$E_{k',s} = k'^2/2m + sJ$, and $E_k = k^2/2m$. Eq. (4.49) was derived for $h_{\boldsymbol{k'}}$ but it does not restrict us to consider any other function or operator. Therefore, the solution applies very well to any term in Eqs. (4.46) and (4.47). We proceed now to solve the expression,

$$\mathscr{C} = \int \frac{dE}{2\pi} (\Sigma^K G^A - G^R \Sigma^K), \tag{4.51}$$

which is given by subtracting Eqs. (4.46)-(4.47), i.e.,

$$\mathscr{C} = u_{1B}\int\frac{dE}{2\pi}\int\frac{d^3\boldsymbol{k'}}{(2\pi)^3}\Big[\xi^2\Big(\hat{\boldsymbol{\sigma}}\cdot\boldsymbol{n}G^R_{k'}h_{k'}\hat{\boldsymbol{\sigma}}\cdot\boldsymbol{n}G^A_k + G^R_k\hat{\boldsymbol{\sigma}}\cdot\boldsymbol{n}h_{k'}G^A_{k'}\hat{\boldsymbol{\sigma}}\cdot\boldsymbol{n}\Big)$$
$$+ G^R_{k'}h_{k'}G^A_k + G^R_k h_{k'}G^A_{k'} + i\xi\Big([G^R_{k'}h_{k'},\hat{\boldsymbol{\sigma}}\cdot\boldsymbol{n}]G^A_k + G^R_k[h_{k'}G^A_{k'},\hat{\boldsymbol{\sigma}}\cdot\boldsymbol{n}]\Big)$$
$$+\frac{\xi}{2}\left[\boldsymbol{\sigma}\times(\boldsymbol{k}-\boldsymbol{k'})G^R_{\boldsymbol{k'}}(\nabla_{\boldsymbol{R}}h_{\boldsymbol{k'}})G^A_{\boldsymbol{k}} + G^R_{\boldsymbol{k'}}(\nabla_{\boldsymbol{R}}h_{\boldsymbol{k'}})\boldsymbol{\sigma}\times(\boldsymbol{k}-\boldsymbol{k'})G^A_{\boldsymbol{k}}\right]$$
$$+\frac{\xi}{2}[G^R_k\boldsymbol{\sigma}\times(\boldsymbol{k}-\boldsymbol{k'})(\nabla_{\boldsymbol{R}}h_{\boldsymbol{k'}})G^A_{\boldsymbol{k'}} + G^R_k(\nabla_{\boldsymbol{R}}h_{\boldsymbol{k'}})G^A_{\boldsymbol{k'}}\boldsymbol{\sigma}\times(\boldsymbol{k}-\boldsymbol{k'})]\Big] \tag{4.52}$$

Considering Eq. (4.49), we get for each term of Eq. (4.52),

$$\int\frac{dE}{2\pi}(G^R_{k'}h_{k'}G^A_k + G^R_k h_{k'}G^A_{k'}) = 2\pi h_{k'}\delta_\Sigma, \tag{4.53}$$

$$\int\frac{dE}{2\pi}\xi^2(\hat{\boldsymbol{\sigma}}\cdot\boldsymbol{n}G^R_{k'}h_{k'}\hat{\boldsymbol{\sigma}}\cdot\boldsymbol{n}G^A_k + G^R_k\hat{\boldsymbol{\sigma}}\cdot\boldsymbol{n}h_{k'}G^A_{k'}\hat{\boldsymbol{\sigma}}\cdot\boldsymbol{n}) = 2\pi\xi^2\hat{\boldsymbol{\sigma}}\cdot\boldsymbol{n}h_{k'}\hat{\boldsymbol{\sigma}}\cdot\boldsymbol{n}\delta_\Sigma, \tag{4.54}$$

$$\int\frac{dE}{2\pi}i\xi([G^R_{k'}h_{k'},\hat{\boldsymbol{\sigma}}\cdot\boldsymbol{n}]G^A_k + G^R_k[h_{k'}G^A_{k'},\hat{\boldsymbol{\sigma}}\cdot\boldsymbol{n}]) = 2i\xi\pi[h_{k'},\hat{\boldsymbol{\sigma}}\cdot\boldsymbol{n}]\delta_\Sigma$$
$$-\frac{\xi\pi}{2}\{h_{k'},\hat{\boldsymbol{\sigma}}\cdot(\boldsymbol{m}\times\boldsymbol{n})\}\delta_\Delta, \tag{4.55}$$

$$\int\frac{dE}{2\pi}\frac{\xi}{2}\left[\boldsymbol{\sigma}\times(\boldsymbol{k}-\boldsymbol{k'})G^R_{\boldsymbol{k'}}(\nabla_{\boldsymbol{R}}h_{\boldsymbol{k'}})G^A_{\boldsymbol{k}} + G^R_{\boldsymbol{k'}}(\nabla_{\boldsymbol{R}}h_{\boldsymbol{k'}})\hat{\boldsymbol{\sigma}}\times(\boldsymbol{k}-\boldsymbol{k'})G^A_{\boldsymbol{k}}\right] =$$
$$\frac{\xi\pi}{2}\left\{\hat{\boldsymbol{\sigma}}\times(\boldsymbol{k}-\boldsymbol{k'}),(\nabla_{\boldsymbol{R}}h_{\boldsymbol{k'}})\right\}\delta_\Sigma + \frac{\xi\pi}{8}(\hat{\boldsymbol{\sigma}}\times(\boldsymbol{k}-\boldsymbol{k'}))[\hat{\boldsymbol{\sigma}}\cdot\boldsymbol{m},\boldsymbol{\nabla}_R h_{k'}]\delta_\Delta$$
$$+\frac{\xi\pi}{8}[\hat{\boldsymbol{\sigma}}\cdot\boldsymbol{m},\boldsymbol{\nabla}_R h_{k'}\hat{\boldsymbol{\sigma}}\times(\boldsymbol{k}-\boldsymbol{k'})]\delta_\Delta, \tag{4.56}$$

$$\int\frac{dE}{2\pi}\frac{\xi}{2}[G^R_k\boldsymbol{\sigma}\times(\boldsymbol{k}-\boldsymbol{k'})(\nabla_{\boldsymbol{R}}h_{\boldsymbol{k'}})G^A_{\boldsymbol{k'}} + G^R_k(\nabla_{\boldsymbol{R}}h_{\boldsymbol{k'}})G^A_{\boldsymbol{k'}}\boldsymbol{\sigma}\times(\boldsymbol{k}-\boldsymbol{k'})] =$$
$$\frac{\xi\pi}{2}\left\{\boldsymbol{\sigma}\times(\boldsymbol{k}-\boldsymbol{k'}),(\nabla_{\boldsymbol{R}}h_{\boldsymbol{k'}})\right\}\delta_\Sigma + \frac{\xi\pi}{8}[\hat{\boldsymbol{\sigma}}\times(\boldsymbol{k}-\boldsymbol{k'})(\nabla_{\boldsymbol{R}}h_{\boldsymbol{k'}}),\hat{\boldsymbol{\sigma}}\cdot\boldsymbol{m}]\delta_\Delta$$
$$+\frac{\xi\pi}{8}[\nabla_{\boldsymbol{R}}h_{\boldsymbol{k'}},\hat{\boldsymbol{\sigma}}\cdot\boldsymbol{m}](\hat{\boldsymbol{\sigma}}\times(\boldsymbol{k}-\boldsymbol{k'}))\delta_\Delta, \tag{4.57}$$

where $\delta_\Delta = \delta(E_{k',+} - E_{k,-}) - \delta(E_{k',-} - E_{k,+})$ and $\delta_\Sigma = \delta(E_{k'} - E_k)$. Then,

$$\mathscr{C} \approx 2\pi u_{1B} \int \frac{d^3\boldsymbol{k'}}{(2\pi)^3}\Big[h_{k'} + i\xi[h_{k'}, \hat{\boldsymbol{\sigma}}\cdot\boldsymbol{n}] + \xi^2\hat{\boldsymbol{\sigma}}\cdot\boldsymbol{n}h_{k'}\hat{\boldsymbol{\sigma}}\cdot\boldsymbol{n} + \frac{\xi}{2}\left\{\boldsymbol{\sigma}\times(\boldsymbol{k}-\boldsymbol{k'}), (\nabla_{\boldsymbol{R}}h_{\boldsymbol{k'}})\right\}\Big]\delta_\Sigma$$
$$+ \frac{\pi u_{1B}}{2}\int \frac{d^3\boldsymbol{k'}}{(2\pi)^3}\Big[-\xi\{h_{k'}, \hat{\boldsymbol{\sigma}}\cdot(\boldsymbol{m}\times\boldsymbol{n})\} + \frac{\xi}{4}(\hat{\boldsymbol{\sigma}}\times(\boldsymbol{k}-\boldsymbol{k'}))[\hat{\boldsymbol{\sigma}}\cdot\boldsymbol{m}, \boldsymbol{\nabla}_R h_{k'}]$$
$$+ \frac{\xi}{4}[\hat{\boldsymbol{\sigma}}\cdot\boldsymbol{m}, \boldsymbol{\nabla}_R h_{k'}\hat{\boldsymbol{\sigma}}\times(\boldsymbol{k}-\boldsymbol{k'})] + \frac{\xi}{4}[\hat{\boldsymbol{\sigma}}\times(\boldsymbol{k}-\boldsymbol{k'})(\nabla_{\boldsymbol{R}}h_{\boldsymbol{k'}}), \hat{\boldsymbol{\sigma}}\cdot\boldsymbol{m}]$$
$$+ \frac{\xi}{4}[\nabla_{\boldsymbol{R}}h_{\boldsymbol{k'}}, \hat{\boldsymbol{\sigma}}\cdot\boldsymbol{m}](\hat{\boldsymbol{\sigma}}\times(\boldsymbol{k}-\boldsymbol{k'}))\Big]\delta_\Delta \tag{4.58}$$

Introducing a more familiar distribution function, $g_{\boldsymbol{k}} = (1 - h_{\boldsymbol{k}})/2$, Eq. (4.58) becomes

$$\mathscr{C} = 2\pi u_{1B}\int \frac{d^3\boldsymbol{k'}}{(2\pi)^3}\Big[-2g_{k'} + (1+\xi^2\boldsymbol{n}^2) - 2i\xi[g_{k'}, \hat{\boldsymbol{\sigma}}\cdot\boldsymbol{n}] - 2\xi^2\hat{\boldsymbol{\sigma}}\cdot\boldsymbol{n}g_{k'}\hat{\boldsymbol{\sigma}}\cdot\boldsymbol{n}$$
$$-\xi\left\{\boldsymbol{\sigma}\times(\boldsymbol{k}-\boldsymbol{k'}), (\nabla_{\boldsymbol{R}}g_{\boldsymbol{k'}})\right\}\Big]\delta_\Sigma$$
$$+ \pi u_{1B}\int \frac{d^3\boldsymbol{k'}}{(2\pi)^3}\Big[\xi\{g_{k'}, \hat{\boldsymbol{\sigma}}\cdot(\boldsymbol{m}\times\boldsymbol{n})\} - \frac{\xi}{4}(\hat{\boldsymbol{\sigma}}\times(\boldsymbol{k}-\boldsymbol{k'}))[\hat{\boldsymbol{\sigma}}\cdot\boldsymbol{m}, \boldsymbol{\nabla}_R g_{k'}]$$
$$- \frac{\xi}{4}[\hat{\boldsymbol{\sigma}}\cdot\boldsymbol{m}, \boldsymbol{\nabla}_R g_{k'}\hat{\boldsymbol{\sigma}}\times(\boldsymbol{k}-\boldsymbol{k'})] - \frac{\xi}{4}[\hat{\boldsymbol{\sigma}}\times(\boldsymbol{k}-\boldsymbol{k'})(\nabla_{\boldsymbol{R}}g_{\boldsymbol{k'}}), \hat{\boldsymbol{\sigma}}\cdot\boldsymbol{m}]$$
$$- \frac{\xi}{4}[\nabla_{\boldsymbol{R}}g_{\boldsymbol{k'}}, \hat{\boldsymbol{\sigma}}\cdot\boldsymbol{m}](\hat{\boldsymbol{\sigma}}\times(\boldsymbol{k}-\boldsymbol{k'}))\Big]\delta_\Delta \tag{4.59}$$

Similarly, the momentum relaxation in terms of $g_{\boldsymbol{k'}}$ reads,

$$\frac{1}{\boldsymbol{\tau}} \approx \frac{1}{\tau_0}(1 + \frac{4}{3}k^2\xi^2 m\epsilon_F - \beta\hat{\boldsymbol{\sigma}}\cdot\boldsymbol{m}) = 2\pi u_{1B}\int \frac{d^3\boldsymbol{k'}}{(2\pi)^3}(1+\xi^2\boldsymbol{n}^2 - \beta\{g_{k'}, \hat{\boldsymbol{\sigma}}\cdot\boldsymbol{m}\})\delta_\Sigma, \tag{4.60}$$

$$\{2g_k, \frac{1}{2\boldsymbol{\tau}}\} \approx \{g_k, 2\pi u_{1B}\int \frac{d^3\boldsymbol{k'}}{(2\pi)^3}(1+\xi^2\boldsymbol{n}^2 - \beta\hat{\boldsymbol{\sigma}}\cdot\boldsymbol{m})\delta_\Sigma\}, \tag{4.61}$$

Therefore the *collision term* (*coll*), given in Eq. (4.42) reads,

$$
\begin{aligned}
coll = 2\pi u_{1B} \int \frac{d^3\boldsymbol{k'}}{(2\pi)^3} \Big[& 2(1+\xi^2 \boldsymbol{n}^2)(g_k - g_{k'}) - \beta\{\hat{\boldsymbol{\sigma}} \cdot \boldsymbol{m}, g_k - g_{k'}\} - 2i\xi[g_{k'}, \hat{\boldsymbol{\sigma}} \cdot \boldsymbol{n}] \\
& + 2\xi^2(\boldsymbol{n}^2 g_{k'} - \hat{\boldsymbol{\sigma}} \cdot \boldsymbol{n} g_{k'} \hat{\boldsymbol{\sigma}} \cdot \boldsymbol{n}) - \xi \left\{ \boldsymbol{\sigma} \times (\boldsymbol{k} - \boldsymbol{k'}), (\nabla_{\boldsymbol{R}} g_{\boldsymbol{k'}}) \right\} \Big] \delta_\Sigma \\
+ \pi u_{1B} \int \frac{d^3\boldsymbol{k'}}{(2\pi)^3} \Big[& \xi\{g_{k'}, \hat{\boldsymbol{\sigma}} \cdot (\boldsymbol{m} \times \boldsymbol{n})\} - \frac{\xi}{4}(\hat{\boldsymbol{\sigma}} \times (\boldsymbol{k} - \boldsymbol{k'}))[\hat{\boldsymbol{\sigma}} \cdot \boldsymbol{m}, \boldsymbol{\nabla}_R g_{k'}] \\
& - \frac{\xi}{4}[\hat{\boldsymbol{\sigma}} \cdot \boldsymbol{m}, \boldsymbol{\nabla}_R g_{k'} \hat{\boldsymbol{\sigma}} \times (\boldsymbol{k} - \boldsymbol{k'})] - \frac{\xi}{4}[\hat{\boldsymbol{\sigma}} \times (\boldsymbol{k} - \boldsymbol{k'})(\nabla_{\boldsymbol{R}} g_{\boldsymbol{k'}}), \hat{\boldsymbol{\sigma}} \cdot \boldsymbol{m}] \\
& - \frac{\xi}{4}[\nabla_{\boldsymbol{R}} g_{\boldsymbol{k'}}, \hat{\boldsymbol{\sigma}} \cdot \boldsymbol{m}](\hat{\boldsymbol{\sigma}} \times (\boldsymbol{k} - \boldsymbol{k'})) \Big] \delta_\Delta, \qquad (4.62)
\end{aligned}
$$

where we added and subtracted the term $4\pi n_i V_0^2 \int \frac{d^3\boldsymbol{k'}}{(2\pi)^3} \xi^2 \boldsymbol{n}^2 g_{k'} \delta_\Sigma$ to give a proper form to the collision term.

Consequently, the kinetic equation given in Eq. (4.42) becomes,

$$
-i[h_{\boldsymbol{k}}, J\hat{\boldsymbol{\sigma}} \cdot \boldsymbol{m}] + \frac{\partial h_{\boldsymbol{k}}}{\partial T} + \frac{1}{2}\{\frac{\partial h_{\boldsymbol{k}}}{\partial \boldsymbol{R}}, \frac{\boldsymbol{k}}{m}\} = coll. \qquad (4.63)
$$

Replacing $h_k = 1 - 2g_k$, it simplifies to

$$
-2\bigg(- i[g_k, J\hat{\boldsymbol{\sigma}} \cdot \boldsymbol{m}] + \frac{\partial g_k}{\partial t} + \frac{\boldsymbol{k}}{m}\frac{\partial g_k}{\partial \boldsymbol{r}} \bigg) = coll. \qquad (4.64)
$$

where we have replaced $(\boldsymbol{R}, T) \rightarrow (\boldsymbol{r}, t)$ for simplicity. Finally our kinetic equation reads,

$$
\begin{aligned}
&- i[g_k, J\hat{\boldsymbol{\sigma}}\cdot\boldsymbol{m}] + \frac{\partial g_k}{\partial t} + \frac{\boldsymbol{k}}{m}\frac{\partial g_k}{\partial \boldsymbol{r}} = 2\pi u_{1B}\int \frac{d^3\boldsymbol{k'}}{(2\pi)^3}\Big[(g_{k'} - g_k) + i\xi[g_{k'}, \hat{\boldsymbol{\sigma}}\cdot\boldsymbol{n}] \\
&\quad + \xi^2(\hat{\boldsymbol{\sigma}}\cdot\boldsymbol{n} g_{k'}\hat{\boldsymbol{\sigma}}\cdot\boldsymbol{n} - \boldsymbol{n}^2 g_{k'}) + \frac{\xi}{2}\{\boldsymbol{\sigma}\times(\boldsymbol{k}-\boldsymbol{k'}), (\nabla_{\boldsymbol{R}} g_{\boldsymbol{k'}})\} + \frac{\beta}{2}\{\hat{\boldsymbol{\sigma}}\cdot\boldsymbol{m}, g_k - g_{k'}\}\Big]\delta_\Sigma \\
&- \frac{\pi u_{1B}}{2}\int \frac{d^3\boldsymbol{k'}}{(2\pi)^3}\Big[\xi\{g_{k'}, \hat{\boldsymbol{\sigma}}\cdot(\boldsymbol{m}\times\boldsymbol{n})\} - \frac{\xi}{4}(\hat{\boldsymbol{\sigma}}\times(\boldsymbol{k}-\boldsymbol{k'}))[\hat{\boldsymbol{\sigma}}\cdot\boldsymbol{m}, \boldsymbol{\nabla}_R g_{k'}] \\
&\qquad - \frac{\xi}{4}[\hat{\boldsymbol{\sigma}}\cdot\boldsymbol{m}, \boldsymbol{\nabla}_R g_{k'}\hat{\boldsymbol{\sigma}}\times(\boldsymbol{k}-\boldsymbol{k'})] - \frac{\xi}{4}[\hat{\boldsymbol{\sigma}}\times(\boldsymbol{k}-\boldsymbol{k'})(\nabla_{\boldsymbol{R}} g_{\boldsymbol{k'}}), \hat{\boldsymbol{\sigma}}\cdot\boldsymbol{m}] \\
&\qquad - \frac{\xi}{4}[\nabla_{\boldsymbol{R}} g_{\boldsymbol{k'}}, \hat{\boldsymbol{\sigma}}\cdot\boldsymbol{m}](\hat{\boldsymbol{\sigma}}\times(\boldsymbol{k}-\boldsymbol{k'}))\Big]\delta_\Delta. \qquad (4.65)
\end{aligned}
$$

4.2.6 Quantum Boltzmann equations

To consider a set of quantum Boltzmann equations we partition the distribution function, g_k, into its charge, f_k, and spin components, $\boldsymbol{s_k}$, i.e., $g_k = f_k + \hat{\boldsymbol{\sigma}}\cdot\boldsymbol{s_k}$. The following relations hold for the coherent term,

$$
\begin{aligned}
-i[g_k, J\hat{\boldsymbol{\sigma}}\cdot\boldsymbol{m}] &= 2J\hat{\boldsymbol{\sigma}}\cdot(\boldsymbol{s_k}\times\boldsymbol{m}), && (4.66)\\
\frac{\partial g_k}{\partial t} &= \frac{\partial f_k}{\partial t} + \hat{\boldsymbol{\sigma}}\cdot\frac{\partial \boldsymbol{s_k}}{\partial t}, && (4.67)\\
\frac{\boldsymbol{k}}{m}\frac{\partial g_k}{\partial \boldsymbol{r}} &= \frac{\boldsymbol{k}\boldsymbol{\nabla}}{m} f_k + \frac{\boldsymbol{k}\boldsymbol{\nabla}}{m}(\hat{\boldsymbol{\sigma}}\cdot\boldsymbol{s_k}), && (4.68)
\end{aligned}
$$

and for the collision term,

$$g_{k'} - g_k = f_{k'} - f_k + \hat{\boldsymbol{\sigma}} \cdot \boldsymbol{s_{k'}} - \hat{\boldsymbol{\sigma}} \cdot \boldsymbol{s_k}, \tag{4.69}$$

$$[g_{k'}, \hat{\boldsymbol{\sigma}} \cdot \boldsymbol{n}] = 2i[\hat{\boldsymbol{\sigma}} \cdot (\boldsymbol{s_{k'}} \times \boldsymbol{n})], \tag{4.70}$$

$$\hat{\boldsymbol{\sigma}} \cdot \boldsymbol{n} g_{k'} \hat{\boldsymbol{\sigma}} \cdot \boldsymbol{n} - \boldsymbol{n}^2 g_{k'} = \hat{\boldsymbol{\sigma}} \cdot \boldsymbol{n}(\boldsymbol{s_{k'}} \boldsymbol{n}) - \hat{\boldsymbol{\sigma}} \cdot (\boldsymbol{n} \times (\boldsymbol{s_{k'}} \times \boldsymbol{n})) - \boldsymbol{n^2} \hat{\boldsymbol{\sigma}} \cdot \boldsymbol{s_{k'}}, \tag{4.71}$$

$$\{\boldsymbol{\sigma} \times (\boldsymbol{k} - \boldsymbol{k'}), (\nabla_{\boldsymbol{R}} g_{\boldsymbol{k'}})\} = 2\hat{\boldsymbol{\sigma}} \cdot ((\boldsymbol{k} - \boldsymbol{k'}) \times \boldsymbol{\nabla}) f_{\boldsymbol{k'}} + 2((\boldsymbol{k} - \boldsymbol{k'}) \times \boldsymbol{\nabla}) \boldsymbol{s_{k'}} \tag{4.72}$$

$$\{\hat{\boldsymbol{\sigma}} \cdot \boldsymbol{m}, g_k - g_{k'}\} = 2\hat{\boldsymbol{\sigma}} \cdot \boldsymbol{m}(f_k - f_{k'}) + 2(\boldsymbol{s_k} - \boldsymbol{s_{k'}}) \boldsymbol{m}, \tag{4.73}$$

$$\{g_{k'}, \hat{\boldsymbol{\sigma}} \cdot (\boldsymbol{m} \times \boldsymbol{n})\} = 2 f_{k'} \hat{\boldsymbol{\sigma}} \cdot (\boldsymbol{m} \times \boldsymbol{n}) + 2 \boldsymbol{s_{k'}} (\boldsymbol{m} \times \boldsymbol{n}), \tag{4.74}$$

$$\begin{aligned}(\hat{\boldsymbol{\sigma}} \times (\boldsymbol{k} - \boldsymbol{k'}))[\hat{\boldsymbol{\sigma}} \cdot \boldsymbol{m}, \boldsymbol{\nabla}_R g_{k'}] &= 2i((\boldsymbol{k} - \boldsymbol{k'}) \times \boldsymbol{\nabla})(\boldsymbol{m} \times \boldsymbol{s_{k'}}) \\ &\quad - 2\hat{\boldsymbol{\sigma}} \cdot (((\boldsymbol{k} - \boldsymbol{k'}) \times \boldsymbol{\nabla}) \times (\boldsymbol{m} \times \boldsymbol{s_{k'}})),\end{aligned} \tag{4.75}$$

$$\begin{aligned}[\hat{\boldsymbol{\sigma}} \cdot \boldsymbol{m}, \boldsymbol{\nabla}_R g_{k'} \hat{\boldsymbol{\sigma}} \times (\boldsymbol{k} - \boldsymbol{k'})] &= 2i\hat{\boldsymbol{\sigma}} \cdot (\boldsymbol{m} \times ((\boldsymbol{k} - \boldsymbol{k'}) \times \boldsymbol{\nabla})) f_{k'} \\ &\quad + 2\hat{\boldsymbol{\sigma}} \cdot (\boldsymbol{m} \times (((\boldsymbol{k} - \boldsymbol{k'}) \times \boldsymbol{\nabla}) \times \boldsymbol{s_{k'}})),\end{aligned} \tag{4.76}$$

$$\begin{aligned}[\hat{\boldsymbol{\sigma}} \times (\boldsymbol{k} - \boldsymbol{k'})(\nabla_{\boldsymbol{R}} g_{\boldsymbol{k'}}), \hat{\boldsymbol{\sigma}} \cdot \boldsymbol{m}] &= -2i\hat{\boldsymbol{\sigma}} \cdot (\boldsymbol{m} \times ((\boldsymbol{k} - \boldsymbol{k'}) \times \boldsymbol{\nabla})) f_{k'} \\ &\quad + 2\hat{\boldsymbol{\sigma}} \cdot (\boldsymbol{m} \times (((\boldsymbol{k} - \boldsymbol{k'}) \times \boldsymbol{\nabla}) \times \boldsymbol{s_{k'}})),\end{aligned} \tag{4.77}$$

$$\begin{aligned}[\nabla_{\boldsymbol{R}} g_{\boldsymbol{k'}}, \hat{\boldsymbol{\sigma}} \cdot \boldsymbol{m}](\hat{\boldsymbol{\sigma}} \times (\boldsymbol{k} - \boldsymbol{k'})) &= -2i((\boldsymbol{k} - \boldsymbol{k'}) \times \boldsymbol{\nabla})(\boldsymbol{m} \times \boldsymbol{s_{k'}}) \\ &\quad - 2\hat{\boldsymbol{\sigma}} \cdot (((\boldsymbol{k} - \boldsymbol{k'}) \times \boldsymbol{\nabla}) \times (\boldsymbol{m} \times \boldsymbol{s_{k'}})),\end{aligned} \tag{4.78}$$

where $\boldsymbol{\nabla} \cdot (\hat{\boldsymbol{\sigma}} \times (\boldsymbol{k} - \boldsymbol{k'})) = \hat{\boldsymbol{\sigma}} \cdot ((\boldsymbol{k} - \boldsymbol{k'}) \times \boldsymbol{\nabla})$. In Eqs. (4.66)-(4.78) we take the trace to separate between the charge ($Tr[...]$) and spin equations ($Tr[\hat{\boldsymbol{\sigma}}...]$); therefore,

$$\begin{aligned}\frac{\partial f_k}{\partial t} + \frac{\boldsymbol{k}\boldsymbol{\nabla}}{m} f_k = 2\pi u_{1B} \int \frac{d^3\boldsymbol{k'}}{(2\pi)^3} \Big[(f_{k'} - f_k) + \xi((\boldsymbol{k} - \boldsymbol{k'}) \times \boldsymbol{\nabla}) \boldsymbol{s_{k'}} + \beta(\boldsymbol{s_k} - \boldsymbol{s_{k'}}) \boldsymbol{m} \Big] \delta_\Sigma \\ - \xi \pi u_{1B} \int \frac{d^3\boldsymbol{k'}}{(2\pi)^3} \boldsymbol{s_{k'}} (\boldsymbol{m} \times \boldsymbol{n}) \delta_\Delta.\end{aligned} \tag{4.79}$$

and

$$\frac{\partial \boldsymbol{s_k}}{\partial t}+\frac{\boldsymbol{k\nabla}}{m}\boldsymbol{s_k}+2J(\boldsymbol{s_k}\times\boldsymbol{m})=2\pi u_{1B}\int\frac{d^3\boldsymbol{k'}}{(2\pi)^3}\Big[(\boldsymbol{s_{k'}}-\boldsymbol{s_k})+\xi((\boldsymbol{k}-\boldsymbol{k'})\times\boldsymbol{\nabla})f_{k'}$$
$$+\beta(f_k-f_{k'})\boldsymbol{m}\Big]\delta_\Sigma-4\pi u_{1B}\int\frac{d^3\boldsymbol{k'}}{(2\pi)^3}\Big[\xi(\boldsymbol{s_{k'}}\times\boldsymbol{n})+\xi^2(\boldsymbol{n}\times(\boldsymbol{s_{k'}}\times\boldsymbol{n}))\Big]\delta_\Sigma$$
$$-\xi\pi u_{1B}\int\frac{d^3\boldsymbol{k'}}{(2\pi)^3}f_{k'}(\boldsymbol{m}\times\boldsymbol{n})\delta_\Delta-\frac{\xi\pi u_{1B}}{2}\int\frac{d^3\boldsymbol{k'}}{(2\pi)^3}\Big[\boldsymbol{s}_{k'}\times(\boldsymbol{m}\times((\boldsymbol{k}-\boldsymbol{k'})\times\boldsymbol{\nabla}))\Big]\delta_\Delta \tag{4.80}$$

We consider the distribution function to be partitioned into $f'_k=\bar{f}+f^{odd}_{k'}$ and $\boldsymbol{s'_k}=\bar{\boldsymbol{s}}+2J\tau_0(\bar{\boldsymbol{s}}\times\boldsymbol{m})+\boldsymbol{s}^{odd}_{\boldsymbol{k'}}$, where the former term is an even function, i.e. $\bar{f}=\int\frac{d^3\boldsymbol{k'}}{(2\pi)^3}f_{k'}/\frac{d^3\boldsymbol{k'}}{(2\pi)^3}$, and the latter is an odd function. This is a general approach and applies to any function. We remark the following relationships of an odd function

$$\int\frac{d^3\boldsymbol{k'}}{(2\pi)^3}f^{odd}_{k'}=0,\qquad\int\frac{d^3\boldsymbol{k'}}{(2\pi)^3}k'^2_i f^{odd}_{k'}=0,\qquad\int\frac{d^3\boldsymbol{k'}}{(2\pi)^3}k'_ik'_j\delta f^{odd}_{k'}=0. \tag{4.81}$$

Consequently, our quantum Boltzmann transport equations (BTEs) simplify to,

$$\frac{\partial f_k}{\partial t}+\frac{\boldsymbol{k\nabla}}{m}f_k=\frac{\tilde{\bar{f}}-\tilde{f}_k}{\tau_0}+2\xi\pi u_{1B}\int\frac{d^3\boldsymbol{k'}}{(2\pi)^3}((\boldsymbol{k}-\boldsymbol{k'})\times\boldsymbol{\nabla})\boldsymbol{s_{k'}}\delta_\Sigma$$
$$-\xi\pi u_{1B}\int\frac{d^3\boldsymbol{k'}}{(2\pi)^3}\boldsymbol{s_{k'}}(\boldsymbol{m}\times\boldsymbol{n})\delta_\Delta, \tag{4.82}$$

$$\frac{\partial \boldsymbol{s_k}}{\partial t}+\frac{\boldsymbol{k\nabla}}{m}\boldsymbol{s_k}+\Delta(\boldsymbol{s_k}\times\boldsymbol{m})=\frac{\tilde{\bar{\boldsymbol{s}}}+\Delta\tau_0(\bar{\boldsymbol{s}}\times\boldsymbol{m})-\tilde{\boldsymbol{s}}_{\boldsymbol{k}}}{\tau_0}+2\xi\pi u_{1B}\int\frac{d^3\boldsymbol{k'}}{(2\pi)^3}((\boldsymbol{k}-\boldsymbol{k'})\times\boldsymbol{\nabla})f_{k'}\delta_\Sigma$$
$$-\frac{4}{3}\frac{\xi^2\epsilon_F m}{\tau_0}(k^2\bar{\boldsymbol{s}}+\boldsymbol{k}(\bar{\boldsymbol{s}}\boldsymbol{k}))-4\pi u_{1B}\int\frac{d^3\boldsymbol{k'}}{(2\pi)^3}\xi(\boldsymbol{s_{k'}}\times\boldsymbol{n})\delta_\Sigma-\xi\pi u_{1B}\int\frac{d^3\boldsymbol{k'}}{(2\pi)^3}f_{k'}(\boldsymbol{m}\times\boldsymbol{n})\delta_\Delta$$
$$-\frac{\xi\pi u_{1B}}{2}\int\frac{d^3\boldsymbol{k'}}{(2\pi)^3}\Big[\boldsymbol{s}_{k'}\times(\boldsymbol{m}\times((\boldsymbol{k}-\boldsymbol{k'})\times\boldsymbol{\nabla}))\Big]\delta_\Delta, \tag{4.83}$$

where $\tilde{f}_k = f_k - \beta \boldsymbol{s_k} \boldsymbol{m}$ and $\tilde{\boldsymbol{s}}_{\boldsymbol{k}} = \boldsymbol{s_k} - \beta f_k \boldsymbol{m}$. $\Delta = 2J$ in order to differentiate it from β and $\delta_\Delta \propto J$. To solve (4.82) and (4.83) we first need to express the delta functions in terms of k'. We have,

$$\delta_\Sigma = \delta(\epsilon_{k'} - \epsilon_k) = \frac{\delta(k' - k)}{|k/m|}, \tag{4.84}$$

$$\delta_\Delta = \delta(\epsilon_{k'} - \epsilon_k + 2J) - \delta(\epsilon_{k'} - \epsilon_k - 2J) = \frac{\delta(k' - \sqrt{k^2 - 4mJ})}{|\sqrt{k^2 - 4mJ}/m|} - \frac{\delta(k' - \sqrt{k^2 + 4mJ})}{|\sqrt{k^2 + 4mJ}/m|} \tag{4.85}$$

Therefore, the integrals will have solutions of the form

$$\int \frac{d^3\boldsymbol{k'}}{(2\pi)^3} \delta_\Sigma \approx \frac{k_F m}{2\pi^2}, \tag{4.86}$$

$$\int \frac{d^3\boldsymbol{k'}}{(2\pi)^3} k_i'^2 \delta_\Sigma \approx \frac{k_F^3 m}{6\pi^2}, \tag{4.87}$$

$$\int \frac{d^3\boldsymbol{k'}}{(2\pi)^3} k_i'^2 \delta_\Delta \approx -2\frac{k_F m^2 J}{\pi^2}, \tag{4.88}$$

$$\int \frac{d^3\boldsymbol{k'}}{(2\pi)^3} \delta_\Delta \approx -2\frac{m^2 J}{k_F \pi^2}, \tag{4.89}$$

where we have assumed $k \approx k_F$. These solutions require an approximation to be taken in the distribution function. The zeroth-order approximation is given by neglecting exchange ($J = \beta = 0$) and spin-orbit coupling ($\xi = 0$) in Eqs. (4.82) and (4.83). Therefore the BTEs become,

$$\frac{\partial f_k}{\partial t} + \frac{\boldsymbol{k}\boldsymbol{\nabla}}{m} f_k = \frac{(\bar{f} - f_k)}{\tau_0}, \qquad \frac{\partial \boldsymbol{s_k}}{\partial t} + \frac{\boldsymbol{k}\boldsymbol{\nabla}}{m} \boldsymbol{s_k} = \frac{(\bar{\boldsymbol{s}} - \boldsymbol{s_k})}{\tau_0}, \tag{4.90}$$

and the solutions in steady state are,

$$f_k \approx \bar{f} - \frac{\tau_0}{m}(\boldsymbol{k}\boldsymbol{\nabla})\bar{f}, \qquad \boldsymbol{s_k} \approx \bar{\boldsymbol{s}} - \frac{\tau_0}{m}(\boldsymbol{k}\boldsymbol{\nabla})\bar{\boldsymbol{s}}. \tag{4.91}$$

Replacing Eqs. (4.86), (4.89), and (4.91) in the integrals with δ_Δ then,

$$-\xi\pi u_{1B}\int \frac{d^3\boldsymbol{k'}}{(2\pi)^3}\boldsymbol{s_{k'}}(\boldsymbol{m}\times\boldsymbol{n})\delta_\Delta = -2J\xi\bar{\boldsymbol{s}}(\boldsymbol{m}\times(\boldsymbol{\nabla}\times\boldsymbol{k})), \tag{4.92}$$

$$-\xi\pi u_{1B}\int \frac{d^3\boldsymbol{k'}}{(2\pi)^3}f_{k'}(\boldsymbol{m}\times\boldsymbol{n})\delta_\Delta = -2J\xi\boldsymbol{m}\times(\boldsymbol{\nabla}\times\boldsymbol{k})\bar{f}, \tag{4.93}$$

$$-\frac{\xi\pi u_{1B}}{2}\int \frac{d^3\boldsymbol{k'}}{(2\pi)^3}\Big[\boldsymbol{s}_{k'}\times(\boldsymbol{m}\times((\boldsymbol{k}-\boldsymbol{k'})\times\boldsymbol{\nabla}))\Big]\delta_\Delta = \frac{\xi J}{2\epsilon_F\tau_0}\bar{\boldsymbol{s}}\times(\boldsymbol{m}\times(\boldsymbol{k}\times\boldsymbol{\nabla})) \tag{4.94}$$

Replacing Eqs. (4.92)-(4.94) in Eqs. (4.82)-(4.83) we have,

$$\frac{\partial f_k}{\partial t} + \frac{\boldsymbol{k}\boldsymbol{\nabla}}{m}f_k = \frac{\tilde{\bar{f}} - \tilde{f}_k}{\tau_0} + 2\xi\pi u_{1B}\int \frac{d^3\boldsymbol{k'}}{(2\pi)^3}((\boldsymbol{k}-\boldsymbol{k'})\times\boldsymbol{\nabla})\boldsymbol{s_{k'}}\delta_\Sigma - 2J\xi\bar{\boldsymbol{s}}(\boldsymbol{m}\times(\boldsymbol{\nabla}\times\boldsymbol{k})), \tag{4.95}$$

and

$$\begin{aligned}\frac{\partial \boldsymbol{s_k}}{\partial t} + \frac{\boldsymbol{k}\boldsymbol{\nabla}}{m}\boldsymbol{s_k} + \Delta(\boldsymbol{s_k}\times\boldsymbol{m}) &= \frac{\tilde{\bar{\boldsymbol{s}}} + \Delta\tau_0(\bar{\boldsymbol{s}}\times\boldsymbol{m}) - \tilde{\boldsymbol{s}}_{\boldsymbol{k}}}{\tau_0} \\ &+ 2\xi\pi u_{1B}\int \frac{d^3\boldsymbol{k'}}{(2\pi)^3}((\boldsymbol{k}-\boldsymbol{k'})\times\boldsymbol{\nabla})f_{k'}\delta_\Sigma - \frac{4}{3}\frac{\xi^2\epsilon_F m}{\tau_0}(k^2\bar{\boldsymbol{s}} + \boldsymbol{k}(\bar{\boldsymbol{s}}\boldsymbol{k})) \\ &- 4\pi u_{1B}\int \frac{d^3\boldsymbol{k'}}{(2\pi)^3}\xi(\boldsymbol{s_{k'}}\times\boldsymbol{n})\delta_\Sigma - 2J\xi\boldsymbol{m}\times(\boldsymbol{\nabla}\times\boldsymbol{k})\bar{f} + \frac{\xi J}{2\epsilon_F\tau_0}\bar{\boldsymbol{s}}\times(\boldsymbol{m}\times(\boldsymbol{k}\times\boldsymbol{\nabla})).\end{aligned} \tag{4.96}$$

To solve the $\delta_\Sigma-$ integrals we consider the BTEs in the presence of exchange

coupling. i.e.,

$$f_k = \bar{f} - \beta\tau_0(\boldsymbol{v}\boldsymbol{\nabla})\bar{\boldsymbol{s}}\boldsymbol{m} - \tau_0(\boldsymbol{v}\boldsymbol{\nabla})\bar{f} \tag{4.97}$$

$$\boldsymbol{s_k} = \bar{\boldsymbol{s}} - \tau_0(\boldsymbol{v}\boldsymbol{\nabla})\bar{\boldsymbol{s}} - \beta\tau_0(\boldsymbol{v}\boldsymbol{\nabla})\bar{f}\boldsymbol{m} + \Delta\tau_0^2(\boldsymbol{v}\boldsymbol{\nabla})\bar{\boldsymbol{s}} \times \boldsymbol{m} \tag{4.98}$$

Consequently ,

$$\begin{aligned}
2\xi\pi u_{1B}\int \frac{d^3\boldsymbol{k'}}{(2\pi)^3}((\boldsymbol{k}-\boldsymbol{k'})\times\boldsymbol{\nabla})f_{k'}\delta_\Sigma &= 2\xi\pi u_{1B}\int \frac{d^3\boldsymbol{k'}}{(2\pi)^3}(\boldsymbol{k}\times\boldsymbol{\nabla})\bar{f}\delta_\Sigma \\
&= \frac{\xi}{\tau_0}(\boldsymbol{k}\times\boldsymbol{\nabla})\bar{f}, \qquad (4.99)\\
2\xi\pi u_{1B}\int \frac{d^3\boldsymbol{k'}}{(2\pi)^3}((\boldsymbol{k}-\boldsymbol{k'})\times\boldsymbol{\nabla})\boldsymbol{s_{k'}}\delta_\Sigma &= 2\xi\pi u_{1B}\int \frac{d^3\boldsymbol{k'}}{(2\pi)^3}(\boldsymbol{k}\times\boldsymbol{\nabla})\bar{\boldsymbol{s}}\delta_\Sigma \\
&= \frac{\xi}{\tau_0}(\boldsymbol{k}\times\boldsymbol{\nabla})\bar{\boldsymbol{s}}, \qquad (4.100)\\
-4\pi u_{1B}\int \frac{d^3\boldsymbol{k'}}{(2\pi)^3}\xi(\boldsymbol{s_{k'}}\times\boldsymbol{n})\delta_\Sigma &= -4\pi u_{1B}\xi\int \frac{d^3\boldsymbol{k'}}{(2\pi)^3}\Big[-\tau_0(\boldsymbol{v'}\boldsymbol{\nabla})(\bar{\boldsymbol{s}}+\beta\bar{f}\boldsymbol{m})\times\boldsymbol{n} \\
&\qquad + \Delta\tau^2(\boldsymbol{v'}\boldsymbol{\nabla})(\bar{\boldsymbol{s}}\times\boldsymbol{m})\times\boldsymbol{n}\Big] \\
&= -\frac{4}{3}\xi\epsilon_F(\bar{\boldsymbol{s}}+\beta\bar{f}\boldsymbol{m})\times(\boldsymbol{k}\times\boldsymbol{\nabla}) \\
&\quad + \frac{4}{3}\Delta\xi\tau_0\epsilon_F[(\bar{\boldsymbol{s}}\times\boldsymbol{m})\times(\boldsymbol{k}\times\boldsymbol{\nabla})]. \qquad (4.101)
\end{aligned}$$

Replacing the expressions in our BTEs, we have,

$$\frac{\partial f_k}{\partial t} + \frac{\boldsymbol{k}\boldsymbol{\nabla}}{m}f_k = \frac{\tilde{\bar{f}} - \tilde{f}_k}{\tau_0} + \frac{\xi}{\tau_0}(\boldsymbol{k}\times\boldsymbol{\nabla})\bar{\boldsymbol{s}} - 2J\xi\bar{\boldsymbol{s}}(\boldsymbol{m}\times(\boldsymbol{\nabla}\times\boldsymbol{k})), \tag{4.102}$$

and

$$\frac{\partial \boldsymbol{s_k}}{\partial t} + \frac{\boldsymbol{k\nabla}}{m}\boldsymbol{s_k} + \Delta(\boldsymbol{s_k} \times \boldsymbol{m}) = \frac{\tilde{\bar{\boldsymbol{s}}} + \Delta\tau_0(\bar{\boldsymbol{s}} \times \boldsymbol{m}) - \tilde{\boldsymbol{s}}_{\boldsymbol{k}}}{\tau_0} + \frac{\xi}{\tau_0}(\boldsymbol{k} \times \boldsymbol{\nabla})\bar{f}$$
$$- \frac{4}{3}\frac{\xi^2\epsilon_F m}{\tau_0}(k^2\bar{\boldsymbol{s}} + \boldsymbol{k}(\bar{\boldsymbol{s}}\boldsymbol{k})) - \frac{4}{3}\xi\epsilon_F(\bar{\boldsymbol{s}} + \beta\bar{f}\boldsymbol{m}) \times (\boldsymbol{k} \times \boldsymbol{\nabla}) + \frac{4}{3}\Delta\xi\tau_0\epsilon_F[(\bar{\boldsymbol{s}} \times \boldsymbol{m}) \times (\boldsymbol{k} \times \boldsymbol{\nabla})]$$
$$- 2J\xi\boldsymbol{m} \times (\boldsymbol{\nabla} \times \boldsymbol{k})\bar{f} + \frac{\xi J}{2\epsilon_F\tau_0}\bar{\boldsymbol{s}} \times (\boldsymbol{m} \times (\boldsymbol{k} \times \boldsymbol{\nabla})). \tag{4.103}$$

Simplifying the expressions,

$$\frac{\partial f_k}{\partial t} + \frac{\boldsymbol{k\nabla}}{m}f_k = \frac{\tilde{\bar{f}} - \tilde{f}_k}{\tau_0} + \frac{\xi}{\tau_0}(\boldsymbol{k} \times \boldsymbol{\nabla})\bar{\boldsymbol{s}} - 2J\xi\bar{\boldsymbol{s}}(\boldsymbol{m} \times (\boldsymbol{\nabla} \times \boldsymbol{k})), \tag{4.104}$$

and

$$\frac{\partial \boldsymbol{s_k}}{\partial t} + \frac{\boldsymbol{k\nabla}}{m}\boldsymbol{s_k} + \Delta(\boldsymbol{s_k} \times \boldsymbol{m}) = \frac{\tilde{\bar{\boldsymbol{s}}} + \Delta\tau_0(\bar{\boldsymbol{s}} \times \boldsymbol{m}) - \tilde{\boldsymbol{s}}_{\boldsymbol{k}}}{\tau_0} + \frac{\xi}{\tau_0}(\boldsymbol{k} \times \boldsymbol{\nabla})\bar{f}$$
$$- \frac{4}{3}\xi\epsilon_F(\bar{\boldsymbol{s}} + \beta\bar{f}\boldsymbol{m}) \times (\boldsymbol{k} \times \boldsymbol{\nabla}) - 2J\xi\boldsymbol{m} \times (\boldsymbol{\nabla} \times \boldsymbol{k})\bar{f} + \frac{4}{3}\Delta\xi\tau_0\epsilon_F[(\bar{\boldsymbol{s}} \times \boldsymbol{m}) \times (\boldsymbol{k} \times \boldsymbol{\nabla})]$$
$$+ \frac{\xi J}{2\epsilon_F\tau_0}\bar{\boldsymbol{s}} \times (\boldsymbol{m} \times (\boldsymbol{k} \times \boldsymbol{\nabla})) \tag{4.105}$$

Vanishing the time dependence we have,

$$\begin{aligned} f_k &= \bar{f} - \beta\bar{\boldsymbol{s}}\boldsymbol{m} + \beta\boldsymbol{s_k}\boldsymbol{m} - \tau_0\frac{\boldsymbol{k\nabla}}{m}f_k + \xi(\boldsymbol{k} \times \boldsymbol{\nabla})\bar{\boldsymbol{s}} - 2J\xi\tau_0\bar{\boldsymbol{s}}(\boldsymbol{m} \times (\boldsymbol{\nabla} \times \boldsymbol{k})) \\ &= \bar{f} - \tau_0\beta(\boldsymbol{v\nabla})\boldsymbol{s}\boldsymbol{m} + \xi\beta(\boldsymbol{k} \times \boldsymbol{\nabla})\bar{f}\boldsymbol{m} - \frac{4}{3}\tau_0\xi\beta\epsilon_F[\bar{\boldsymbol{s}} \times (\boldsymbol{k} \times \boldsymbol{\nabla})]\boldsymbol{m} - \tau_0\frac{\boldsymbol{k\nabla}}{m}\bar{f} \\ &\quad + \xi(\boldsymbol{k} \times \boldsymbol{\nabla})\bar{\boldsymbol{s}} - 2J\xi\tau_0\bar{\boldsymbol{s}}(\boldsymbol{m} \times (\boldsymbol{\nabla} \times \boldsymbol{k})) \\ &= \bar{f} - \tau_0(\boldsymbol{v\nabla})(\bar{f} + \beta\boldsymbol{s}\boldsymbol{m}) + \xi(\boldsymbol{k} \times \boldsymbol{\nabla})(\bar{\boldsymbol{s}} + \beta\bar{f}\boldsymbol{m}) - (\frac{4}{3}\tau_0\xi\beta\epsilon_F + 2J\xi\tau_0)[\bar{\boldsymbol{s}} \times (\boldsymbol{k} \times \boldsymbol{\nabla})]\boldsymbol{m} \end{aligned} \tag{4.106}$$

and

$$
\begin{aligned}
\boldsymbol{s_k} &= \bar{\boldsymbol{s}} - \beta\bar{f}\boldsymbol{m} + \beta f_k\boldsymbol{m} - \tau_0\frac{\boldsymbol{k}\boldsymbol{\nabla}}{m}\boldsymbol{s_k} + \Delta\tau_0(\bar{\boldsymbol{s}}\times\boldsymbol{m}) - \Delta\tau_0(\boldsymbol{s_k}\times\boldsymbol{m}) + \xi(\boldsymbol{k}\times\boldsymbol{\nabla})\bar{f} \\
&\quad - \frac{4}{3}\xi\epsilon_F\tau_0(\bar{\boldsymbol{s}} + \beta\bar{f}\boldsymbol{m})\times(\boldsymbol{k}\times\boldsymbol{\nabla}) - 2J\xi\tau_0\boldsymbol{m}\times(\boldsymbol{\nabla}\times\boldsymbol{k})\bar{f} \\
&\quad + \frac{4}{3}\Delta\xi\tau_0^2\epsilon_F[(\bar{\boldsymbol{s}}\times\boldsymbol{m})\times(\boldsymbol{k}\times\boldsymbol{\nabla})] + \frac{\xi J}{2\epsilon_F\tau_0}\bar{\boldsymbol{s}}\times(\boldsymbol{m}\times(\boldsymbol{k}\times\boldsymbol{\nabla})) \\
&= \bar{\boldsymbol{s}} - \beta\tau_0(\boldsymbol{v}\boldsymbol{\nabla})\bar{f}\boldsymbol{m} + \xi\beta[(\boldsymbol{k}\times\boldsymbol{\nabla})\bar{\boldsymbol{s}}]\boldsymbol{m} - \tau_0(\boldsymbol{v}\boldsymbol{\nabla})\bar{\boldsymbol{s}} + \Delta\tau_0^2(\boldsymbol{v}\boldsymbol{\nabla})(\bar{\boldsymbol{s}}\times\boldsymbol{m}) \\
&\quad - \Delta\xi\tau_0(\boldsymbol{k}\times\boldsymbol{\nabla})\times\boldsymbol{m}\bar{f} + \frac{4}{3}\xi\Delta\tau_0^2\epsilon_F(\bar{\boldsymbol{s}}\times(\boldsymbol{k}\times\boldsymbol{\nabla}))\times\boldsymbol{m} + \xi(\boldsymbol{k}\times\boldsymbol{\nabla})\bar{f} \\
&\quad - \frac{4}{3}\xi\epsilon_F\tau_0(\bar{\boldsymbol{s}} + \beta\bar{f}\boldsymbol{m})\times(\boldsymbol{k}\times\boldsymbol{\nabla}) - 2J\xi\tau_0\boldsymbol{m}\times(\boldsymbol{\nabla}\times\boldsymbol{k})\bar{f} \\
&\quad + \frac{4}{3}\Delta\xi\tau_0^2\epsilon_F[(\bar{\boldsymbol{s}}\times\boldsymbol{m})\times(\boldsymbol{k}\times\boldsymbol{\nabla})] + \frac{\xi J}{2\epsilon_F\tau_0}\bar{\boldsymbol{s}}\times(\boldsymbol{m}\times(\boldsymbol{k}\times\boldsymbol{\nabla})) \\
&= \bar{\boldsymbol{s}} - \tau_0(\boldsymbol{v}\boldsymbol{\nabla})(\bar{\boldsymbol{s}} + \beta\bar{f}\boldsymbol{m}) + \xi\beta[(\boldsymbol{k}\times\boldsymbol{\nabla})\bar{\boldsymbol{s}}]\boldsymbol{m} + \Delta\tau_0^2(\boldsymbol{v}\boldsymbol{\nabla})(\bar{\boldsymbol{s}}\times\boldsymbol{m}) \\
&\quad + (\Delta\xi\tau_0 + 2J\xi\tau_0)\boldsymbol{m}\times(\boldsymbol{k}\times\boldsymbol{\nabla})\bar{f} + \frac{4}{3}\xi\Delta\tau_0^2\epsilon_F(\bar{\boldsymbol{s}}\times(\boldsymbol{k}\times\boldsymbol{\nabla}))\times\boldsymbol{m} + \xi(\boldsymbol{k}\times\boldsymbol{\nabla})\bar{f} \\
&\quad - \frac{4}{3}\xi\epsilon_F\tau_0(\bar{\boldsymbol{s}} + \beta\bar{f}\boldsymbol{m})\times(\boldsymbol{k}\times\boldsymbol{\nabla}) + \frac{4}{3}\Delta\xi\tau_0^2\epsilon_F[(\bar{\boldsymbol{s}}\times\boldsymbol{m})\times(\boldsymbol{k}\times\boldsymbol{\nabla})] \\
&\quad + \frac{\xi J}{2\epsilon_F\tau_0}\bar{\boldsymbol{s}}\times(\boldsymbol{m}\times(\boldsymbol{k}\times\boldsymbol{\nabla}))
\end{aligned}
\tag{4.107}
$$

4.2.7 Diffusion Equations

To derive the set of diffusion equations we consider the steady state solution of f_k and $\boldsymbol{s_k}$ to the first order in exchange and spin-orbit coupling. Integrating Eqs. (4.106)-(4.107) over k we obtain the spin densities. To derive the current densities we consider the velocity operator given by $\boldsymbol{v} = \frac{\boldsymbol{k}}{m} - \frac{\xi}{\tau_0}\boldsymbol{k}\times\hat{\boldsymbol{\sigma}} + \frac{\xi\beta}{\tau_0}\boldsymbol{k}\times\boldsymbol{m}$, e.g., the charge current density is given by $\boldsymbol{j}_e = \int\frac{d^3\boldsymbol{k}}{(2\pi)^3}(\frac{\boldsymbol{k}}{m}f_k - \frac{\xi}{\tau_0}\boldsymbol{k}\times\boldsymbol{s}_k + \frac{\xi\beta}{\tau_0}\boldsymbol{k}\times\boldsymbol{m}f_k)$. Therefore our final expressions become

$$\frac{\partial \mu_c}{\partial t} = \boldsymbol{\nabla}^2[\mu_c + \beta \boldsymbol{\mu} \cdot \boldsymbol{m}], \tag{4.108}$$

$$\frac{\partial \boldsymbol{\mu}}{\partial t} = -\boldsymbol{\nabla} \cdot \boldsymbol{Q}_j + \frac{1}{\tau_\phi}(\boldsymbol{\mu} \times \boldsymbol{m}) \times \boldsymbol{m} - \frac{1}{\tau_L}(\boldsymbol{\mu} \times \boldsymbol{m}) - \frac{1}{\tau_{sf}}\boldsymbol{\mu}, \tag{4.109}$$

$$\frac{\boldsymbol{j}_e}{D} = -\boldsymbol{\nabla}(\mu_c + \beta \boldsymbol{\mu} \cdot \boldsymbol{m}) + \alpha_{sj}\boldsymbol{\nabla} \times (\boldsymbol{\mu} + \frac{\beta}{2}\mu_c \boldsymbol{m}) - \alpha_{sw}\beta \boldsymbol{\nabla} \times (\boldsymbol{\mu} \times \boldsymbol{m}), \tag{4.110}$$

$$\frac{\boldsymbol{Q}_j}{D} = -\boldsymbol{Q}_j^0 + \alpha_{sj}\boldsymbol{\nabla} \times (\mu_c \hat{\boldsymbol{e}}_j + \beta m_j \boldsymbol{\mu}) - \alpha_{sw}\boldsymbol{\nabla} \times (\hat{\boldsymbol{e}}_j \times (\boldsymbol{\mu} + \beta \mu_c \boldsymbol{m}))\big] \tag{4.111}$$

μ_c and $\boldsymbol{\mu}$ are the charge and spin accumulations. $\boldsymbol{j}_e$ and $\boldsymbol{Q}_j$ are the charge and spin current densities, where subindex j represents the spin orientation. $\boldsymbol{Q}_j^0 = \boldsymbol{\nabla} \cdot (\mu_j + \beta \mu_c m_j - \frac{\tau_0}{\tau_L}(\boldsymbol{\mu} \times \boldsymbol{m})_j + \frac{\tau_0}{\tau_\phi}((\boldsymbol{\mu} \times \boldsymbol{m}) \times \boldsymbol{m})_j)$. The spin-flip relaxation time due to the spin-orbit interaction, $\tau_{so} = \frac{9}{8}\frac{\tau_0}{\alpha^2}$, and the dephasing term of ferromagnets [93], $\tau_\phi = \hbar^2/4J^2\tau_0$, are given at higher order in spin-orbit coupling and exchange interaction, respectively. Eqs. (4.108)-(4.111) correspond to one of the major results of this work. In the absence of SOC, these equations are equivalent to Petitjean et al. [93], and in the absence of exchange, to Shchelushkin and Brataas [56]. $D = \tau_0 v_F^2/3$ is the diffusion coefficient and $\alpha = \xi_{so} k_F^2$ is the dimensionless spin-orbit coupling parameter. $\alpha_{sw} = 2\alpha/3$ and $\alpha_{sj} = \alpha/l_F k_F$ are the dimensionless spin swapping and side-jump terms, respectively. v_F is the Fermi velocity, $l_F = \tau_0 v_F$ is the mean-free path, and $\tau_L = \hbar/2J$ is the spin precessional time around the magnetization, known as Larmor precessional time. The present model was derived for weak - compared to the Fermi enegy - ferromagnets. In a magnetic system with SOC, the competition between spin precession, spin relaxation, spin Hall and spin swapping effects are governed by the ratio between the different characteristic lengths: spin dephasing, spin relaxation and spin precession lengths. In a bulk homogeneous ferromagnet, spin swapping and spin Hall effects are not operative ($\boldsymbol{\nabla}$=0), and only survive close to the interfaces. Therefore, in a strong ferromagnet where dephasing is shorter than spin relaxation, one expects that these two effects will vanish. Consequently, any

spin that is transverse to the magnetization will eventually align or anti-align in the direction of $\boldsymbol{m}$ [92]. In contrast, in weak ferromagnets, the dephasing length is larger and these effects can become prominent.

4.3 Results and discussion

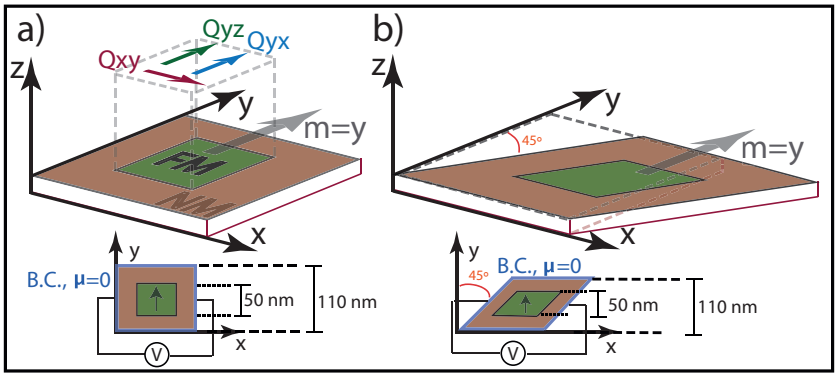

Figure 4.1: (Color online) Schematic view of the device in 3D (top) and 2D (bottom). Two types of geometries are considered: a) squared-lattice, b) diamond-like. In the squared-lattice-geometry the ferromagnet (shaded green) is $50 \times 50\ nm^2$ and the normal metal (shaded red) is $110 \times 110\ nm^2$. In the diamond-like-geometry the lateral sides are tilted 45° with respect to the base. Current flows along $\hat{x}$ and $\boldsymbol{m} = \hat{y}$. As boundary condition we set $\boldsymbol{\mu} = 0$ in all sides of the normal metal (blue lines in 2D schemes). Three spin current densities are defined in the ferromagnetic layer, Q_{xy}, Q_{yz}, and Q_{yx}.

Fig. 1 depicts the two types of geometries considered in this work, a) squared-lattice, b) diamond-like. In both cases, all sides of the ferromagnet are in contact with normal metals. We impose $\boldsymbol{\mu} = 0$ as boundary condition in the normal metal and set $\boldsymbol{m} = \hat{\boldsymbol{y}}$ in the ferromagnet. As shown in the top scheme in Fig. 4.2, a charge current flowing along $\hat{\boldsymbol{x}}$ in the normal metal becomes spin polarized along $\hat{\boldsymbol{y}}$ in the ferromagnet, i.e., a spin current density $Q_{xy} \sim -D\nabla_x \mu_y$ is induced in the magnetic layer, where Q_{ij} is the spin current density component with spatial direction given along i and spin orientation defined along j. Due to the interplay between Larmor precession and spin flip relaxation, spin accumulation along $\hat{\boldsymbol{y}}$ is localized at the

normal metal/ferromagnet interfaces along the transport direction, in agreement with Valet-Fert theory [94].

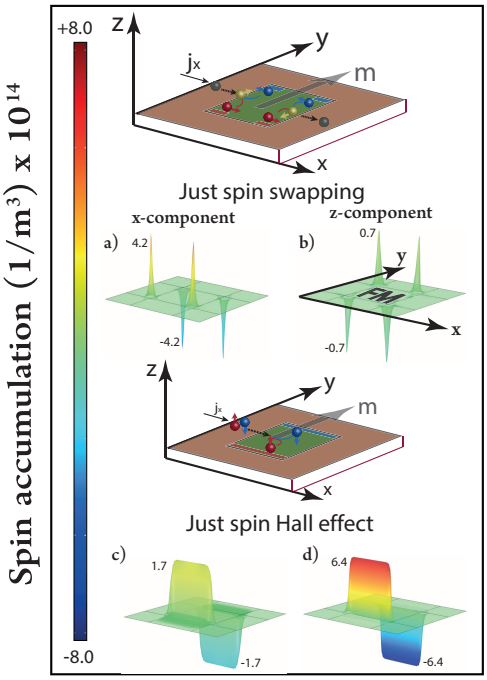

Figure 4.2: (Color online) Spin accumulation profiles μ_x (left) and μ_z (right) in a squared-lattice geometry. (a)(b) Top panels refer to the accumulations when only spin swapping and Larmor precession are considered, (c)(d) Bottom panels refer to the case when only spin Hall effect and Larmor precession are considered. $\boldsymbol{m} = \hat{\boldsymbol{y}}$ and transport is given along $\hat{\boldsymbol{x}}$. The spin diffusion length is $l_{sf} = \sqrt{D\tau_{sf}} = 2$ nm, the Larmor precessional length is $l_J = \sqrt{D\tau_L} = 2$ nm, and the dephasing length is $l_\phi = \sqrt{D\tau_\phi} = 3.4$ nm. The mean free path is $l_F = \tau_0 v_F = 2.5$ nm, the velocity is $v_F = 5\times10^5$ m/s, and the Fermi wave-vector is $k_F = 4.3$ nm^{-1}. $\epsilon_F = 0.7$ eV, $J = 0.15$ eV, and $\alpha^* = 0.1$ eV.nm, where $\alpha^* = \alpha\hbar v_F$.

Before presenting the complete numerical results for this system, we first attempt to give some insight of the impact of Larmor precession on spin swapping, for this we consider a toy model where we vanish in Eq. (4.111) the side-jump contribution, the polarization factor, and the dephasing term. The equation then reduces to,

$$\frac{Q_{yx}}{D} = -\nabla_y \mu_x - \frac{\tau_0}{\tau_L}\nabla_y \mu_z + \frac{2}{3}\alpha_{sw}\nabla_x \mu_y, \tag{4.112}$$

$$\frac{Q_{yz}}{D} = -\nabla_y \mu_z + \frac{\tau_0}{\tau_L}\nabla_y \mu_x. \tag{4.113}$$

Eq. (4.112) shows that due to spin swapping mechanism, $Q_{xy} \sim -D\nabla_x \mu_y$ builds $Q_{yx} \sim -D\nabla_y \mu_x$, in agreement with previous results reported in normal metals [58], where the spin accumulation generated, μ_x, vanishes far from the interfaces due to spin-flip mechanisms. In top scheme in Fig. 4.2 we depict this situation for the case of ferromagnets, where, in contrast to normal metals, an additional term arises that couples Q_{yx} to Q_{yz}, see Eq. (4.113). It means that spin swapping builds also spin accumulation polarized along z, which resembles spin Hall effect (this is not spin Hall Effect, this is spin swapping + precession). On Figs. 4.1(a)(b) we plot the $x-$ and $z-$ components of the spin accumulation. Similar results are obtained if we neglect spin swapping and focus on spin Hall effect instead, see Ref [95], where the authors considered an external magnetic field. In this case, depicted in bottom scheme in Fig. 4.2, the spin accumulations do not vanish far from the interfaces as the driven source is the charge current density [96]. Results are shown in Figs. 4.2(c)(d).

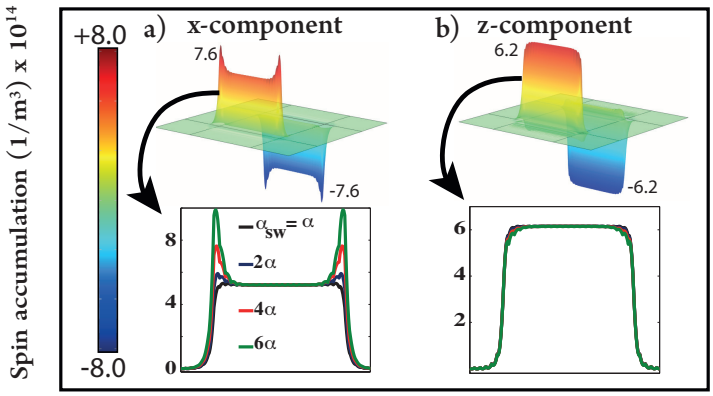

Figure 4.3: (Color online) Spin accumulation profiles μ_x (left) and μ_z (right) described by Eqs. (4.108)-(4.111) in a squared-lattice geometry. Parameters are given in Fig. 4.2.

We now proceed to give the complete numerical results of Eqs (4.108)-(4.111) for a squared-lattice geometry. μ_z is dominated by the spin Hall effect, giving rise to a robust accumulation at the lateral sides of the ferromagnet, see Fig. 4.3(b). Meanwhile, the accumulation μ_x strongly depends on the contribution of spin swapping, see Fig. 4.3(a) where we have considered $\alpha_{sw} = 4\alpha$. On bottom insets we display the spin accumulation profiles for different values of α_{sw}. To enhance the contribution of spin swapping, we can decrease the side-jump contribution by increasing the mean free path or the momentum relaxation time.

In the following we introduce the diamond-like geometry, depicted in Fig. 4.1(b). The importance of the geometry to control magnetization switching was discussed in Ref. [97]. In this case, we explore the role of the geometry in nucleation and propagation of domain walls in systems involving spin swapping, spin Hall effect, and Larmor precession. In contrast to the squared-lattice geometry, in a diamond-like structure spin flip scattering lengths near the tilted sides of the ferromagnet become asymmetric, giving rise to a symmetry breaking of the spin accumulations, i.e., in contrast to the symmetric profiles given in Figs. 4.3(a)(b), here, the spin accumulation at one side is larger than at the other side, see Figs. 4.4(a)(b). Considering that spin swapping is localized near the edges, this geometry may contribute to nucleation of domain walls in the regions where the spin swapping magnitude is higher. Eventually, due to spin transfer mechanism, this domain wall will propagate, leading to possible new avenues in magnetization switching, see top scheme in Fig. 4.4

Notice that in Figs. 4.4(a)(b) we have considered different spin flip relaxation lengths in the normal metal, i.e., we set $l_{sf} = 3$ nm in the top NM region (T), $l_{sf} = 1$ nm in the bottom NM region (B), and $l_{sf} = 2$ nm in the middle region (M), see Fig. 4.4(a). Therefore, in this configuration, spins at the top interface, in contrast to the spins at the bottom interface, will experience longer times to relax, giving rise to an enhancement of the spin accumulations.

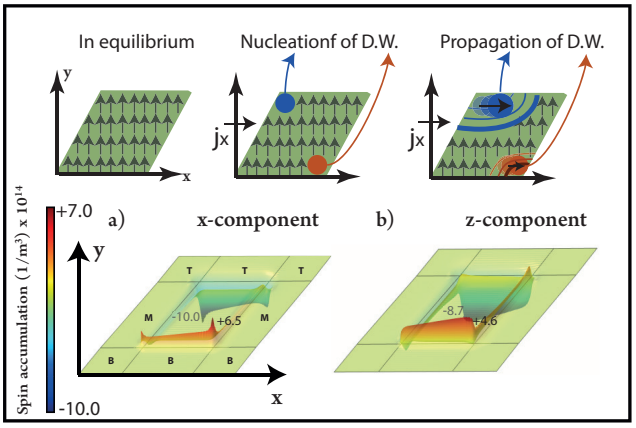

Figure 4.4: (Color online) Spin accumulation profiles, a) μ_x and b) μ_z in a diamond like geometry. $\boldsymbol{m} = \hat{\boldsymbol{y}}$ and transport is given along $\hat{\boldsymbol{x}}$. In the normal metal, the bottom region (B) is set to $l_{sf} = 1$ nm, the middle region (M) to $l_{sf} = 2$ nm, and the top region (T) to $l_{sf} = 3$ nm. The ferromagnet is kept with $l_{sf} = 2$ nm. Other parameters are given in Fig. 4.1.

4.4 Conclusions

We have studied the spin accumulation in 2 types of ferromagnetic films in the presence of spin-orbit coupled impurities. In the first configuration, a squared-lattice geometry, we showed that μ_x and μ_z are driven by the competing terms of spin Hall effect and spin swapping. μ_x strongly depends on the spin swapping mechanism, exhibiting higher amplitudes at the lateral edges of the sample. Meanwhile, μ_z is dominated by spin Hall effect, exhibiting a robust accumulation at both sides of the ferromagnet. In the second configuration, a diamond-like geometry, we showed that tilting the sides of the ferromagnet and considering different spin-flip relaxation lengths contribute to a symmetry breaking of the spin accumulation, which may lead to spin orbit torque effects governed by spin swapping. In contrast to the conventional Rashba torque and spin Hall torque, which act in the full system, spin swapping torque is localized at the interfaces, opening novel avenues in nucleation and propagation of domain walls.

Chapter 5

Concluding Remarks

5.1 Summary

The intensive search for innovative ways in MRAM technology to control and measure magnetization orientation in nanodevices has led to the discovery of spin torques. In the present thesis we have investigated two kind of spin torques: i) spin transfer torques and ii) spin-orbit torques. The former appears as a result of angular momentum transfer from the conductive electrons to the localized magnetization vector, whereas the latter appears as a result of spin-orbit fields acting in the sample.

In Chap. 2 we studied *spin transfer torques in spin filter tunnel junctions*. In contrast to conventional magnetic tunnel junctions, where two non-collinear ferromagnetic electrodes are separated by a thin insulating barrier, in spin filter tunnel junctions the ferromagnetic electrodes are separated by a magnetic insulator. We showed that the spin transfer torque amplitude in spin filter tunnel junctions is much higher than in conventional magnetic tunnel junctions, as a result of spin filtering effect acting in the magnetic barrier. Of particular interest in our calculations is the angular dependence of the spin transfer torque. We showed that the torque amplitude can be tuned over a wide range just by rotation of the magnetization vector in the magnetic insulator. These results open promising novelties in the fabrication of STT-MRAM devices.

In Chap. 3 we studied *Rashba torque in ferromagnetic films*. In contrast to the spin transfer torque mechanism, the spin-orbit torque, referred to as Rashba, appears even in collinear homogeneous ferromagnetic layers. Therefore, memory devices based on Rashba require a stack of layers much lower than the ones given in tunnel junctions, offering efficient ways of achieving magnetization reversal and excitations. We showed that the spin-orbit torque is dominated by the out-of-plane component, as a result of inverse spin galvanic effect, which generates a continuous non-equilibrium spin density along the Rashba field. Moreover, to provide a better understanding to the key mechanisms behind the experimental results and be able to distinguish this effect from the so called *spin Hall torque*, the angular dependence of the Rashba torque has been studied. We showed that in the strong Rashba regime, the in-plane torque component exhibits a strong angular dependence. The origin of the angular dependence within this model is the anisotropy of the spin relaxation, which arises naturally since the Rashba spin-orbit interaction is responsible for the anisotropic D'yakonov-Perel spin relaxation mechanism. For the out-of-plane torque component, in contrast, we found it to be almost constant even when the spin relaxation is anisotropic. Experimentally however, both spin torque components depend strongly on magnetization orientation, and therefore, further studies have been considered very recently (to the date of publication of this thesis) to quantitatively distinguish the contributions of spin Hall and Rashba torques. Nonetheless, this type of structure remains a promising candidate in future developments of SOT-MRAM devices.

In Chap. 4 we studied *spin swapping and spin Hall effect in ferromagnetic films* arising from the spin-orbit coupled impurities in the sample. In contrast to Chap. 3, which is referred to as an intrinsic spin-orbit coupling effect, in Chap. 4 we discussed the nature of extrinsic spin-orbit coupling in ferromagnetic films. We showed that spin orbit torques may appear in the form of spin swapping torque and spin Hall torque. However, in diamond-like geometries, the torque is governed by spin swapping as it

is highly localized at the interfaces, offering the possibility to nucleate and propagate domain walls.

In conclusion, we have discussed new ways to control and measure magnetization orientation in nanodevices that may impact the future of spintronics technology.

5.2 Perspectives

Electric currents and the magnetic moments of elementary particles give rise to a magnetic field, which acts on other currents and magnetic moments. This well established concept has given rise to outstanding applications in our everyday life, ranging from compasses to tapes and disk drives. In spintronics, the remarkable discovery of *Giant Magnetoresistance* has led to many applications in diverse fields. For instance, in medicine it is well used to track bacterias through magnetic biosensors, and in computer technology, it is used to read and store information in magnetic random access memories. The key ingredient of spintronics is the spin, a quantum mechanical property that appears in particles such as the electron. It is described as a tiny magnetic moment that the particle has and allows it to interact with other magnetic moments and fields. The most promising material for spintronics technology has been the ferromagnet, e.g., a magnetic tunnel junction is based on two non-collinear ferromagnetic layers separated by a thin oxide. More recently, new types of materials have been discovered to be useful for a new generation of spintronics technology, e.g., antiferromagnets, spin-orbit coupled heavy metals, magnetic insulators, skyrmions, topological insulators, graphene, transition metal dichalcogenides, organic semiconductors, etc. Due to the inclusion of these exotic materials, spintronics is regarded nowadays as a broader and multidisciplinary field; however, the concept of memory devices based on current induced magnetization reversal and excitation remains to be the main objective in spintronics research. For this reason as a perspective work we

aim to take one step forward and study the interaction of electromagnetic waves with the spin of the electron and open possible novel avenues in a new type of memory devices. This approach comes by understanding that technology is currently moving towards the capacity of playing with single particles, such as single electron transistors and inverters, which are at the scope of current nano-electronics technology. Therefore, at this quantum level, electromagnetic waves are no longer regarded as beams because the wavelengths become comparable to the dimensions of the system. In the near future we may start speaking of single spin technology and its interaction with light. In this sense, we propose to study Casimir effect and surface plasmons in exotic materials related to spin-electronics. The former appears due to the zero-point quantum fluctuations of the electromagnetic field, whereas the latter appears in the presence of visible light. To simplify the picture, in this section we discuss Casimir effect only.

Casimir effect is of great interest nowadays as it offers the possibility to use the ground state energy to generate forces. Richard Feynman once said, "there is plenty of room at the bottom," referring to the advantages of nanotechnology over microtechnology. Casimir effect can be regarded as, "there is plenty of energy at the bottom," as there is a huge amount of zero-point energy that can be used for free once we reach the level of single particle technology. In his seminal work [98], Casimir showed that the force acting on a pair of two perfectly conducting plates in vacuum is attractive and decays as $1/a^4$, being a the separation distance between the plates. This effect was explained in terms of the zero-point quantum fluctuations of the electromagnetic field in vacuum under variations of the boundary condition which yields a finite change of the zero-point energy of the system, and therefore results in an observable force, i.e., the radiation pressure of the field outside two plates is slightly greater than that between the plates. Later, Lifshitz [99] generalized this result considering two slabs with dielectric functions ϵ_L and ϵ_R, immersed in a fluid (ϵ_B), and found that

when $\epsilon_L < \epsilon_B < \epsilon_R$ the force becomes repulsive, yielding possible outcomes in quantum levitation. Nowadays, there is a broader literature of Casimir effect in condensed matter physics and the interest is increasing because they dominate the interaction between nanostructures and are responsible for the adhesion or repulsion between moving parts in small devices such as micro- and nano- electromechanical systems. In spintronic devices, Casimir effect is showing its presence since the discovery of ferromagnetic slabs inducing variations in the Casimir force due to the magneto-optical Kerr effect. In particular, in a recent paper [100] it was shown that when considering a ferromagnet plate next to an isotropic metallic mirror one obtains a Casimir energy that depends on magnetization orientation, meaning that Casimir effect gives rise to magnetic anisotropy in the ferromagnetic layer due to the magneto-optical Kerr effect. Consequently, any system with magneto-optical properties are good candidates to be studied. In our case we propose to consider one of the slabs to be a magnetic dielectric material. The system is likely to be solved considering the generalized Lifshitz approach and therefore a repulsive Casimir force may be expected. Besides ferromagnetic slabs, new kind of exotic materials are under investigation regarding the Casimir effect, such as topological insulators. Topological insulators in contact with the exchange interaction of a magnetic material suffers time-reversal symmetry breaking and therefore its surface states (metallic states) give rise to magneto-electric properties such as quantum anomalous Hall effect. These magneto-electric effects can be probed optically using linearly-polarized light, resulting in Faraday rotation in the transmitted light and Kerr rotation in the reflected light, leading to dramatic magneto-optical effects [101] that will eventually affect the Casimir force when considering two slabs in vacuum [102]. Similarly, here we propose to study Casimir effect in two slabs of graphene samples, as it has been shown that graphene in contact with the exchange interaction of atoms or substrates induces a Zeeman field on graphene itself. Moreover, the combine influence of induced Rashba spin-orbit coupling and

Zeeman field opens up a band gap at the Dirac point of graphene, resulting in a quantum anomalous Hall effect [103]. Of relevant interest also is the interaction between scatterers in two dimensional systems, which results in a Casimir-type problem [104], and more recently, the concept of Casimir-induced-spin-torques between local spins in noncollinear quantum antiferromagnets [105] is opening novel avenues in Casimir-spin-effects.

REFERENCES

[1] W. Gerlach and O. Stern, Z. Phys. **9** 349 (1922).

[2] A. Sommerfeld, "Atomic Structure and Spectral Lines," New York, E.P. Dutton, (1923).

[3] M. N. Baibich, J. M. Broto, A. Fert, F. Nguyen van Dau, F. Petroff, P. Eitenne, G. Creuzet, A. Friederich, and J. Chazelas, Phys. Rev. Lett. **61**, 2472 (1988); G. Binasch, P. Grunberg, F. Saurenbach, and W. Zinn, Phys. Rev. B **39**, 4828 (R) (1989).

[4] W. Thomson, Proc. Royal Soc. London **8**, 546 (1857). T. McGuire and R. Potter, IEEE Trans. on Mag. **11**, 1018 (1975).

[5] P. M. Tedrow and R. Meservey, Phys. Rev. Lett. **26**, 192195 (1971).

[6] Julliere, M. Phys Lett. A **54**, 225 (1975).

[7] W. H. Butler, X.-G. Zhang, T. C. Schulthess, and J. M. MacLaren, Phys. Rev. B 63, 054416 (2001); J. Mathon and A. Umerski, Phys. Rev. B **63**, 220403 (2001).

[8] M. Bowen et al., Appl. Phys. Lett. **79**, 1655 (2001).

[9] S Yuasa, T Nagahama, A Fukushima, Y Suzuki, and K Ando, Nat. Mat. **3** 868 (2004); S. S. P. Parkin et al., Nat. Mat. **3** 862 (2004); S Yuasa and D. D. Djayaprawira, J. Phys. D: Appl. Phys. **40** R337 (2007).

[10] S. Ikeda, J. Hayakawa, Y. Ashizawa, Y.M. Lee, K. Miura, H. Hasegawa, M. Tsunoda, F. Matsukura and H. Ohno, Appl. Phys. Lett. **93**, 082508 (2008).

[11] J. C. Slonczewski, J. Magn. Magn. Mat., **159**, L1 (1996); L. Berger, Phys. Rev. B **54**, 9353 (1996).

[12] D.C. Ralph and M. D. Stiles, J. Magn. and Magn. Mat. **320**, 1190 (2008).

[13] Yiming Huai, AAPPS Bulletin **18**, 6 (2008); S. I. Kiselev, J. C. Sankey, I. N. Krivorotov, N. C. Emley, R. J. Schoelkopf, R. A. Buhrman, and D. C. Ralph, Nature (London) **425**, 380 (2003).

[14] A. Brataas, A. D. Kent, and H. Ohno, Nat. Mat. **11**, 372 (2012).

[15] M. Tsoi, A. G. M. Jansen, J. Bass, W.-C. Chiang, M. Seck, V. Tsoi, and P. Wyder, Phys. Rev. Lett. **80**, 4281 (1998); ibid. **81**, 493 (E) (1998); E. B. Myers, D. C. Ralph, J. A. Katine, R. N. Louie, and R. A. Buhrman, Science **285**, 867 (1999); J. A. Katine, F. J. Albert, R. A. Buhrman, E. B. Myers, and D. C. Ralph, Phys. Rev. Lett. **84**, 3149 (2000).

[16] Yiming Huai, Frank Albert, Paul Nguyen, Mahendra Pakala, and Thierry Valet, Appl. Phys. Lett. **84**, 3118 (2004); G. D. Fuchs, N. C. Emley, I. N. Krivorotov, P. M. Braganca, E. M. Ryan, S. I. Kiselev, J. C. Sankey, D. C. Ralph, R. A. Burman, and J. A. Katine, Appl. Phys. Lett. **85**, 1205 (2004);

[17] J. Hayakawa, S. Ikeda, Y. M. Lee, R. Sasaki, T. Meguro, F. Matsukura, H. Takahashi, and H. Ohno, Jpn. J. Appl. Phys. Exp. Lett. **44**, 37, L1267 (2005); Z. Diao, D. Apalkov, M. Paka- la, Y. Ding, A. Panchula, and Y. Huai, Appl. Phys. Lett. **87**, 232502 (2005).

[18] W. H. Butler, X.-G. Zhang, T. C. Schulthess, and J. M. MacLaren, Phys. Rev. B **63**, 054416 (2001); J. Mathon and A. Umerski, Phys. Rev. B **63**, 220403 (2001).

[19] M. Bowen, V. Cros, F. Petroff, A. Fert, C. Martnez Boubeta, J. L. Costa-Kramer, J. V. Anguita, A Cebollada, F. Briones, J. M. de Teresa, L. Morelln, M. R. Ibarra, F. Guell, F. Peir, and A. Cornet, Appl. Phys. Lett. **79**, 1655 (2001); S. Yuasa, T. Nagahama, A. Fukushima, Y. Suzuki, and K. Ando, Nat. Mat. **3** 868 (2004); S. S. P. Parkin, C. Kaiser, A. Panchula, P. M. Rice, B. Hughes, M. Samant, and S.-H. Yang, Nat. Mat. **3** 862 (2004); S. Yuasa and D. D. Djayaprawira, J. Phys. D: Appl. Phys. **40** R337 (2007).

[20] C. Heiliger and M. D. Stiles, Phys. Rev. Lett. **100**, 186805 (2008); M. Wilczynski, J. Barnas, and R. Swirkowicz, Phys. Rev. B **77**, 054434 (2008); J. Xiao and G. E. Bauer, Phys. Rev. B **77**, 224419 (2008); A. Manchon, N. Ryzhanova, N. Strelkov, A. Vedyayev, and B. Dieny, J. Phys.: Condens. Matter **19**, 165212 (2007).

[21] I. Theodonis, N. Kioussis, A. Kalitsov, M. Chshiev, and W. H. Butler, Phys. Rev. Lett. **97** 237205 (2006); I. Theodonis, N. Kioussis, A. Kalitsov, M. Chshiev, W. H. Butler, and A. Vedyayev, Journ. Appl. Phys. **99**, 08G501 (2006); A. Kalitsov, M. Chshiev, I. Theodonis, N. Kioussis, and W. H. Butler, Phys. Rev. B **79**, 174416 (2009); M. Chshiev, I. Theodonis, A. Kalitsov, N. Kioussis, and W. H. Butler, IEEE Trans. Mag. **44**, 2543 (2008).

[22] S.-C. Oh, S.-Y. Park, A. Manchon, M. Chshiev, J.-H. Han, H.-W. Lee, J.-E. Lee, K.-T. Nam, Y. Jo, Y.-C. Kong, B. Dieny and K.-J. Lee, Nat. Phys. **5**, 898 (2009).

[23] Y.-H. Tang, N. Kioussis, A. Kalitsov, W. H. Butler, and R. Car, Phys. Rev. Lett. **103**, 057206 (2009); ibis. Phys. Rev. B **81**, 054437 (2010).

[24] A. Kalitsov, W. Silvestre, M. Chshiev, and J. P. Velev, Phys. Rev. B **88**, 104430 (2013).

[25] A. Manchon, S. Zhang, and K.-J. Lee, Phys. Rev. B **82**, 174420 (2010).

[26] Y.-H. Tang and N. Kioussis, Phys. Rev B **85**, 104413 (2012).

[27] W. Eerenstein, N. D. Mathur, and J. F. Scott, Nature **442**, 759 (2006); H. Bea, M. Gajek, M. Bibes, and A. Barthélémy, J. Phys.: Condens. Matter **20**, 434221 (2008).

[28] J. S. Moodera, X. Hao, G. A. Gibson, and R. Meservey, Phys. Rev. Lett. **61**, 637 (1988).

[29] J. S. Moodera, J. Phys.: Condens. Matter. **19**, 165202 (2007).

[30] K. Uchida, J. Xiao, H. Adachi, J. Ohe, S. Takahashi, J. Ieda, T. Ota, Y. Kajiwara, H. Umezawa, H. Kawai, G. E. W. Bauer, S. Maekawa, and E. Saitoh. Nat Mat. **9**, 894 (2010); Y. Kajiwara, K. Harii, S. Takahashi, J. Ohe, K. Uchida, M. Mizuguchi, H. Umezawa, H. Kawai, K. Ando, K. Takanashi, S. Maekawa, and E. Saitoh. Nature **464**, 262 (2010).

[31] N. Jutong, I. Rungger, C. Schuster, U. Eckern, S. Sanvito, and U. Schwingenschlogl, Phys. Rev. B **86**, 205310 (2012).

[32] D. C. Worledge and T. H. Geballe. J. Appl. Phys. **88**, 5277 (2000); Z.-W. Xie and B.-Z. Li, J. Appl. Phys. **93**, 9111 (2003); M. Wilczynski, J. Magn. Magn. Mater. **325**, 94 (2013).

[33] A. Saffarzadeh, J. Magn. Magn. Mater. **269**, 327 (2004); M. G. Chapline and S. X. Wang, J. Appl. Phys. **100**, 123909 (2006).

[34] D. Jin, Y. Ren, Z.-Z. Li, M.-W. Xiao, G. Jin, and A. Hu, Phys. Rev. B **73**, 012414 (2006).

[35] P. LeClair, J. K. Ha, H. J. M. Swagten, J. T. Kohlhepp, C. H. van de Vin, and W. J. M. de Jonge, Appl. Phys. Lett. **80**, 625 (2002); G.-X. Miao, M. Muller, and J. S. Moodera, Phys. Rev. Lett. **102**, 076601 (2009).

[36] J. S. Moodera, R. Meservey, and X. Hao, Phys. Rev. Lett. **70**, 853 (1993).

[37] T. S. Santos and J. S. Moodera, Phys. Rev. B **69**, 241203(R) (2004).

[38] M. G. Chapline and S. X. Wang, Phys. Rev. B **74**, 014418 (2006); A. V. Ramos, M. J. Guittet, J. B. Moussy, R. Mattana, C. Deranlot, F. Petroff, and C. Gatel, Appl. Phys. Lett. **91**, 122107 (2007).

[39] U. Luders, M. Bibes, K. Bouzehouane, E. Jacquet, J.-P. Contour, S. Fusil, J.-F. Bobo, J. Fontcuberta, A. Barthélémy, and A. Fert, Appl. Phys. Lett. **88**, 082505 (2006); U. Luders, M. Bibes, S. Fusil, K. Bouzehouane, E. Jacquet, C. B. Sommers, J.-P. Contour, J.-F. Bobo, A. Barthélémy, A. Fert, and P. M. Levy, Phys. Rev. B **76**, 134412 (2007).

[40] B. B. Nelson-Cheeseman, R. V. Chopdekar, L. M. B. Alldredge, J. S. Bettinger, E. Arenholz, and Y. Suzuki, Phys. Rev. B **76**, 220410 (R) (2007).

[41] M. Gajek, M. Bibes, A. Barthélémy, K. Bouzehouane, S. Fusil, M. Varela, J. Fontcuberta, and A. Fert, Phys. Rev. B **72**, 020406 (R) (2005).

[42] R. V. Chopdekar, B. B. Nelson-Cheeseman, M. Liberati, E. Arenholz, and Y. Suzuki, Phys. Rev. B **83**, 224426 (2011).

[43] J.-I. Inoue, J. Appl. Phys. **111**, 07C902 (2012); ibis. Phys. Rev. B **84**, 180402 (R) (2011).

[44] A. Manchon and S. Zhang, Phys. Rev. B **78**, 212405 (2008); ibis, Phys. Rev. B **79**, 212405 (2009); I. Garate and A. H. MacDonald, Phys. Rev. B **80**, 134403 (2009); A. Matos-Abiague and R. L. Rodriguez-Suarez, Phys. Rev. B **80**, 094424 (2009).

[45] A. Chernyshov, M. Overby, X. Liu, J. K. Furdyna, Y. Lyanda-Geller, and L. P. Rokhinson, Nature Phys. **5**, 656 (2009); D. Fang, H. Kurebayashi, J. Wunderlich, K. Výborný, L. P. Zârbo, R. P. Campion, A. Casiraghi, B. L. Gallagher, T. Jungwirth, and A. J. Ferguson, Nature Nanotech. **6**, 413 (2011); K. M. D. Hals, A. Brataas and Y. Tserkovnyak, Europhys. Lett. **90**, 47002 (2010).

[46] I. M. Miron, G. Gaudin, S. Auffret, B. Rodmacq, A. Schuhl, S. Pizzini, J. Vogel, and P. Gambardella, Nature Mater. **9**, 230 (2010); U. H. Pi, K. W. Kim, J. Y. Bae, S. C. Lee, Y. J. Cho, K. S. Kim, and S. Seo, Appl. Phys. Lett. **97**, 162507 (2010); I. M. Miron, K. Garello, G. Gaudin, P.-J. Zermatten, M. V. Costache, S. Auffret, S. Bandiera, B. Rodmacq, A. Schuhl, and P. Gambardella, Nature (London) **476**, 189 (2011).

[47] K.-W. Kim, S.-M. Seo, J. Ryu, K. -J. Lee, and H. -W. Lee, Phys. Rev. B **85** 180404(R) (2012); D. A. Pesin and A. H. MacDonald, Phys. Rev. B **86** 014416 (2012); E. van der Bijl and R. A. Duine, Phys. Rev. B **86**, 094406 (2012).

[48] X. Wang and A. Manchon, Phys. Rev. Lett. **108**, 117201 (2012).

[49] J. E. Hirsch, Phys. Rev. Lett. **83**, 1834 (1999); S. Zhang, Phys. Rev. Lett. **85**, 393 (2000).

[50] L. Liu, O. J. Lee, T. J. Gudmundsen, D. C. Ralph, and R. A. Buhrman, Phys. Rev. Lett. **109**, 096602 (2012); L. Liu, C.-F. Pai, Y. Li, H. W. Tseng, D. C. Ralph, and R. A. Buhrman, Science **336**, 555 (2012); L. Liu, T. Moriyama, D. C. Ralph, and R. A. Buhrman, Phys. Rev. Lett. **106** 036601 (2011).

[51] P.M. Haney, H.-W. Lee, K.-J. Lee, A. Manchon, M. D. Stiles, Phys. Rev. B. **87**, 174411 (2013).

[52] N. Nagaosa, J. Sinova, S. Onoda, A. H. McDonald, N. P. Ong, Rev. of Mod. Phys. **82**, 1539 (2010).

[53] A. Crepieux, P. Bruno, Phys. Rev. B **64**, 014416 (2001).

[54] S. K. Lyo and T. Holstein, Phys. Rev. Lett. **29**, 423 (1972).

[55] M. B. Lifshits and M. I. Dyakonov, Phys. Rev. Lett. **103**, 186601 (2009)

[56] R. V. Shchelushkin and A. Brataas, Phys. Rev. B **72**, 073110 (2005).

[57] S. Sadjina, A. Brataas, and A. G. Mal'shukov, Phys. Rev. B **85**, 115306 (2012).

[58] H. Saidaoui and A. Manchon, Phys. Rev. B **92**, 024417 (2015).

[59] D. J. Griffiths, Introduction to Quantum Mechanics, Addison-Wesley, 2nd edition (2004).

[60] J. C. Slonczewski, Phys. Rev. B, **39**, 6995 (1989).

[61] T. Valet and A. Fert, Phys. Rev. B, **48** (10), 7099 (1993)

[62] L. V. Keldysh, Sov. Phys. JETP, **20** 4 (1965); C. Caroli, R. Combescot, P. Nozieres, and D. Saint-James, J. Phys. C **4**, 916 (1971).

[63] H. Kubota, A. Fukushima, K. Yakushiji, T. Nagahama, S. Yuasa, K. Ando, H. Maehara, Y. Nagamine, K. Tsunekawa, D. D. Djayaprawira, N. Watanabe, and Y. Suzuki, Nat. Phys. **4**, 37 (2008); J. C. Sankey, Y. -T. Cui, J. Z. Sun, J. C. Slonczewski, R. A. Buhrman, and D. C. Ralph, Nat. Phys. **4**, 67 (2008); C. Wang, Y.-T. Cui, J. Z. Sun, J. A. Katine, R. A. Buhrman, and D. C. Ralph, Phys. Rev. B **79**, 224416 (2009).

[64] W. H. Butler, Sci. Tech. Adv. Mater. **9**, 014106 (2008).

[65] T. Nagahama, T. S. Santos, and J. S. Moodera, Phys. Rev. Lett. **99**, 016602 (2007); G. X. Miao and J. S. Moodera. J. Appl. Phys. **106**, 023911 (2009).

[66] C. O. Pauyac, A. Kalitsov, A. Manchon, and M. Chshiev, Phys. Rev. B **90** 235417 (2014).

[67] X. Fan, H. Celik, J. Wu, C. Ni, K.-J. Lee, V. O. Lorenz, and J. Q. Xiao, Nat. Comm. **5** 3042 (2014); J. Kim, J. Sinha, M. ayashi, M. Yamanouchi, S. Fukami, T. Suzuki, and H. Ohno, Nat. Mat. **12** 240-245 (2013).

[68] X. Wang, C. O. Pauyac, and A. Manchon, Phys. Rev. B **89** 054405 (2014).

[69] K. Garello, I. M. Miron, C. O. Avci, F. Freimuth, Y. Mokrousov, S. Blügel, S. Auffret, O. Boulle, G. Gaudin, and P. Gambardella, Nat. Nanotech. **8**, 587 (2013).

[70] X. Qiu, P. Deorani, K. Narayanapillai, K.-S. Lee, K.-J. Lee, H.-W. Lee, and H. Yang, Sci. Rep. **4** 4491 (2014).

[71] A. I. Larkin and Yu. N. Ovchinnikov, Zh. Eksp. Teor. Fiz. **68,** 1915-1927 (1975).

[72] J. Rammer and H. Smith, Rev. Mod. Phys. **58**, 323 (1986).

[73] E. G. Mishchenko, A. V. Shytov, and B. I. Halperin, Phys. Rev. Lett. **93**, 226602 (2004).

[74] J. Rammer, *Quantum Field Theory of Non-equilibrium States* (Cambridge University Press, Cambridge, 2007).

[75] M. I. D'yakonov and V. I. Perel, Sov. Phys. JETP Lett. **13**, 467 (1971).

[76] V. M. Edelstein, Solid State Commun. **73**, 233 (1990).

[77] S. Zhang and Z. Li, Phys. Rev. Lett. **93**, 127204 (2004).

[78] C. Petitjean, D. Luc, and X. Waintal, Phys. Rev. Lett. **109** 117204 (2012); Y. Tserkovnyak, A. Brataas, and G. E. W. Bauer, J. Magn. Magn. Mater. **320**, 1282 (2008).

[79] Y. K. Kato, R. C. Myers, A. C. Gossard, and D. D. Awschalom, Science 306, 1910 (2004).

[80] H.-A. Engel, E. I. Rashba, and B. I. Halperin, Phys. Rev. Lett. **98**, 036602 (2007).

[81] N. Nagaosa, J Sinova, S. Onoda, A. H. McDonald, and N. P. Ong, Rev. Mod. Phys. **82** 1539 (2010)

[82] M. I. Dyakonov and V. I. Perel, Sov. Phys. JETP Lett. **13**, 467 (1971). ibis, Phys. Lett. A **35** (6), 459 (1971). J. E. Hirsch, Phys. Rev. Lett. **83**, 1834 (1999).

[83] C. Gould, C. Ruster, T. Jungwirth, E. Girgis, G. M. Schott, R. Giraud, K. Brunner, G. Schmidt, and L. W. Molenkamp, Phys. Rev. Lett. **93**, 117203 (2004). H. Saito, S. Yuasa, and K. Ando, Phys. Rev. Lett. **95**, 086604 (2005). L. Gao, X. Jiang, S. Yang, J. D. Burton, E. Y. Tsymbal, and S. S. P. Parkin, Phys. Rev. Lett. **99**, 226602 (2007).

[84] M. K. Niranjan, C. G. Duan, S. S. Jaswal, and E. Y. Tsymbal, Appl. Phys. Lett. **96**, 222504 (2010).

[85] C. O. Pauyac, X. Wang, M. Chshiev, A. Manchon, Appl. Phys. Lett., **102**, 252403 (2013).

[86] W. Kohn and J. M. Luttinger, Phys. Rev. **108**, 590 (1957).

[87] G. D. Mahan, Many Particle Physics, 3rd edition, Kluwer Academic / Plenum Publishers, NY, Boston (2000).

[88] J. Rammer and H. Smith, Rev. Mod. Phys. **58**, 323 (1986).

[89] E. G. Mishchenko, A. V. Shytov, and B. I. Halperin, Phys. Rev. Lett. **93**, 226602 (2004). X. Wang and A. Manchon, Phys. Rev. Lett. **108**, 117201 (2012). W. Wang, C. Ortiz Pauyac, A. Manchon, Phys. Rev. B **89**, 054405 (2014).

[90] A. A. Burkov and D. G. Hawthorn, Phys. Rev. Lett. **105**, 066802 (2010). P. B. Ndiaye, C. A. Akosa, M. H. Fischer, A. Vaezi, E-A. Kim, and A. Manchon. ArXiv:1509.06929 (2015).

[91] S. Takahashi and S. Maekawa, J. Phys. Soc. Jpn. **77**, 031009 (2008).

[92] T. Taniguchi, J. Grollier, and M. D. Stiles, arXiv:1411.4863 (2014).

[93] C. Petitjean, D. Luc, and X. Waintal, Phys. Rev. Lett. **109**, 117204 (2012).

[94] T. Valet and A. Fert, Phys. Rev B **48**, 7099 (1993).

[95] K. Shen, R. Raimondi, and G. Vignale, Phys. Rev. B **92**, 035301 (2015).

[96] Y. K. Kato, R. C. Myers, A. C. Gossard, D. D. Awschalom, Science **306** 5703 (2004).

[97] C. K. Safeer, E. Ju, A. Lopez, L. Buda-Prejbeanu, S. Auffret, S. Pizzini, O. Boulle, I. M. Miron, and G. Gaudin, Nat. Nanotech. doi:10.1038/nnano.2015.252 (2015).

[98] H. B. G. Casimir, Proc. K. Ned. Akad. Wet. **51**, 791 (1948).

[99] E. M. Lifshitz, Sov. Phys. JETP **2**, 73 (1956). I. E. Dzyaloshinski, E. M. Lifshitz, and L. P. Pitaevski, Adv. Phys. **10**, 165 (1965).

[100] P. Bruno, Phys. Rev. Lett. **88**, 240401 (2002). G. Metalidis and P. Bruno, Phys. Rev. A **66**, 062102 (2002). G. Metalidis and P. Bruno, Phys. Rev. A **81**, 022123 (2010).

[101] W.-K. Tse and A. H. MacDonald, Phys. Rev. Lett. **105**, 057401 (2010). W.-K. Tse and A. H. MacDonald, Phys. Rev. B (R) **82**, 161104 (2010). W.-K. Tse and A. H. MacDonald, Phys. Rev. B **84**, 205327 (2011).

[102] W. Nie, R. Zeng, Y. Lan and S. Zhu, Phys. Rev. B **88**, 085421 (2013).

[103] Z. Qiao, S. A. Yang, W. Feng, W.-K. Tse, J. Ding, Y. Yao, J. Wang, and Q. Niu, Phys. Rev. B (R) **82**, 161414 (2010). W.-K. Tse, Z. Qiao, Y. Yao, A. H. MacDonald, and Q. Niu, Phys. Rev. B **83** 155447 (2011). Z. Qiao, W.-K. Tse, H. Jiang, Y. Yao, and Q. Niu, Phys. Rev. Lett. **107**, 256801 (2011).

[104] D. Zhabinskaya and E. J. Mele, Phys. Rev. B **80**, 155405 (2009).

[105] Z. Z. Du, H. M. Liu, Y. L. Xie, Q. H. Wang, and J.-M. Liu **92**, 214409 (2015).